Improving the adhesion properties of a shoulder implant using plasma technology

Karen Vloebergh

Supervisors: Prof. dr. Rino Morent, Prof. dr. ir. Nathalie De Geyter
Counsellor: Ir. Stijn Van Vrekhem

Master's dissertation submitted in order to obtain the academic degree of
Master of Science in Biomedical Engineering

UNIVERSITEIT
GENT

Version 1.0.0

compiled on: June 3, 2016

Improving the adhesion properties of a shoulder implant using plasma technology

Karen Vloebergh

Supervisors: Prof. dr. Rino Morent, Prof. dr. ir. Nathalie De Geyter
Counsellor: Ir. Stijn Van Vrekhem

Master's dissertation submitted in order to obtain the academic degree of
Master of Science in Biomedical Engineering

Department of Applied Physics
Chair: Prof. dr. ir. Christophe Leys
Faculty of Engineering and Architecture
Academic year 2015-2016

UNIVERSITEIT
GENT

Foreword

First of all I would like to thank the Research Unit Plasma Technology (RUPT) at UGent for the opportunity they gave me to do this research. My acknowledgements go to Prof. dr. ir. Nathalie De Geyter and Prof. dr. Rino Morent for their guidance during this master thesis. I would like to thank dr. Heidi Declerq and Johanna Aernoudt for the help regarding cell experiments. A big thanks to Joris Peelman for his technical knowledge and assistance. I really enjoyed my time at RUPT and I would like to thank all the people at the department, especially Rim, Rouba, Gaelle, Annick and Pieter for their warm welcome, lunch-breaks and horoscope guidelines. I would also like to thank my college thesis students Valerie, Caroline and Lieve for their support.

My greatest acknowledgement and appreciation goes to Stijn Van Vrekhem, I was very lucky to have him as my mentor. His patience, care, motivation and knowledge helped me succeed and I think we made a great team. I wish him all the best during the rest of his PhD.

At last, I want to thank my family, my mom, dad and big sister and also my boyfriend, who listened patiently to my whining and kept me motivated. Without them I would definitely not stand where I am today.

IMPROVING THE ADHESION PROPERTIES OF A SHOULDER IMPLANT USING PLASMA TECHNOLOGY

Karen Vloebergh[1]

[1]Masterstudent of Science in Biomedical Engineering
Faculty of Engineering and Architecture, University of Ghent

Promotor: Prof. dr. R. Morent, & Prof. dr. ir. N. De Geyter

Co-supervisor: ir. S. Van Vrekhem

Research Unit Plasma Technology (RUPT), Department of Applied Physics
Faculty of Engineering and Architecture, University of Ghent

ABSTRACT − **Insufficient glenoid fixation is one of the reasons why total shoulder arthroplasty often tends to fail. This is mainly due to the inert nature of the ultra high molecular weight polyethylene (UHMWPE) glenoid surface, leading to low adhesion towards bone cement. In this study, plasma activation is used to increase polarity of the UHMWPE surface, aiming to improve glenoid performance. Five different plasma activation conditions are selected and analyzed to see how they change surface hydrophilicity, roughness and chemical composition. Ageing tests examine the stability of the modified surface over time and cell tests look at the interaction of osteoblast in regard to adhesion and proliferation. In a final test the changes in adhesive strength between the activated UHMWPE implant and bone cement are investigated by means of a pull-out test.**

Keywords - Atmospheric pressure plasma jet, Plasma activation, UHMWPE, Adhesion, Shoulder prosthesis, Process characterization

1 INTRODUCTION

Total shoulder arthroplasty (TSA) indicates a total shoulder joint replacement by means of a prosthesis. Here the shoulder, which consist of a humerus-part located at the upper arm and a glenoid cavity located in the shoulder blade, is replaced by artificial components. Just like other total joint arthroplasties, the frequency of TSA increases every year. In the United States a 319 % increase in the procedure rate has been seen from 1993 to 2007, corresponding to an annual growth of 10.6 % [1, 2]. Indications regarding TSA are diseases of the gleno-humeral joint such as symptomatic osteoarthritis, rheumatoid arthritis or avascular necrosis [3]. Anatomic TSA has become the golden standard for treating advanced shoulder osteoarthritis with an intact and functioning rotator cuff after failure of non-operative actions [4]. During surgery the superior end of the humerus is replaced by a metallic stem that ends in a round ball. Additionally, the glenoid plane is restored by placing an ultra high molecular weight polyethylene (UHMWPE) prosthetic compartment. More than other total joint replacements, TSA is associated with a multitude of complications. Complication rates regarding anatomic TSA range from 10 % to 16 %. The two most common causes of failure include glenoid component loosening and prosthesis instability [1, 2]. The origin can be multi-factorial and is subdivided in two main categories: incorrect placement of the component, causing eccentric loading of the glenoid, and insufficient component fixation. The traditional choice regarding fixation includes a cemented all polymer glenoid, using poly methyl methacrylate (PMMA), which contains ester-functionalities [5]. As an alternative to the cemented glenoid component, the metal-backed glenoid was developed where the fixation is done either by a screw construct or by using press-fit metal pegs. Nevertheless the general failure rate of an uncemented (metal-back) glenoid component is reported to be higher than those of cemented PE components [6]. UHMWPE is known for its sufficient mechanical bulk characteristics but it is an inert, non-polar material and has therefore low adhesive binding properties towards bone cement [7]. By modifying the surface of UHMWPE it is however possible to increase these adhesion properties, which may lead to improved glenoid fixation and might decrease complications regarding TSA.

There are several ways available to introduce these polar functional groups on the surface such as wet-chemical

methods, ozone treatment, UV-treatment, self-assembly, high-energy radiation and plasma treatment [8, 9]. Plasma technology has some major advantages as it does not affect the mechanical properties of the bulk material, it is relatively inexpensive and reproducible, it can be used on complex surfaces and has a relative short treatment time [10]. Also the use of hazardous solvents is avoided, as plasma is a solvent free technique [11]. Plasma activations includes a two-step process starting with the formation of free radicals on the polymer surface during plasma treatment, followed by the reaction of these free radicals with the atmosphere and thereby introducing functional groups [7]. This chemical modification can alter physical surface properties like polarity and surface roughness but also enables chemical binding of biological compounds on the surface. There are a lot of different types of set-ups regarding non-thermal atmospheric plasma sources. A new and upcoming trend in plasma source technology includes the atmospheric pressure plasma jet, it is often referred to as remote plasma treatment as surface treatment occurs in the afterglow of the plasma.

The aim of this study is to increase the adhesion between the UHMWPE surface and bone cement (PMMA) in order to improve glenoid fixation. For an optimal result, the influence of process parameters regarding plasma activation treatment have to be determined. In order to get an insight regarding the modifications made to the surface a varied set of surface characterization techniques are used like static water contact angle (WCA) measurement, atomic force microscopy (AFM) and X-ray photoelectron (XPS). Next, ageing, cell tests and pull-out tests are performed to further verify the influence of surface modification for five selected plasma activation conditions.

2 MATERIALS AND METHODS

2.1 Experimental set-up
Plasma is generated at atmospheric pressure within a quartz capillary, which has an inside and outside diameter of 1.3 and 3.0 mm and serves as a dielectric barrier. The needle (tungsten wire) within the quartz capillary is connected to a high voltage source and represents the high voltage electrode. Plasma is created by applying an AC high voltage, with a fixed frequency of 27 KHz to the high voltage electrode; it has a diameter of 0.5 mm and a half-sphere-shaped tip. The average discharge power for a voltage of 4 kV and a flow of 2 l/min is 1.60 $\pm$0.02 W and for a voltage of 5 kV and a flow of 0.75 l/min, this is equal to 2.62 $\pm$0.08 W. The ring electrode surrounding the quartz capillary is grounded and has a height of 10 mm. It is placed at a distance of 35 mm from the high voltage electrode and 20 mm from the lower edge of the capillary. Bronckhorst EL-flow gas flow controllers regulate the Ar gas feed. UHMWPE samples are modified by scanning the surface using a CNC portal milling machine PF 600 P from BZT (Germany), the jet is programmed to scan the whole

sample area using WINPC-NC software. The UHMWPE samples are placed 20 mm from the lower end of the capillary. Variable parameters include treatment time [0.13, 6 s], scan repetition [1, 45], jet velocity (50, 150 or 450 mm/min), gas feed (0.75 or 2 l/min) and applied power (1.60 or 2.62 W). Figure 1 gives a schematic overview of the plasma jet configuration.

UHMWPE-film with a thickness of 0.50 mm is purchased from GoodFellow (England). With regard to the pull-out tests, medical grade UHMWPE blocks (Quadrant, Belgium) are used, which are 30 mm in length, 9 mm wide and 4 mm high.
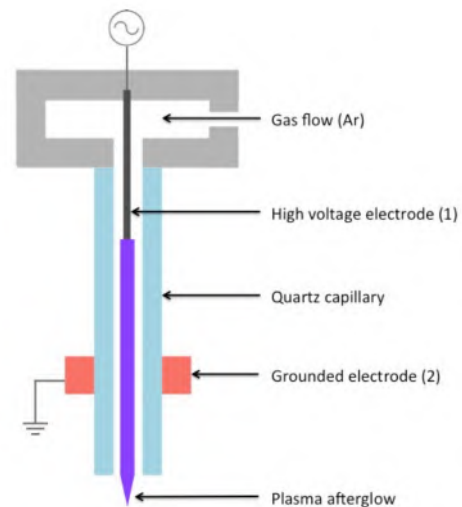

Figure 1. The atmospheric pressure plasma jet configuration used during experiments.

2.2 Surface characterization techniques
Static contact angle measurements are obtained using Easydropp and Drop Shap Analysis (DSA), both acquired from the company Krüss (Germany). The liquid used to deposit the water droplet is deionized water, 1 μl drops are produced at a speed of 150 μl /min. During AFM experiments a cantilever (PPP-NCHR) XE-70 set-up from Park systems (Korea) is used in non-contact mode. The image quality is set on 256x256 with a scan size of 30 μm and a scan rate of 0.3 to 1.0 Hz. The operating software (XEP) and data processing software (XEI) both come from Park systems. XPS surface analysis measurements are performed on a Physical Electronics PHI (United States), 5000 VersaProbe II spectrometer employing a monochromatic Al Kα X-ray source (hυ= 1486.6 eV). Experimental parameters include a pressure lower than 5.10^{-6} Pa, a point measurement of 200 μm, an area measurement of 600 μm x 100 μm and an applied power of 50 W. For the spectrum recordings a survey scan region of 0 to 1100 eV is taken, with a survey pass energy of 187.75 eV. This was done for three points per sample. The detail scan region is set on 20 eV with a detail pass energy of 23.5 eV. The survey scans are processed using PHI MultiPak software (Physical Electronics PHI, United States) and from the peak area ratios, the elemental composition can be determined. PHI

MultiPak is used to curve-fit the high resolution C1s peaks, the calibration point is taken at 285 eV for C-C bond.

2.3 Ageing tests

After plasma treatment, samples are stored for a selected time slot of 4 h, 8 h, 24 h, 7 days and 14 days in vacuum, ambient air of PBS and subsequently the WCA is measured. Additional XPS-measurements are performed after a storage time of 7 days. The temperature of the vacuum oven is programmed at approximately 20 °C. Ambient air treated samples are incubated at 20 °C and a humidity of 50 %, resembling controlled open-air conditions. In order to mimic physiological conditions a 1 liter PBS solution is made using 8.0 g sodium chloride (NaCl), 0.2 g potassium chloride (KCl), 1.42 g di-sodium phosphate (Na_2HPO_4), 0.24 g mono-potassium phosphate (KH_2PO_4), solved in 800 ml of deionized water, supplemented with hydrogen chloride (HCl) to reach a pH of 7.4. The solution is further diluted using deionized water in order to reach a total volume of 1 l. Samples are incubated at 37 °C and after incubation they are washed with deionized water and dried using dry air or N_2.

2.4 Cell tests

Mouse calvaria 3T3 (MC3T3) subclone pre-osteoblast cells are cultured onto UHMPWE samples for 24 h and 7 days regarding adhesion and proliferation tests. For the adhesion tests a cell amount of 100 000 cells/well is seeded and after 24 h visual inspection and quantitative measurements are conducted. Regarding proliferation a cell amount of 40 000 cells/well are seeded and measurements are conducted at day 1 and day 7. Cell morphology, viability and density are assessed by a LIVE/DEAD cell viability assay (duplicates). Each sample is washed two times with 0.5 ml of PBS and incubated in a solution containing 0.5 ml PBS, 2.5 μl calcein AM (Anaspec, United States) and 2.5 μl propidium iodide (PI) (Sigma Aldrich). Quantitative cell viability tests include a CellTiter 96 Aqueous Non-Radioactive Cell Proliferation MTS (3-(4,5-dimethylthiazol-2-yl)-5-(3-carboxymethoxyphenyl)-2-(4-sulfophenyl)-2H tetrazolium) assay and a PrestoBlue assay (triplicates). The MTS assay measures the cellular conversion of the MTS into a soluble formazan dye by mitochondrial NADH/NADPH- dependent de-hydrogenase. Each sample (well) is washed with PBS and a solution containing 0.5 ml of colorless media and 100 μl PMS/MTS mixture (1 μl PMS per 20 μl MTS) is added. After 4 h of incubation at a temperature of 37 °C, 400 μl of the colored compound is taken out and the absorbance is measured with a 490 nm Universal Microplate Reader EL 800 (BioTek Instruments, USA). PrestoBlue (Invitrogen, United States) is a resazurin-based compound, which is converted to its reduced form by mitochondrial enzymes of viable cells. As a consequence of the reduction, the reagent exhibits a shift in its fluorescence. To each well 450 µl culture media is added together with 50 µl PrestoBlue compound. After 1 h incubation at 37 °C, 400 µl of the colored PrestoBlue

solution is taken out and its fluorescence is measured at 535-605 nm.

2.5 Pull-out tests

For this test medical grade UHMWPE (Chirulen 1020, Quadrant, Belgium) is used. In regard to plasma activation, the top and bottom of the medical grade UHMWPE samples are treated. Bone cement is made by mixing 24 g of radiopaque polymer powder (Denture base polymers from Huge Dent, China) and 11 ml of MMA monomer liquid (Huge Dent, China). This results in a bone cement paste that hardens after 20 to 30 minutes. The activated part of the sample is cemented in the mold for a length of about 4 mm. For each of the five activation conditions, 10 samples are prepared and fixed in bone cement right after plasma treatment. Also 10 untreated samples are cemented. Next a universal testing machine LRX plus (Lloyd Instruments, Bognor Regis, UK) is used to perform a uni-axial pull-out test on each sample, with a fixed moving speed of 2 mm/min.

3 RESULTS AND DISCUSSION

3.1 Surface characterization

Surface characterization examines the effect of plasma activation with regard to surface alterations. Three tests are performed to study this surface modification: WCA measurement, AFM and XPS. Measuring the WCA of a droplet on a surface gives a fast and basic idea on surface hydrophilicity. By gradually increasing treatment time and keeping flow and power fixed (2 l/min and 1.60 W) for three different jet velocities (50, 150 and 450 mm/min), an exponential decrease in WCA is seen, which reaches a plateau value of approximately 47° after 3.6 s for all three velocities. Further treatment does no longer influence the measured WCA as is seen in Figure 2. These saturation points are labelled Saturation 1 (450 mm/min), Saturation 2 (150 mm/min) and Saturation 3 (50 mm/min). Tamada et al. suggest that cell adhesion is best on PE plasma modified surfaces with a measured contact angle of 70° [12]. In order to obtain a surface modification that corresponds more to these findings, the same configuration is taken (same gas flow and power), but the treatment time is set much shorter. This condition is referred to as Condition B. Literature also suggest that too much oxygen can lead to the production of free radicals, which are highly reactive towards vital molecules like DNA and proteins, leading to cell lysis [13]. In an attempt to find a contact angle even lower than the Saturation point, the fixed configuration (gas flow and power) is adjusted as literature states that a lower flow and a higher power lead to more reactive particles and so a more pronounced surface modification [14]. By applying 2.62 W instead of 1.60 W and by using a gas flow of 0.75 l/min instead of 2 l/min, the WCA decreases from 87° to 25.5°. The treatment time and jet velocity is taken at 3.6 s and 50 mm/min. This condition is labelled Condition F. Hereby five different plasma activation conditions are selected, Table 1 gives a final overview. It is known that plasma activation can lead to surface etching, which might smoothen or roughen the

surface [7]. When looking at the root mean square surface roughness (Rq) of untreated and plasma activated UHMWPE surface (Table 1), no significant difference is seen and so surface etching can be neglected regarding this set-up. This corresponds to literature as Wang et al. already reported that the hydrophilic effect of remote Ar plasma enhances radical reactions and restrain electron and ion etching effects [15]. In order to see how different plasma activation conditions influence surface chemistry, treated samples are analyzed using XPS. Table 2 expresses the ratio of the relative percentages of carbon and oxygen. As expected Condition B has an oxygen concentration that is much smaller compared to Saturation 1 (C/O ratio of 0.26 and 0.42), as the treatment time is 14 times shorter. Lower treatment times thus result in a lower oxygen concentration. This also corresponds with the WCA measurements. The oxygen concentration of all three Saturation points is approximately 30 %, this corresponds and explains the results from the WCA measurements, which decrease after plasma treatment. Based on XPS results, a higher power and lower flow, used during Condition F does not affect the amount of oxygen incorporation (no statistical difference between Saturation 3 and Condition F) but

WCA measurements state otherwise, as the measured contact angle does further decrease compared to the Saturation conditions. This conflicting outcome can be due to the fact that when the WCA is measured only the top surface, with a depth of approximately 1 nm is analyzed, while XPS measurements have a analyzing depth of approximately 10 nm [16]. By deconvolving the C1s peaks the relative percentage of functional groups present on the surface is determined (Table 2). It is seen that longer treatment times (Saturation 1 compared to Condition B), lead to equal concentrations of C-O and a statistical increase in O=C-O functionalities ($p < 0.01$). The use of different jet velocities leads to a similar hydrophilicity (similar amounts of oxygen), but different functional group incorporation. Higher jet velocities like Saturation 1 (450 mm/min) compared to Saturation 3 lead to a higher amount of C=O and O-C=O functionalities, with a statistical difference ($p < 0.01$) between Saturation 1 and Saturation 3 regarding O-C=O, a statistical difference ($p < 0.05$) for O=C and no statistical significance regarding relative oxygen percentage. Also between Saturation 2 and Saturation 3 there is a strong statistical difference ($p < 0.01$) in O-C=O functionalities.
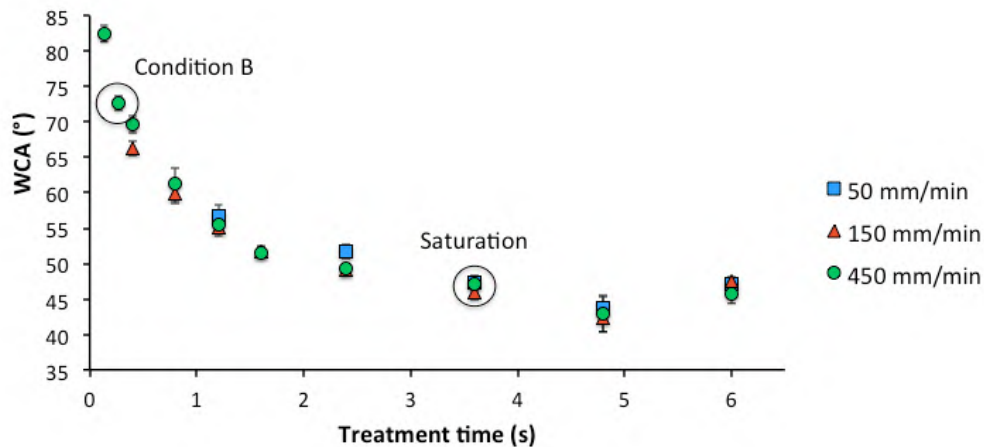

Figure 2. WCA measurements during different treatment times for three types of jet velocities, using a power of 1.6 W and a gas flow of 2 l/min.

Table 1. The different parameters of the selected plasma treatments and the WCA and Rq value for untreated and treated samples.

Label	Jet velocity (mm/min)	Treatment time (s)	Flow (l/min)	Power (W)	WCA (°)	Rq (nm)
Untreated					87.0	139 ±8
Saturation 1	450	3.6	2	1.60	47.1	145 ±22
Saturation 2	150	3.6	2	1.60	46.0	142 ±34
Saturation 3	50	3.6	2	1.60	47.3	140 ±27
Condition B	450	0.27	2	1.60	72.6	124 ±19
Condition F	50	3.6	0.75	2.62	25.5	133 ±27

Table 2. The ratio of the relative carbon oxygen concentration and the relative percentage of functional groups present on the surface for each plasma activation condition.

Label	C/O ratio	C – C %	C – O %	C = O %	O – C = O %
Saturation 1	0.43 ±0.03	63.2 ±2.4	14.2 ±3.7	10.0 ±2.1	12.6 ± 1.2
Saturation 2	0.41 ±0.03	62.3 ±4.9	17.2 ±5.8	8.0 ±1.5	12.5 ±1.0
Saturation 3	0.40 ±0.02	65.9 ±6.4	18.5 ±7.8	6.4 ±1.6	9.1 ±1.2
Condition B	0.26 ±0.03	72.6 ±3.1	14.0 ±3.5	8.4 ±0.9	5.0 ±0.6
Condition F	0.42 ±0.02	62.0 ±3.7	20.5 ±5.4	8.0 ±2.2	9.5 ±0.8

3.2 Ageing tests

Ageing of plasma-treated polymers has been investigated by several researchers as chemical changes induced by plasma activation are often found to be either partially or totally reversible as time increases. Williams et al. indicate two main events that take place, (i) post-treatment chemical reactions and (ii) surface relaxation [16]. During this ageing experiment treated samples are stored for a selected time slot of 4 h, 8 h, 24 h, 7 days and 14 days in vacuum air or PBS and subsequently the WCA is measured. For each plasma activation condition a relaxation plateau value is reached after approximately 24 h. The loss in treatment efficiency L (%) during storage up to 14 days is calculated using the following equation [17]:

$$L = 100 \cdot \frac{\vartheta_{s1} - \vartheta_{s2}}{\vartheta_{s1} - \vartheta_{untreated}} \qquad (1)$$

Where ϑ_{s1} is the saturation value of the WCA after plasma treatment, ϑ_{s2} is the plateau value of the WCA after 14 days of storage (average WCA from day 1 till day 14) and $\vartheta_{untreated}$ is the WCA value of the untreated material, which in this case is equal to 87°. Table 3 shows the plateau values and treatment efficiencies of all five conditions. Ageing as a function of time shows that after plasma treatment the WCA quickly increases during the first hours of storage, except for Condition B, here the increase is minimal. Hydrophobic recovery of treated UHMWPE is most pronounced for Saturation 3 and less apparent for Condition B for both vacuum and air. In order to see how ageing influences the chemical composition of an activated UHMWPE surface XPS measurements are performed after 7 days of storage in vacuum, air and PBS. XPS-results show that there is a decrease of oxygen concentration for all environments. The decrease is most pronounced in the PBS-environment and lowest in vacuum. Based on the XPS-results it is possible to say that double bonds like in C=O and O-C=O functionalities are more stable regarding ageing in vacuum and air than single bond C-O, as functional reorganization is much more pronounced for the latter. From XPS data measured at day zero it is concluded that higher jet velocities like Saturation 1 contain more of these double bonds, compared to Saturation 3, what might explain the fact that hydrophobic recovery is much more pronounced for Saturation 3.

3.3 Cell tests

Based on fluorescent images, cell adhesion regarding plasma activated UHMWPE shows better cell morphology, viability and density compared to untreated UHMWPE, see Figure 3. For this set-up (cell amount > 100 000 cells/well) the MTS assay gives a more reliable outcome compared to PrestoBlue measurements as the latter is too sensitive for this high cell amount. MTS quantification suggests that plasma activation leads to an increase in cell adhesion. Overall plasma activation seems to improve initial biocompatibility of UHMWPE as cell configurations on treated samples indicate sufficient surface adhesion, elongated cell morphology and higher quantitative amounts based on MTS results. When quantifying small cell amounts, like for the proliferation test after 24 h (cell amount > 40 000 cells/well), it is better to use PrestoBlue, as it is much more sensitive towards smaller cell amounts compared to MTS [18]. Visual inspection through fluorescent imaging suggests good cell morphology, density and viability, similar to the positive control, at day 7 of the proliferation test. Quantitative measurements (PrestoBlue) regarding cell proliferation do not show a significant improvement regarding plasma activation of UHMWPE and also no statistical difference regarding different plasma treatment methods is observed. Further tests are needed to draw a clearer conclusion regarding visual inspection and quantitative measurements.
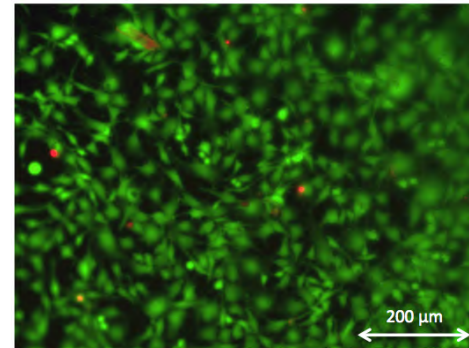

Figure 3. Fluorescence images of MC3T3 cells after 7 days in culture regarding proliferation test. Green indicates living cells, red indicates dead cells. The image presented is Saturation 1.

Table 3. Ageing of plasma activated samples. In the table ϑ_{s1} is the saturation value of the WCA after plasma treatment, ϑ_{s2} is the plateau value of the WCA after 14 days of storage in either vacuum or air, L_{vacuum} and L_{air} indicate the loss in treatment efficiency L (%) during storage up to 14 days.

Label	ϑ_{s1}	$\vartheta_{s2-Vacuum}$	ϑ_{s2-Air}	L_{Vacuum}	L_{Air}
Saturation 1	47.5	52.9 ±3.9	54.2 ±2.2	14 ±10	17 ± 6
Saturation 2	46.5	51.9 ±0.9	55.2 ±1.0	13 ±2	21 ±3
Saturation 3	45.0	52.5 ±2.9	57.4 ±4.2	18 ±7	30 ±10
Condition B	68.6	69.8 ±1.3	69.6 ±0.3	7 ±7	6 ±2
Condition F	25.5	33.3 ±2.0	37.8 ±0.8	13 ±3	20 ±1

3.4   Pull-out tests

A glenoid prosthesis is made out of medical grade UHMWPE, which is a linear homo-polymer, making it non-polar. Bone cement (PMMA), which is used in regard to prosthesis fixation, is more polar and contains ester-functionalities. By the use of plasma surface modification the amount of oxygen functionalities increases and when this oxygen-rich surface comes in contact with PMMA, which also contains oxygen (ester) functionalities, an increase in intermolecular forces (mainly Van der Waals forces) improves surface adhesion, leading to better component fixation. In order to assess the effect of plasma treatment regarding adhesion of UHMWPE and bone cement (PMMA), pull-out test are performed. During pull-out tests the maximal force needed to pull the UHMWPE samples out of bone cement is measured. By normalizing this value over the measured contact area, the pull-out stress is determined. The mean stress needed to pull the sample out of the bone cement is about 0.11 MPa for an untreated sample and between 0.31 and 0.97 MPa for the plasma activated samples. The mean pull-out stress thus clearly increases after plasma treatment. Figure 4 displays these values and indicates a statistical significant difference ($p < 0.05$) regarding (all) treated versus untreated samples. In order to give a good overview only Condition B and Untreated is marked as significantly different on this figure. So even for a plasma treatment time of only 0.27 s (Condition B), a significant increase in pull-out stress is obtained. Increasing treatment time (Condition B versus Saturation 1), leads to a significant increase ($p < 0.01$) in pull-out stress. This correlates to the significant increase ($p < 0.01$) in oxygen concentrations between both conditions. There is also a significant difference ($p < 0.05$) between the pull-out stress of Saturation 1 and Saturation 3. As said before, higher carboxyl-functionalities lead to greater Van der Waals interaction and thus better surface adhesion towards PMMA. Higher jet velocities (450 mm/min compared to 50 mm/min) during plasma activation results in an equal amount of oxygen concentrations but a statistical higher amount of

carboxyl-functionalities which leads to this significant increase in pull-out stress regarding higher jet velocities.

4   CONCLUSION

The aim of this master thesis was to improve the adhesion properties of an UHMWPE glenoid component towards bone cement (PMMA) and bone by looking at the influence of different plasma activation parameters like treatment time, jet velocity, gas flow and power. By using an atmospheric pressure plasma jet, selected regions can be modified under normal ambient pressure. Plasma activation using Ar results in an increase in surface hydrophilicity by incorporation of oxygen containing functional groups and does not significantly affect surface roughness. Longer treatment times lead to more incorporation of C=O and O-C=O and have overall a higher relative amount of oxygen present on the surface. Even for a short treatment time, the pull-out stress is significantly increased compared to untreated UHMWPE. Different jet velocities at equal treatment time lead to the same oxygen concentration but different types of functional groups are incorporated. Faster jet movements have a statistical higher amount of C=O and O-C=O functionalities, slower movements seem to have more C-O functionalities. This is reflected in the pull-out tests as faster jet velocities have a higher mean pull-out stress, due to increased adhesion towards PMMA which contains ester functionalities. A higher power and a smaller flow result in a further decrease of the WCA but the overall amount of oxygen based on XPS results is not further influenced, also no difference in pull-out stress is observed. Based on cell morphology, plasma activation seems to have a positive effect on cell adhesion and proliferation, which should benefit anatomical integration of the glenoid component. However, plasma activation is a transient type of surface modification as hydrophobic recovery will take place. Storage of plasma-treated UHMWPE in vacuum, air or PBS modifies the surface chemistry and wettability. During WCA and XPS measurements it was seen that the oxygen concentration decreased for all environments. Faster jet movements have a statistical higher amount of C=O and O-C=O
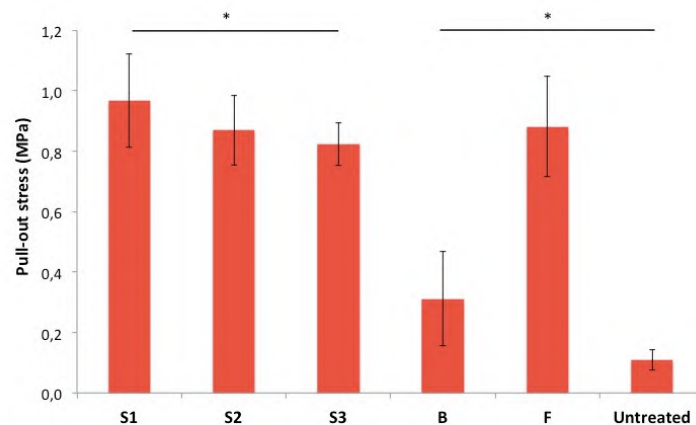

Figure 4. Pull-out stress for the plasma activated and untreated UHMWPE samples, with a statistical difference between Saturation 1 and 3. All treated samples have a pull-out stress that is significant higher than the pull-out stress of the untreated sample. This figure only displays the statistical difference regarding Untreated and Condition B.

functionalities, slower movements seem to have higher C-O functionalities. In respect to ageing these double bonds lead to a more stable configuration and therefore hydrophobic recovery was less profound for fast jet velocities.

It is obvious that TSA glenoid fixation using bone cement can benefit from plasma activation and might tackle current complications leading to an improved performance.

5   ACKNOWLEDGEMENTS

6   REFERENCES

1.   Bohsali, K.I., M.A. Wirth, and C.A. Rockwood, Jr., *Complications of total shoulder arthroplasty.* J Bone Joint Surg Am, 2006. **88**(10): p. 2279-92.

2.   Day, J.S., et al., *Prevalence and projections of total shoulder and elbow arthroplasty in the United States to 2015.* J Shoulder Elbow Surg, 2010. **19**(8): p. 1115-20.

3.   Kaback, L., A. Green, and T. Blaine, *Glenohumeral arthritis and total shoulder replacement.* Medicine and Health, 2012. **95**(4): p. 120-4.

4.   Chillemi, C. and V. Franceschini, *Shoulder osteoarthritis.* Arthritis, 2013. **2013**: p. 1-7.

5.   Young, A.A. and G. Walch, *Fixation of the glenoid component in total shoulder arthroplasty: what is modern cementing technique?* J Shoulder Elbow Surg, 2010. **19**(8): p. 1129-36.

6.   Schrumpf, M., et al., *The glenoid in total shoulder arthroplasty.* Curr Rev Musculoskelet Med, 2011. **4**(4): p. 191-9.

7.   Cools, P., et al., *The use of DBD plasma treatment and polymerization for the enhancement of biomedical UHMWPE.* Thin Solid Films, 2014. **572**: p. 251-259.

8.   Desmet, T., et al., *Nonthermal plasma technology as a versatile strategy for polymeric biomaterials surface modification: A review.* Bio-macromolecules, 2009. **10**(9): p. 2351-69.

9.   Strobel, M., C.S. Lyons, and K.L. Mittal, *Plasma surface modification of polymers: relevance to adhesion*, ed. VSP. 1994.

10.   Chu, P.K., et al., *Plasma-surface modification of biomaterials.* Materials science and engineering, 2002. **36**: p. 143-206.

11.   Yoshida, S., et al., *Surface modification of polymers by plasma treatments for the enhancement of biocompatibility and controlled drug release.* Surface and Coatings Technology, 2013. **233**: p. 99-107.

12.   Tamada, Y. and Y. Ikada, *Cell adhesion to plasma-treated polymer surfaces.* Polymer, 1992. **34**(10): p. 2208-12.

13.   Stern, V. *The oxygen dilemma: Can to much O2 kill?* Mind 2008.

14.   Van Deynse, A., et al., *Surface activation of polyethylene with an argon atmospheric pressure plasma jet: Influence of applied power and flow rate.* Applied Surface Science, 2014. **328**: p. 269-78.

15.   Chen, W., C. Jie-rong, and L. Ru, *Studies on surface modification of poly(tetrafluoroethylene) film by remote and direct Ar plasma.* Applied Surface Science, 2008. **254**(9): p. 2882-88.

16.   Williams, R.L., D.J. Wilson, and N.P. Rhodes, *Stability of plasma-treated silicone rubber and its influence on the interfacial aspects of blood compatibility.* Biomaterials, 2004. **25**(19): p. 4659-73.

17.   Van Deynse, A., et al., *Surface modification of polyethylene in an argon atmospheric pressure plasma jet.* Surface and Coatings Technology, 2015. **276**: p. 384-90.

18.   Invitrogen, *PrestoBlue Cell Viability Reagent*, in *Documentation*, Thermofisher, Editor. 2012.

Contents

Abbreviations

TSA	Total shoulder arthroplasty
MMA	Methyl methacrylate
PMMA	Poly(methyl methacrylate)
PE	Polyethylene
UHMWPE	Ultra high molecular weight polyethylene
DBD	Dielectric barrier discharge
Ar	Argon
He	Helium
N_2	Nitrogen
WCA	Water contact angle
AFM	Atomic force microscopy
XPS	X-ray photoelectron spectroscopy

Chapter 1

Total shoulder replacement

1.1 Introduction

The shoulder is located between the neck and the upper arm and is one of the largest and most complex joints in the body. The gleno-humeral joint is indicated as a ball and socket configuration. It consists of a humeral head and a glenoid, which corresponds to a smooth cartilage surface. In contrast to other joints the gleno-humeral joint has very little skeletal stability and depends upon the surrounding soft tissue (muscles, tendons, labrum, capsule) [1]. This group of muscles and tendons visualized in Figure 1.1 stabilizes the shoulder and connects the humerus to the scapula, they are called the rotator cuff. The muscles allow the shoulder to rotate and the tendons provide stability to the shoulder. It is the rotator cuff that ensures active containment of the humeral head into the glenoid vault, which is indicated in Figure 1.2 [2]. Each muscle of the rotator cuff inserts at the scapula and has a tendon that attaches to the humerus.

Total shoulder arthroplasty (TSA) indicates a total shoulder joint replacement by means of a prosthesis. In the period of 1880 to 1890 a German physician called Themistocles Gluck performed the first shoulder joint replacement on a living human being using an ivory prosthesis, but unfortunately he never published any results. A few years later another pioneer called Julés-Emile Péan implanted an artificial shoulder made of platinum [5]. Péan performed a shoulder joint replacement after he removed tuberculous arthritis from the shoulder of a 37-year old baker. Despite good results the shoulder got infected, which led to the removal of the prosthesis only 2 years later [6]. In 1955, a next step was made towards TSA, Charles Neer reported that 11 out of 12 patients with proximal humerus arthroplasty were free from pain after placement of a vitallium prosthesis [7]. He developed the first generation shoulder implants, which is called "the monoblock shoulder implant", indicating that the prosthesis consists out of a single piece [8]. It contains a smooth humeral component, which was initially fixated using poly (methyl methacrylate) (PMMA) [8]. This type of replacement is now called
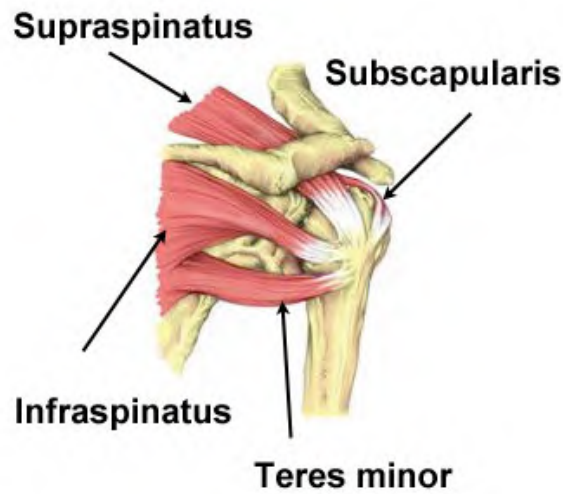
Figure 1.1: Muscles of the rotator cuff [3].
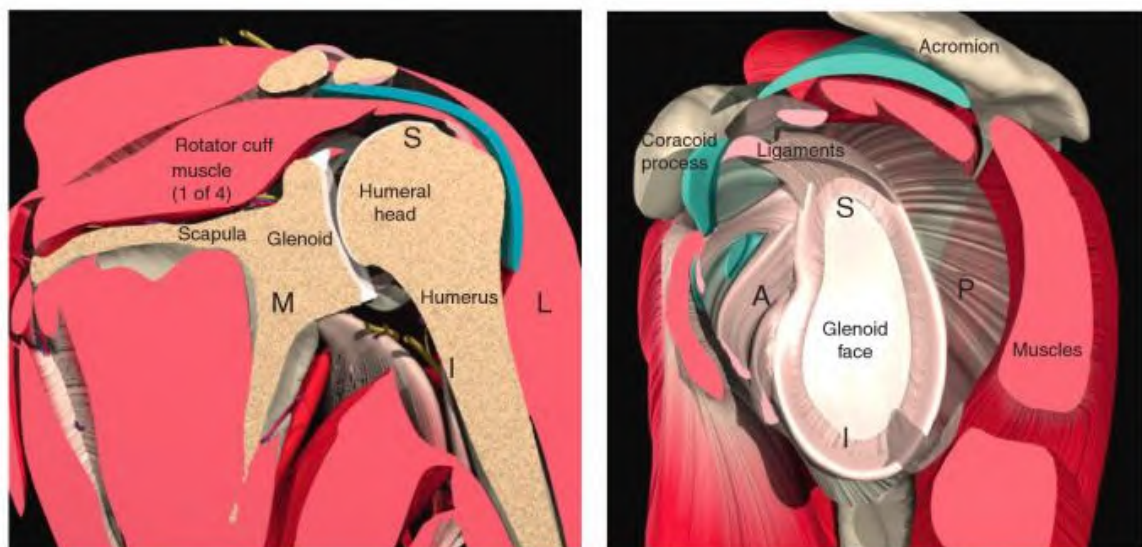
Figure 1.2: Anatomy of a healthy shoulder joint. On the left an anterior view of the shoulder, on the right a lateral perspective of the joint [4].

hemi-arthroplasty, as only the humeral component is replaced. In 1972, Neer added a glenoid part to improve results for patients with an inadequate glenoid, leading to what we now know as TSA [9]. A second generation shoulder implants was named "the modular prosthesis", where the prosthesis consists out of a modular head and a stem covered with ingrowth coating. The fact that the head and the stem became separate parts allows the selection of the ideal head size for each particular patient [8]. Later in the 70s, surgeons experienced difficulties regarding the development of a satisfactory prosthesis for glenoid-humeral arthroplasty

in terms of joint stability and range of motion. Research validated the stabilizing role of the rotator cuff and showed that the loss of these stabilizers can lead to additional forces on the implant and surrounding tissue [10]. It became clear that patients with a deficient rotator cuff only had a limited range of motion after surgery, indicating that the muscles of the shoulder were unable to act in the absence of a stabilizing force. This led to a new type of prosthesis which diverges from anatomy [11]. In 1987, Grammont and Baulot designed a semi-constrained reverse shoulder prosthesis. Later in time this design would be called "the reversed shoulder" [4]. Around the year 1999 a third generation of shoulder implants was developed, which is referred to as the "anatomical" generation due to the fact that they have increased similarities with the actual anatomical shoulder. Depending on the design used, the components allow adjustment of the prosthetic humeral head position. Some implants also allow various degrees of head inclination [8, 12]. Nowadays, two main types of shoulder prosthesises exist. The first type is the anatomic prosthesis, which is mainly used when the rotator cuff is balanced. When the rotator cuff is unstable, reversed shoulder arthroplasty is proven to be superior.

1.2 Clinical manifestation

Just like other total joint arthroplasties, the frequency of TSA increases every year. In the United States a 319 % increase in the procedure rate has been seen from 1993 to 2007, corresponding to an annual growth of 10.6 % [13, 14]. In total, two thirds of all shoulder replacements are performed on people older than 65 and approximately two thirds of all TSAs are carried out on females [1]. Indications regarding shoulder arthroplasty include severe proximal humerus fractures, gleno-humeral osteoarthritis, post-traumatic arthritis, rotator cuff arthroplasty, avascular necrosis, capsulorrhaphy arthropathy, inflammatory arthritis and a failed previous shoulder arthroplasty. However, the most common indication regarding TSA is symptomatic osteoarthritis of the gleno-humeral joint [1].

Osteoarthritis of the shoulder affects up to 32.8 % of the population over the age of sixty [15]. Shoulder osteoarthritis is a non-inflammatory arthritis and is the consequence of destruction of the articular surface of the humeral head and glenoid surface, which results in pain and loss of function [15]. It typically starts on the posterior side of the glenoid and central part of the humeral head with osteophytes present around the neck of the humerus [1]. Osteoarthritis leads to subchondral sclerosis and capsular contractures and eventually results in loss of motion and a painful shoulder joint. There is a distinction between primary and secondary osteoarthritis. Primary osteoarthritis is diagnosed when there are no provoking factors that can lead to this joint malfunction. Secondary osteoarthritis on the other hand occurs as a result of chronic dislocations and recurrent instability, trauma, surgery, avascular

necrosis, inflammatory arthropathy and massive rotator cuff tears [15]. Generally, the rotator cuff remain intact in 95 % of the cases [16]. Treatment of shoulder osteoarthritis is based on the patient's age, severity of the symptoms, level of activity and radiographic findings. Non-operative treatments include activity modification, physical therapy, anti-inflammatory drugs and intra-articular injections. Only if these non-surgical options fail, total shoulder joint arthroplasty is defined as the most effective treatment regarding pain relief and improved function [15]. Patients are diagnosed by a thorough history and physical examination. It is seen that for gleno-humeral osteoarthritis patients, only limited arm elevation is possible. Standard X-ray views are taken to assess gleno-humeral arthritis, from an anterior-posterior and axillary-lateral view [1]. In the case of gleno-humeral osteoarthritis this shows a decreased gleno-humeral joint space, osteophytes, subluxation and bony deformation. Figure 1.3 shows an anterior-posterior view of a left shoulder with advanced gleno-humeral arthritis, indicating the space narrowing and the inferior humeral neck osteophytes. When the integrity of the rotator cuff is uncertain, advanced imaging is required, like Magnetic Resonance Imaging (MRI) or a Computed Tomography (CT) arthrogram. The state of the rotator cuff can be assessed by looking at atrophy and fatty degeneration on these images. Also elevation of the humeral head relative to the glenoid and narrowing of the acromiohumeral space is seen with advanced gleno-humeral osteoarthritis [1]. Before surgery takes place an additional CT scan can be obtained to evaluate the anatomy of the glenoid, bony erosion and wear.

Figure 1.3: Anterior-posterior view of a left shoulder with advanced gleno-humeral osteoarthritis. The solid arrow indicates the space narrowing and the blank arrow points to the inferior humeral neck osteophytes [1].

1.3   Anatomic total shoulder arthroplasty

Anatomic TSA has become the golden standard for treating advanced shoulder osteoarthritis with an intact and functioning rotator cuff after failure of non-operative actions [15]. This

type of prosthesis is also indicated in cases of rheumatoid arthritis, avascular necrosis and post-traumatic arthritis. In this set-up, rotator cuff tears can lead to early implant glenoid loosening and failure. An absolute contraindication regarding the anatomic total shoulder prosthesis is active infection. The goal of this prosthesis is to restore normal bony anatomy and shoulder kinematics by aligning the centre of rotation, which is located at the humeral side and the spinning centre located at the glenoid side, as shown in Figure 1.4 [2].

Figure 1.4: The upper red dots represent the spinning centre at the glenoid side and the lower dots indicate the centre of rotation at the humeral side. The picture on the left shows a non-aligned, diseased shoulder joint. The figure on the right visualizes the restored shoulder by means of an anatomic shoulder prosthesis [2].

During surgery the superior end of the humerus is replaced by a metallic stem that ends in a round ball. Additionally, the glenoid plane is restored by placing a polyethylene (PE) prosthetic compartment. A CT image of an anatomic total shoulder prosthesis is presented in Figure 1.5. Over 95 % of patients will achieve pain relieve and improvement in range of motion and function [1]. However, these benefits come with the risk of glenoid loosening, in particular for younger, more active patients. The overall survival regarding a total shoulder prosthesis is 90 % at 10 years, long-term survival of the glenoid component is a concern as the outcome of glenoid revision is not as promising as a primary TSA [15, 17]. Success rates have been reported to be lower for patients of an age of 50 years and younger [18].

Humeral component

During total shoulder replacement the arthritic boney structure of the upper end of the arm is replaced by a metal ball containing a stem that is placed in the inside of the upper arm bone, namely the humerus. Only the smooth surface of the ball extends from the bone. The stem is usually made of titanium (Ti) or a cobalt-chromium (CoCr) alloy. Fixation of the humeral component is mainly achieved by cement fixation using PMMA and sometimes also through press-fit fixation. When press-fitting is used as a fixation method the stem is porously coated to enhance attachment to the bone, as irregular surfaces allow better bone in-growth [19]. The biggest advantage of this method is that when the prosthesis loosens, revision is more easily performed and bone loss is minimal compared to cement fixation. The disadvantages of this method include the fact that bone ingrowth requires much more time than cement fixation, it
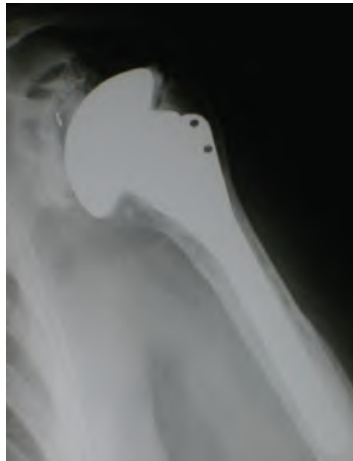
Figure 1.5: An anatomic total shoulder prosthesis [15].

requires faultless positioning and a sufficient bone stock. The method of press-fit fixation is mostly used in younger patients. As most patients are older and therefore have a lower bone density, cement fixation is often the method of choice [18]. In this case, a non-coated stem prosthesis is used. Cementation allows a perfect fit and post-operative stability. The main contraindication is the fact that when the prosthesis loosens, the cement can grind away bone, leading to an adverse condition for revision surgery [13]. Also heat from the bone cement can damage anatomical structures during placement of the prothesis. Even though cement-less stems have the potential to shorten operative time and simplify revision procedures, evidence suggests that cemented stems provide better quality of life, strength and range of motion after two years of implantation [20, 21].

During the late 1980s, a modular humeral component was suggested, as it adds the flexibility of combining multiple head diameters and heights with multiple stem sizes. In this set-up the head and stem are connected by a Morse taper. However, Churchill et al. indicated that this modularity might not contribute to a more successful outcome regarding shoulder arthroplasty for gleno-humeral osteoarthritis [22]. Schoch et al. compared the modular TSA (the second generation) with the monoblock TSA (first generation) and the anatomic TSA (third generation) and indicate that the anatomic TSA continues to provide improvements in pain and range of motion regarding osteoarthritis. The main advantage of the modular set-up is its possibility to remove a humeral head without having to remove a well-fixed humeral stem. Implant modularity facilitates surgery, but similar outcomes can be expected regardless of modularity [23].

Glenoid component

There are several anatomic parameters relevant regarding the design of a prosthetic glenoid, like glenoid height, width, inclination and shape as these parameters vary from patient to patient. The glenoid component almost always consists out of ultra high molecular weight polyethylene (UHMWPE), which is known for its proper mechanical bulk characteristics [24]. The traditional choice regarding fixation includes a cemented all polymer design, using PMMA. This technique includes lavage and drying of the vault, followed by cement insertion by a syringe and pressurization of the component by mechanical means [25]. Some designs also include a metal-back as presented in Figure 1.6. In this case, the fixation of the glenoid part is done either by using a screw construct or by using press-fit metal pegs [26]. The component, which contains an ingrowth coating, is then mechanically locked into the bone. This leads to a stable fixation but can also result in high wear of the polymer glenoid component, implant loosening, component fracture and dislocation [27, 28]. Component loosening causes osteolysis due to polymer and metal wear debris [29]. It is seen that a cemented PE glenoid has an overall stress pattern that more closely resembles the intact native glenoid, as the non-cemented metal-back glenoid is associated with lower stress in the subchondral glenoid bone, indicating stress shielding [29]. An alternative to these two approaches is the hybrid glenoid. Hybrid fixation is a combination of the two previous forms of fixation, using cement and metal-back fixation. This design combines the benefits of a cemented polymer construct with multiple points of mechanical fixation by press-fit metal pegs, which leads to an even better fixation and higher resistance towards shear forces. Churchill et al. state that the high temperature generated through the exothermic reaction during curing of PMMA cement, equal to 82–86 °C, might be responsible for bone necrosis [26, 30]. So minimal cement fixation can be beneficial, also because this requires less removal of bone in case of a revision [29]. Even though this hybrid method is quite new and prospective studies with long-term follow-up are needed to determine whether the hybrid glenoid provides improved long-term results [28]. One new upcoming technique regarding cementation includes pressurized cementation. Choi et al. compared pressurized with unpressurized cementation and found a significant difference between these two set-ups. During unpressurized cementation the surgeon applies minimal manual pressure on the construct. Pressurized cementation contains a three-step pressurization cementation technique before insertion of the implant. The cement is first pressurized by injecting it into each peg hole. Then a highly polished metal pressuring device is pushed in each hole. Finally, the cement is manually pressurized, followed by placement of the final implant. Pressurized cementation leads to fewer post-operative radiolucent lines compared to unpressurized cementation, which suggests better component fixation, however long-term results are not yet available [31].

Today, there are two main designs of the glenoid component available, namely pegged and

Figure 1.6: An image of an anatomic TSA using a metal-backed glenoid prosthesis [32].

keeled, shown in Figure 1.7. According to Gartsman et al. the keeled component is known to induce much more radiolucent lines, insinuating possible component loosening in 39 % of the cases. For the pegged design only in 5 % of the cases radiolucent lines were observed. Mid-term follow-up demonstrates that a keeled component results in a significantly increased translation and rotation compared to the pegged component [26, 33]. A reason for this can be that the keeled design needs more cementation for sufficient fixation. When looking at the glenoid shape, there are again two main types present, the anatomic and the oval version [26]. They are based on observed anatomical data of the glenoid cavity, which can be variable from person to person. Both types have their advantages. The anatomically shaped glenoid stimulates the normal pear-shaped glenoid. The main characteristic of this component design is that it partially avoids internal impingement of soft tissue on the PE component. The pear shape also reduces the contact surface area but may increase the risk of dislocation [26, 34]. The oval design on the other hand imitates the arthritic glenoid and uses the pathologically enlarged glenoid to maximize articular surface area. This leads to an increased superior wall height and decreases the risk for dislocation [26]. A comparison of the pear and oval shaped native glenoid is provided in Figure 1.8. Also the geometry and curvature of the back of the glenoid component has been studied. There exist a flat-back glenoid design, as is shown in Figure 1.7, and a curved-back model, which is displayed in Figure 1.9. According to a two year follow-up, the curved-back has proven to give optimal component seating in 65 % of the cases, for the flat-backed design this resulted in optimal seating for only 26 % of the cases. Additionally, an increased amount of radiolucencies were seen in these flat-back components, stating the curved-back glenoid to be superior over the flat-back geometry [26].
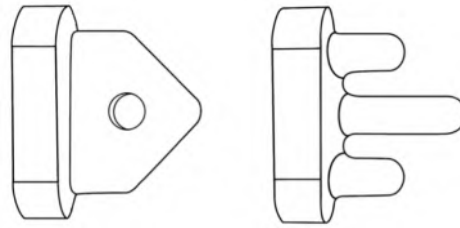
Figure 1.7: Keeled design on the left and pegged design on the right, both designs are flat-backed [35].
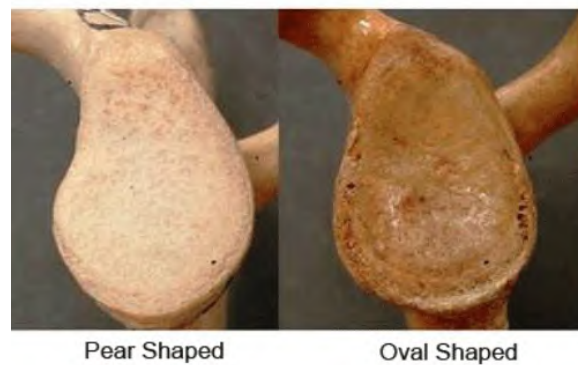
Figure 1.8: Pear and oval shaped native glenoid [36].

Figure 1.9: On the left a pegged curved-back glenoid, on the right a keeled curved-back glenoid [37].

1.4 Other shoulder implants

1.4.1 Reversed total shoulder arthroplasty

A new type of shoulder implant was designed in the 1980s and reversed the normal shoulder anatomy by placing the glenoid socket on the proximal humerus and the prosthetic ball on the glenoid side [6]. In this design, the glenoid has a convex spherical articular surface and the humeral component ends in a PE concave shape, as is shown in Figure 1.10, which represents a CT image of a reversed shoulder prosthesis [8].

Anatomic TSA improves shoulder function by restoring the native gleno-humeral anatomy, demanding that the rotator cuff, which stabilizes the shoulder, is still intact. Reverse shoul-

der arthroplasty, also called constrained TSA, presents an option for patients with cuff tear arthropathy and a cuff-deficient shoulder. This type of prosthesis has only been actively used for about 10 years [13]. The absence of a functional rotator cuff leads to unopposed contraction of the deltoid and results in the displacement of the humeral head in the superior direction, which again leads to a shifted centre of rotation. This then evolves to a state where it is not possible to elevate or abduct the arm, causing pseudoparalysis [38]. Other indications for reverse shoulder arthroplasty are severe inflammatory arthritis with a massive cuff tear, proximal humerus fractures, reconstruction after tumour resection and a previous failed TSA [8]. This reverse system is designed around an instant centre of rotation, which recreates the normal anatomic centre [6]. It is suggested that this reversed design improves motion and strength without the increased risk of dislocation and loosening because of the semi-constrained nature and an improved deltoid lever arm [8]. The reverse total shoulder provides pain relief, improves functional results and reduces the risk of implant failure because of a better primary stability of the glenoid component and due to the medial location of the centre of rotation in respect to its base position [6, 8]. Deltoid integrity is key for a functional reversed TSA as it provides the most power, contributing to restoration of forward elevation and abduction [38]. Adequate glenoid bone stock and quality is necessary for component fixation. Contra-indications also include inadequate infection, neuropathic joint and neurologic deficits.

Figure 1.10: Reversed total shoulder [39].

1.4.2   Hemi-arthroplasty

Patients in an early stage of avascular necrosis and post-traumatic arthritis may have a relative normal glenoid surface and can be treated with a humeral resurfacing implant, or a humeral head replacement also called hemi-arthroplasty [1]. In this case the native glenoid is preserved and only the humeral part is replaced.

Humeral resurfacing

Humeral resurfacing indicates a stem-less humeral head prosthesis where the bone of the humerus supports this artificial head by fitting a metal-alloy cap over the remainder of the head, indicated in Figure 1.11 [15]. Nowadays fixation is mainly accomplished by press-fitting, using a small stem or peggs to aid initial fixation [20]. The main advantage of this design is that it preserves the humeral bone in the event that revision is required [1]. This also leads to shorter operative times and a lower prevalence of humeral peri-prosthetic fractures. In general, this design is indicated for younger, more active patients and some older patients where possible conversion to an alternate prosthesis, possibly reverse shoulder replacement, might be required in the future [1]. Peri-prosthetic fractures, which are a concern for active patients, are less likely to occur here compared to total shoulder replacement because the stem does not pass through the surgical neck. Even though many studies demonstrated the success of this type of arthroplasty on short- and mid-term follow-up, there is a lack of evidence regarding long-term outcome [15].

Figure 1.11: Humeral resurfacing [40].

Humeral head replacement

It is the condition of the glenoid that determines whether humeral head replacement alone can be successful, as during this procedure only the humeral part is replaced and the glenoid part remain [15]. Humeral head replacement can make use of a stemmed humeral implant or a prosthesis that only replaces the humeral head. A stem-less humeral prosthesis is shown in Figure 1.12 and represents the most modern choice. Here, stable fixation is achieved by using a metaphyseal press-fit corolla coated for bony ingrowth [20]. Just like humeral head resurfacing, this technique avoids the replacement of the glenoid component and thereby avoids one of the most complicated parts during surgery, which also post-operatively causes the majority of the problems. However, several studies have proven that total shoulder replacement yields more reliable pain relief compared to humeral head replacement for osteoarthritis where there is minimal involvement of the glenoid [1]. The results of humeral head replacement in

young individuals appear to decline with time and a high rate of patient dissatisfaction and revision surgery remain [32]. Several other studies have confirmed that long-term functional results appear to be compromised by progressive glenoid wear, especially in those individuals with pre-existing asymmetric glenoid erosion [15]. Rotator cuff arthropathy was traditionally treated using hemi-arthroplasty, but the outcomes were very variable which led to the search of an alternative; namely the reversed TSA, as this procedure delivers more predictable and durable results [1].

Figure 1.12: Humeral head replacement, stem-less [41].

1.5 Complications regarding anatomic total shoulder arthroplasty

More than other total joint replacements, TSA is associated with a multitude of complications. Complication rates regarding anatomic TSA range from 10 % to 16 % and include prosthetic loosening on either glenoid and humeral side, gleno-humeral instability, peri-prosthetic fracture, rotator cuff tears, infection, nerve injury and deltoid muscle disfunction [18]. Bohsali et al. indicate that glenoid component loosening accounts for 32 % of all complications regarding anatomic TSA, other causes of failure and their prevalence are noted in Figure 1.13 [13]. The reasons why these arthroplasties often fail is multi-factorial and prolonged follow-up is important in order to assess clinical outcomes, as failure might only appear during mid-term (5- to 10-years) or long-term (over 10 years) follow-up. When looking at constrained TSA, previously described as reversed TSA, complication rates are high according to Bohsali et al. with a mean of 24.4 %. The most common complications regarding the reverse shoulder prosthesis include scapular notching, hematoma formation, glenoid dissociation (like baseplate failure), gleno-humeral dislocation, acromial and/or scapular spine fracture, infection, loosening or dissociation of the humeral component and nerve injury. Sirveaux et al. reported a 4 % short-term revision rate for the reversed shoulder and 8-years post-operatively they found a survival rate of 29.8 % indicating that most complications regarding reverse shoulder arthroplasty only occur during mid- and long-term follow-up [13]. A reversed shoulder is most successful for elderly patients with shoulder arthropathy and clinical pseudoparalysis,

patients must have sufficient bone stock for the implantation of a glenoid component. On the other hand, unconstrained TSA, also known as anatomic TSA, is indicated to be highly successful for the treatment of primary and secondary degenerative shoulders. When comparing the unconstrained shoulder with the constrained shoulder construct, unconstrained shoulder arthroplasty has fewer complications with respect to aseptic loosening, infections and peri-prosthetic fractures. The two most common causes of failure regarding anatomic TSA include component loosening and prosthesis instability [13, 14].

TABLE I Complications Following Unconstrained Total Shoulder Arthroplasties in Studies Reported from 1996 to 2005*			
Complication	No. of Shoulders	Percentage of All Complications	Percentage of All Shoulders
Component loosening	161	39	6.3
Glenoid	134	32	5.3
Humerus	27	6.5	1.1
Instability	124	30	4.9
Superior	77	19	3.0
Posterior	25	6	1.0
Anterior	22	5	0.9
Periprosthetic fracture	46	11	1.8
Intraoperative	27	6.5	1.1
Postoperative	19	4.6	0.7
Rotator cuff tear	32	7.7	1.3
Neural injury	20	4.8	0.8
Infection	19	4.6	0.7
Deltoid detachment	2	0.5	0.08
*Thirty-three series including a total of 2540 shoulders.			

Figure 1.13: A table on the prevalence of different types of complications that occur after anatomic TSA. The study was conducted by Bohsali et al. in 2006 [13].

1.5.1 Component loosening

Humeral component loosening

Aseptic loosening of the humeral component has an overall prevalence of 1 % in regard to anatomic TSA [13]. Humeral component survival is possibly affected by the mode of fixation, press-fit compared to cement fixation. Long-term observation revealed a shift in position of the humeral component of press-fit stems with a prevalence of 49 % indicating cement fixation as the superior fixation technique [42]. Then again, cement fixation might complicate revision. Overall, humeral component loosening is not directly associated with pain.

Glenoid component loosening

Loosening of cemented and uncemented glenoid components is a major problem, affecting long-term survivorship of total shoulder replacement [27]. Overall, the glenoid component of the shoulder implant is much more problematic than the humeral part as the prevalence of glenoid loosening accounts for 32 % of all failures regarding TSA [13]. This complication is

associated with increased pain, decreased shoulder elevation function and the need for revision surgery [29]. The mechanism of glenoid loosening is thought to be multi-factorial and can include aseptic osteolysis, infections, rotator cuff insufficiency and the so-called rocking horse phenomenon [43]. This rocking horse phenomenon is caused by repetitive eccentric loading of the humeral head on the glenoid component. This edge loading produces a torque on the fixation surface and induces tensile stress at the bone-cement-implant interface. Eccentric loading is most commonly caused by incorrect glenoid positioning during surgery and by humeral head migration due to a weak or failing rotator cuff, which destabilises the shoulder joint [29]. Eccentric loading can also be caused by soft tissue instability and incomplete glenoid seating (radial mismatch), which causes misalignment of the centre of rotation and the spinning centre.

There is often a relatively high concentration of radiolucent lines around the glenoid component [44]. The presence of radiolucent lines represents a relatively penetrable X-ray region between the bone and prosthesis interface, suggesting possible component loosening. Iwaki et al. report that linear radiolucent lines appear because of radiopaque cement and a line of sclerosis on the adjacent bone, indicating soft tissue at the interface. The soft tissue presented by radiolucent lines has poor mechanical properties, suggesting a local lack of fixation between bone and implant, enhancing the possibility of relative motion between both parts. Nevertheless, post-operative radiolucent lines lead to a poor prognosis of component loosening. Iwaki et al. state that the presence of radiolucent lines accompanies and promotes loosening but does not necessary cause it [44]. A study conducted by Kwong et al. suggests that radiolucent lines can also occur with well-fixed components and that they commonly represent osteoporosis rather than the presence of a fibrous membrane at the cement-bone interface [45]. Overall, no definite causal relationship between their presence and clinical loosening has been established [13]. Radiographically, a loose glenoid component is characterized by circumferential radiolucent lines of at least 2 mm around the glenoid component, progression of radiolucent lines, cement fragmentation and eventually gross component migration [43].

As an alternative to the cemented glenoid component, the metal-backed glenoid was developed, hoping this would solve the high prevalence of component loosening. General failure rates of an uncemented (metal-back) glenoid component are reported to be higher than those of cemented PE components. On the other hand, overall glenoid loosening is more prevalent in the cemented group [27]. Boileau et al. reported two causes of metal-back glenoid loosening: a mechanical cause, due to the lack of initial stability and a biologic cause, due to osteolysis caused by polymer and metal wear debris [29]. Martin et al. and Boileau et al. have looked into long-term durability of cementless glenoid implants and failure associated with progressive radiolucent lines, osteolysis, tray fracture and screw breakage [19, 46]. After three years of implantation, Boileau et al. reported a significant prevalence of 20 %

of peri-prosthetic radiolucent lines for metal-backed glenoid components [46]. The mid-term (5 to 10 year) results regarding uncemented, metal-backed glenoid components have proven to be unsatisfactory, especially with regard to the higher rate of clinical and radiographic failures. Long-term implantation may amplify issues related to PE wear (as the stiff metal part accelerates PE wear), aseptic loosening and screw breakage. On the other hand, an uncemented prosthesis has the ability to be relatively easily revised to reverse total shoulder prosthesis although glenoid bone loss, due to implant loosening and high wear debris, again increases the difficulty of a revision procedure [13]. An *in vivo* study conducted by Bohsali et al. indicates that the use of a pegged rather than a keeled glenoid component provides a superior mean fixation [13]. The results of a randomized clinical trial involving radiographic comparison of pegged and keeled glenoid components reveal a significantly larger percentage of radiolucent lines around the keeled component (39 %) compared to the pegged design (5 %) [33]. This indicates that the increased technical difficulties of placing a pegged component have potential long-term benefits of fewer radiolucent lines and a lower risk with respect to glenoid loosening. The glenoid component is almost always made out of UHMWPE, which has good load bearing properties, sliding properties, a good impact strength and fatigue resistance. Another material used in regard to the glenoid component is polyetheretherketone (PEEK), which is radiolucent and more closely approximates the modulus of the human cortical bone [47]. For long-term implantation the properties of UHMWPE are compromised by insufficient wear performance, low stiffness and high creep compliance [48]. The combination of irradiation used for sterilization of the component and oxygen exposure leads to a decreased wear resistance and diminished mechanical properties. This results in the formation of wear debris *in vivo*, which cause osteolysis. Small UHMWPE debris particles can activate macrophages as they are phagocytable and therefore biologically active. The exact immune reaction that occurs in peri-prosthetic osteolysis is still unclear [49]. UHMWPE is bio-inert, meaning it does initially not initiate a response or interact when introduced to biological tissue, making it biocompatible. Nevertheless, one must keep in mind that UHMWPE is a hydrophobic "waxy" synthetic polymer, while our body mostly consist out of water and is therefore more hydrophilic, which results in a non-ideal cell-surface match. This inert, non-polar material has therefore low adhesive binding properties also in regard to bone cement [50].

Failed glenoid components can be revised with a new component as long as there is a sufficient amount of glenoid bone stock. Otherwise, revision in the form of hemi-arthroplasty with bone grafting of the glenoid is the only solution, leading to a less satisfying result when compared to glenoid re-implanting [8, 29]. After removal of the loose component, it is important to remove all bone cement present, causing as little damage possible to the surrounding bone. This is followed by the removal of fibrous tissue and exposing healthy subchondral bone [43]. Recently, the reversed total shoulder prosthesis has been used to address the problem of glenoid loosening, particularly when rotator cuff tears and large glenoid bone deficiencies are

present. A reversed prosthesis provides stable fixation of the underlying bone graft with the glenoid baseplate and screws, but this revision technique is also associated with a significant amount of complications and unknown long-term result [43].

1.5.2   Prosthesis instability

The incidence of instability after an anatomic TSA is estimated to be 5 %, making it the second leading cause of complications associated with anatomic total shoulder replacement, accounting for 30 % of all complications [8]. Most instability cases are the result of the combination of poor component positioning and soft tissue imbalance, unable to withstand loading conditions. Moderate loads are counteracted by the deltoid muscle and rotator cuff while larger loads are counterbalanced by capsulolabral structures and bony structures. Anterior and superior instability accounts for 80 % of all instability cases after anatomic TSA. Anterior instability is usually associated with subscapularis deficiency as there is a tear in the subscapularis tendon [8]. Superior instability on the other hand is often reported in association with deficiency of the rotator cuff or the coracoacromial arch. A shoulder with superior instability has a force-couple imbalance between the rotator cuff and the deltoid, which can lead to eccentric forces on the glenoid component, causing the rocking horse phenomenon, accelerated wear and eventual loosening of the glenoid component. Posterior instability is probably caused by multiple factors, including posterior glenoid erosion and soft tissue imbalance. This type of instability usually requires component revision, lengthening of the anterior soft tissue structures and re-tensioning of the posterior capsule and rotator cuff. Inferior instability commonly results from failure in restoring the humeral length when replacement is performed for a proximal humeral fracture or a tumour. Currently, most surgeons favour revising the unstable shoulder arthroplasty to a reverse arthroplasty, making it more constrained [8, 13].

1.6   Conclusion

Anatomic total shoulder arthroplasty is a complex and fast increasing type of total joint replacement. The main problem regarding this type of prosthesis is glenoid component loosening. The cause of this can be multi-factorial and is subdivided in two main categories. On one side, there is incorrect placement of the component, causing eccentric loading of the glenoid. On the other hand, glenoid loosening can be caused by insufficient component fixation as the adhesion properties of bone cement and UHMWPE, out of which the glenoid implant is made, are not optimal. By modifying the surface of UHMWPE it is however possible to increase these adhesion properties, which may lead to increased glenoid fixation. The next chapter will explain the basics of plasma technology and how it is possible to alter the surface chemistry of UHMWPE using this technology.

Chapter 2

Plasma surface treatment

2.1 Introduction

UHMWPE is a biomaterial widely used in joint replacement grafts such as hip, knee and shoulder prosthetics. Approximately one million UHMWPE components are implanted yearly worldwide [24]. It combines initial superior wear resistance and chemical inertness with high fracture toughness and biocompatibility compared to other polymers. It is said that UHMWPE has sufficient bulk properties but non-optimal surface characteristics. A major factor responsible for the failure of UHMWPE in joint replacements is oxidative degradation, which leads to decreased mechanical properties and wear. It is suggested that incorporation of vitamin E into UHMWPE could decrease oxidation and therefore increase prosthesis lifetime [49]. Highly cross-linked UHMWPE has shown dramatic reduction in wear and improved long-term survivorship in total hip replacements [4]. When looking at shoulder joint arthroplasty the major cause of failing is loosening of the UHMWPE glenoid component. Also for this problem, several techniques have been suggested to improve surface adhesion and increase component fixation.

2.1.1 Ultra high molecular weight polyethylene

UHMWPE is a linear homo-polymer with a fairly easy chemical composition, consisting only out of hydrogen and carbon. PE is a polymer formed from ethylene, which has a molecular weight of 28 g/mol, its chemical structure is visualised in Figure 2.1. The mechanical behaviour of PE is related to its average molecular weight. Low-density PE is branched and has a molecular weight of less than 50 000 g/mol. High-density PE is a linear polymer without side branches and has a molecular weight of approximately 20 000 g/mol. Finally, UHMWPE has a molecular weight of over 6 000 000 g/mol, resulting in more abrasion- and wear-resistance properties than lower densities of PE. For UHMWPE, the molecular chain can consist of as many as 200 000 ethylene repeat units [4, 51].
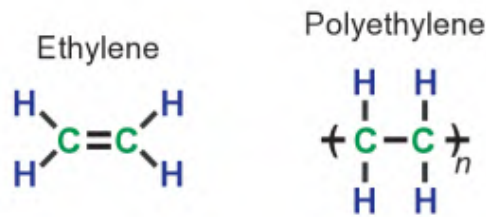
Figure 2.1: Chemical structure of ethylene and PE [4].

Medical graded UHMWPE was first introduced by Sir John Charnley in 1962 with regard to a total hip arthroplasty. In 1970, successful TSAs were performed by Stillbrink, Kenmore and Zipple using PE glenoid components with Neers original humeral component. This was the first recorded use of UHMWPE in the shoulder [52]. For the production of medical graded UHMWPE, ethylene gas has to be polymerised. Secondly, the polymerised UHMWPE in the form of resin powder needs to be consolidated into a sheet or near-net shaped implant by compression moulding or ram extrusion. Then, in most cases the UHMWPE implant is finalized into its final shape by a machine that accommodates a locking mechanism. This procedure consists of milling and turning operations. For the production of UHMWPE used inside the body, special requirements are defined, guaranteeing a pure and safe medical graded UHMWPE powder [4]. After production, sterilization and packaging of the UHMWPE-component takes place. In the 90s, gamma sterilization and air-impermeable packaging was the norm for orthopaedic implants. It is said that for gamma sterilization in a low-oxygen environment, accompanied with an appropriate choice of packaging materials (containing an oxygen barrier) and conditions, oxidation of UHMWPE components may be limited for five to ten years. Other methods of sterilization include gas sterilisation with ethylene oxide, which is very reactive, toxic and difficult to handle. Nowadays sterilisation is often performed by hydrogen peroxide (H_2O_2) plasma treatment. This technique does not generate radicals in the bulk material (only on the surface) and therefore avoids the oxidation cascade reaction, associated with gamma irradiation in low oxygen environments [49].

2.1.2 Surface adhesion, tension and roughness

Adhesion is the tendency of dissimilar particles or surfaces to cling to one another. Cohesion refers to the tendency of identical or similar particles to attach. Literature introduces two main adhesion mechanisms: mechanical coupling and intermolecular interactions. It is important to realize that these chemical and mechanical aspects are linked and cannot be treated as distinct entities, as chemical structures and interactions co-determine the mechanical properties and *vice versa* [53].

Mechanical coupling is also indicated as an interlocking system and is based on adhesive keying into the surface of the substrate, shown in Figure 2.2. There are contradictory findings regarding this mechanism as some researchers insinuate that roughening of a surface is simply increasing the surface area, which results in more molecular interactions and thereby increase adhesion [53]. In surface science one usually always talks about chemical adhesion. In chemical adhesion two materials are held together by molecular interaction and chemical bonds. Intermolecular forces include hydrogen bonds, dipole-dipole interactions (Keesom forces), dispersive interactions (London forces) and induced dipole interactions (Debye forces). These last three types can be summarized as Van der Waals forces. Permanent dipole-dipole interactions, also called Keesom forces, result from molecules that have permanent dipoles due to the electronegative difference between atoms within the molecule. This dipole causes a columbic attraction between molecules with an opposite load. A second type includes the Debye force, this is a dipole-induced interaction between a non-polar and a nearby polar molecule. The induced dipole in the non-polar molecule is now attracted to the permanent dipole, causing an intermolecular interaction. There is also a transient effect that can occur in any molecule as there is random movement of electrons within a molecule, which may result in temporary polarity (instantaneous dipoles) between two non-polar molecules, also defined as London forces. Hydrogen bonds occur between molecules with a hydrogen atom attached to a small, electronegative atom such as fluorine (F), nitrogen (N_2) or oxygen (O_2). Because of the low electronegative capacity of hydrogen and the high electronegative capacity of O_2, N_2 and fluorine and their small size, the electrons move towards these atoms making them slightly negatively charged and the hydrogen thereby gains a slight positive load, leading to attraction of an oppositely charged molecule. The most important source, causing the greatest adhesion force is the ionic interaction, it represents interactions between charged atoms or molecules. The attractive force between oppositely charged ions is described by coulombs law, which states that the force increases as distance decreases [51, 54].
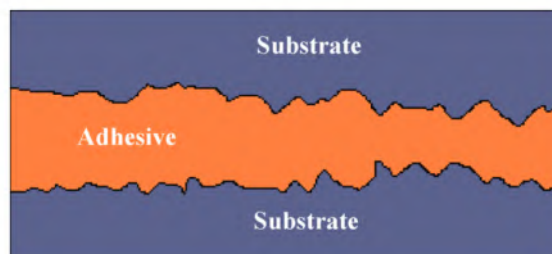

Figure 2.2: Mechanical coupling of two substrates [53].

Wettability depends upon the surface energy of the substrate. Generally, polymers have fairly low surface tension, less then 28 mN/m [55]. An increase in surface tension, equals to

an increase in intermolecular forces, which results in higher wettability and greater adhesion properties. Besides mechanical and chemical adhesion also other adhesion theories are proposed in literature, like electrical adhesion, the rheological mechanism of adhesion and the influence of temperature on adhesion properties. More information regarding this subject can be found in a review paper written by A. Firas on the adhesion of polymers [53].

2.1.3 Types of surface modifications

Modifying the surface of polymers like UHMWPE, by inserting functional groups or by covalent coupling of molecules onto the surface, can result in increased adhesion properties. Interesting polar groups to insert are carboxyl, hydroxyl and amine groups. This can also improve cell-implant interactions as cells consists mostly out of water and favour a similar (hydrophilic) environment. There are several ways available to introduce these functional groups on the surface such as wet-chemical methods, ozone treatment, UV-treatment, self-assembly, high-energy radiation and plasma treatment [56, 57].

An important disadvantage of the wet-chemical method is that these reactions are very aggressive (not environmentally friendly), also irregular surface etching has been reported. A different setback, which is also seen with UV-ozone treatment, is that modification of the chemical composition is not restricted to the surface but also takes place deeper into the bulk material, affecting mechanical characteristics in a negative manner. For UV-ozone treatment, relative long exposure times are required to reach sufficient surface oxidation [58]. Self-assembly surface modification normally uses gold and silver, which limits the applicability of this process. Another technique to adapt surface composition is high-energy radiation, which includes gamma radiation, electron beam radiation and ion beam radiation. This radiation is very energetic and penetrates much deeper into the material, affecting not only surface but also bulk characteristics. In the next part, a detailed introduction regarding plasma technology will follow, explaining why this type of surface modification is superior with regard to improved surface and cell adhesion [55, 56].

2.2 Plasma technology

Plasma treatment can be used to launch different functionalities on inert surfaces. This chemical modification can alter physical surface properties like wettability and surface roughness but also enables chemical binding of biological compounds on the surface. Plasma technology has some major advantages; it does not affect the mechanical properties of the bulk material, it is relatively inexpensive and reproducible, it can be used on complex surfaces and has a relatively short treatment time [59]. Also the use of hazardous solvents is avoided, as plasma

activation is a solvent free technique [60].

Plasma is often referred to as the fourth state of matter. The concept was introduced by Langmuir in 1929 [61]. Plasma is a partly ionized gas and is defined as a quasi-neutral particle system in the form of a gaseous mixture of free electrons, ions, radicals and neutral particles like atoms and molecules. Some of these particles are excited and can return to ground state by emitting energy in terms of a photon. It is this phenomenon that is responsible for the luminosity that characterizes plasma. The plasma state can be obtained by exciting gas into energetic states, by means of radiofrequency, microwaves or electrons from a hot filament discharger [55]. Plasma can be divided into non-equilibrium (non-thermal, cold) and equilibrium (thermal, hot) plasma. Thermal equilibrium implies that all species (electrons, ions, neutrals, *etc.*) have the same temperature. Very high temperatures are required to form this type of plasma, going up to 20 000 K for elements that are hard to ionize like helium (He) [62]. It is not possible to work with these high temperatures onto thermo-sensitive polymer surfaces, as they would degrade. Non-thermal plasmas are generated by an electrical gas discharge; here a strong electric field is applied to a neutral gas, which induces ionization of the gas volume [63]. The applied electrical field accelerates the created charged particles. Especially electrons are affected by the field due to their low mass and thereby gain most energy and high temperatures. On the contrary, heavy ions efficiently exchange their energy with the background gas and thus remain cold. Due to collision between energetic electrons and neutral molecules, radicals are created [63]. Plasma systems with regard to surface modification typically work at low pressures, because at low pressure the discharge is more stable and it is easier to control the plasma reaction. But increasing interest from the industry and the demand for more efficient and flexible techniques have led to the development of atmospheric pressure plasma reactors. As there is no need for vacuum conditions, investment costs are much lower and integration into the industry becomes much easier. The downside to atmospheric plasma production is that instabilities might occur much faster and transition to a thermal arc discharge is likely to take place. This transition is undesirable because it leads to inhomogeneous conditions as the discharge constricts to a narrow current channel and causes an increase in temperature [56, 64].

There are a lot of different types of set-ups regarding non-thermal atmospheric plasma sources. All are based on the fact that a molecule or atom gains energy from an outside excitation source or through interaction (collision) with other particles [59]. One of the most popular set-ups is the dielectric barrier discharge (DBD). The volume discharge arrangement can appear in different forms, one commonly used set-up is presented in Figure 2.3. In this configuration at least one electrode is covered by a dielectric layer, which is an insulator (like glass, quartz polymer or ceramic). One electrode is connected to an alternating current (AC) high voltage source and one is connect to ground. After ionization of the gas in the discharge gap between

the two electrodes, the transported charge accumulates at the dielectric surface. This charge generates an electric field that reduces the field in the gap and interrupts in this way the current flow after a few nanoseconds. The so-called micro-discharges have thereby only a limited lifetime and are uniformly divided over the dielectric surface. The dielectric layer has two functions; it limits the amount of charge transport by a single micro-discharge and distributes the micro-discharges over the entire area of the electrode [64]. A new and upcoming trend in plasma source technology includes the atmospheric pressure plasma jet. The produced plasma is not spatially bound or confined by electrodes and is therefore often referred to as remote plasma treatment. During active plasma treatment, like in a standard DBD reactor, the substrate will be placed between the electrodes and so there is direct contact between plasma and substrate. In remote plasma treatments, the substrate is placed outside, but the gas stream is still loaded with radicals and other active species. The plasma jet normally operates under atmospheric pressure and enables site-specific surface modification [64]. The principle is as follows, gas is blown through a quartz capillary (serving as dielectric barrier), in which a needle under high voltage is placed. Outside the capillary there is a ring electrode connected to ground. When a high voltage of several kilovolts (kV) is applied between these electrodes, the gas gets excited and plasma is created. In this set-up, treatment occurs in the afterglow of the plasma, because gas is blown outside the capillary and part of the plasma will follow. A schematic representation and photograph of an atmospheric pressure plasma jet is provided in Figure 2.4. When working with noble gasses, the afterglow can propagate up to 10 cm [65]. The set-up is easy to integrate into existing production lines and can selectively treat specific parts of a substrate. Unlike the DBD reactor set-up, the plasma jet is not limited to flat and thin substrates, but can also modify large 3D structures. A limiting factor however is the size of the treatment area, as the diameter of the afterglow is only around 1 cm^2 or even smaller [66]. During active plasma treatment, the substrate will interact with a high concentration of active species, while for the plasma jet the amount of active species decreases as the distance between the capillary and the substrate increases. On the other side, remote treatment prevents damages from discharges that run through the substrate like in active plasma treatment. It was reported by Wang et al. that the hydrophilic effect of remote argon (Ar) plasma was more significant than that of direct Ar plasma. They state that remote plasma treatment enhances radical reactions and restrain electron and ion etching effects [67]. A remark when using a plasma jet is the fact that even if pure noble gasses like Ar are used, the plasma afterglow can contain a small amount of O_2 and N_2 species, since the jet generates an afterglow that expands in the surrounding air [68]. Overall, these plasma jets are very promising in the field of surface modifications regarding medical applications and can possibly be used in combination with a robotic arm in order to draw a specific pattern of functional groups on a surface [56, 69].

Plasma is a very reactive environment through which different interactions with the surface
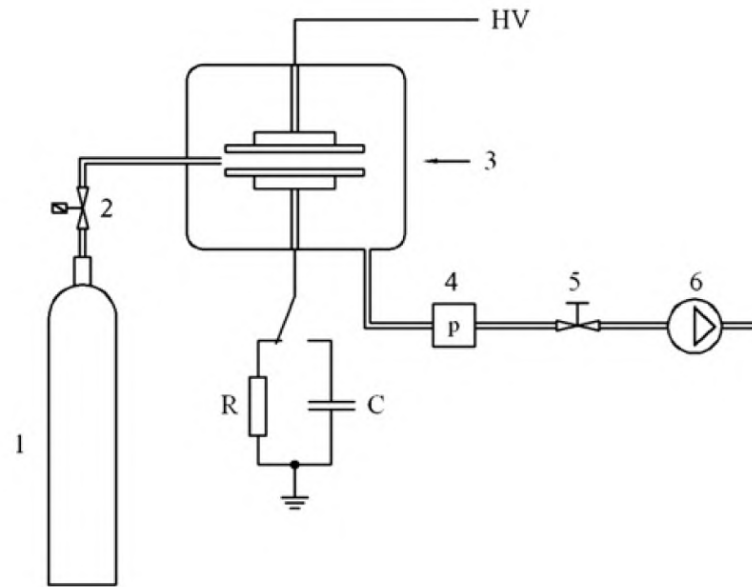
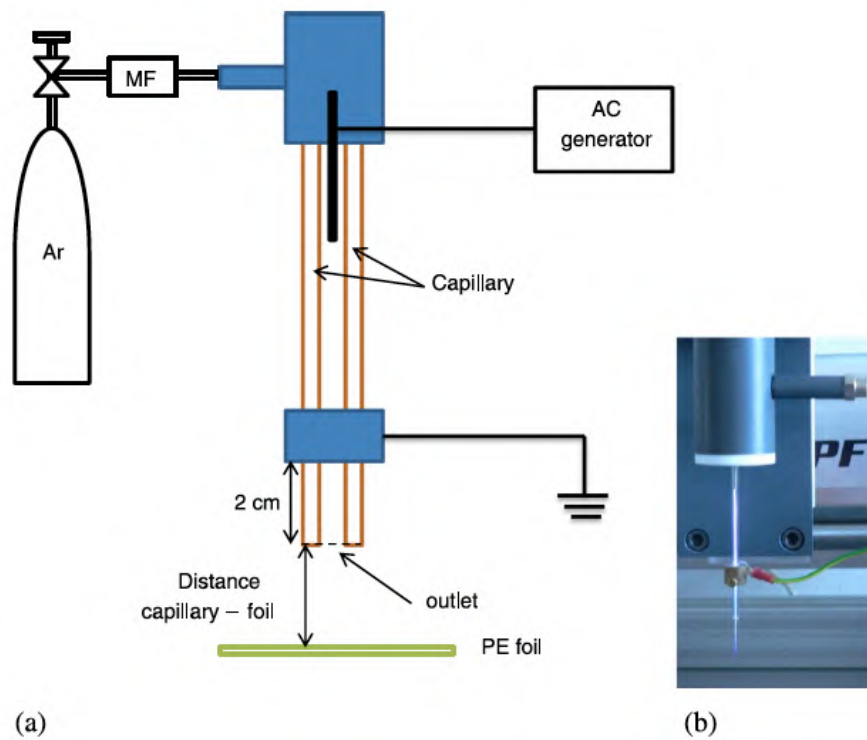**Figure 2.3:** DBD plasma activation reactor [50].

Figure 2.4: Atmospheric pressure plasma jet: (a) diagram, (b) picture [70].

are possible. There are several ways to modify surfaces by using plasma, like plasma crosslink-formation, plasma cleaning, plasma etching (or ablation), plasma polymerisation and plasma activation, visualized in Figure 2.5. Process vapour, substrate and process conditions will determine what process will take the upper hand. Plasma surface crosslink-formation is achieved by direct energy transfer from energetic plasma particles to the polymer surface. When for example, polymers such as PE and polypropylene are treated with plasma, formation of free radicals on the surface is induced. As a result, the radicals induce crosslinking of the polymer chain, increasing molecular weight of the polymer, hardness and wear resistance without damaging the bulk properties of the material. Additionally, crosslink-formation could cause polymer surfaces to form 3D molecular networks, through which the polymer layer can become an insoluble material [60]. Plasma cleaning and plasma sterilisation is extremely interesting in regard to thermo-sensitive polymers. Destruction of bacteria and spores is achieved by the presence of free radicals, ions, electrical interaction, *etc.* Plasma etching indicates a process where material is removed from the surface by chemical reactions. Ions are accelerated towards the substrate by the applied electric field. As the energy is not very high, ions cannot go deep into the substrate and a big portion of their energy is transferred to the surface atoms via elastic and inelastic collisions. Some surface atoms will acquire enough energy and escape from the substrate, the first layer of atoms will be sputtered off, the underlying layers will be exposed and gradually etched [59]. Plasma polymerisation and activation will be further discussed in the following sections [56, 64].
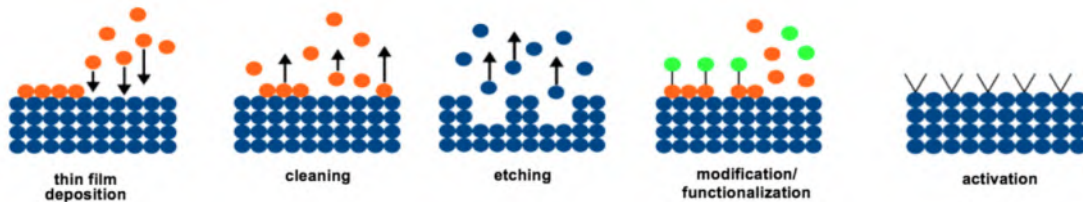

Figure 2.5: Different manners to modify a surface using plasma [64].

Applications regarding plasma in the medical field are quite diverse, going from cleaning, sterilization to changing surface chemistry and coating. Common research areas and applications of plasma treatment in the medical industry include barrier coatings (drugs-release and corrosion protection), tissue engineering (cell growth, adhesion), controlled protein adsorption, blood-compatible surfaces (grafts, catheters, stents, immobilization of biomolecules on the surface), sterilisation of surgical tools and devices, hardening of surfaces (cross-linking), increasing wettability of inert surfaces, *etc.* [59, 64].

2.2.1 Plasma activation

Plasma treatment is based on reactive or inert gasses: after ionization, these gasses will substitute functional groups or create radicals by collision of electrons and neutral molecules onto the surface. Most commonly, gasses like Ar, He, O_2, N_2, ammonia (NH_3) and tetrafluorimethane (CF_4) are used [56]. The type of used gas will determine the various types of functional groups found on the surface. Inert gasses like He and Ar are known not to introduce new functionalities on the surface but mainly generate radicals, which will interact with O_2 from the atmosphere to form peroxides, alcohol groups, *etc.* O_2 plasma leads to the introduction of oxygen containing functional groups like carboxylic acid groups, peroxide groups and hydroxyl groups. N_2 and NH_3 plasmas introduce primary, secondary and tertiary amines and amides on the surface [56, 59]. Plasma activated surfaces lead to a change in chemical and physical properties. The surface can become more hydrophilic as oxygen containing functional groups are introduced, roughness is changed and chain scission and/or cross-linking can occur [56]. Plasma treatment of a polymer only influences the top nm-layers of the material, leaving the bulk material unaffected and so this surface modification does not influence mechanical bulk properties. The final surface properties are a complex combination of substrate, gas, processing parameters (time, voltage, gas flow, *etc.*), cleaning procedure, ageing and environmental conditions. During plasma activation of a surface, damage can occur such as fragmentation by charged particle bombardment or radiation damage. This can be avoided by minimizing the applied energy or by separating the introduction of functionalities on the surface and the direct plasma, leading to a plasma afterglow concept [59, 64].

It is important to keep in mind that activation of a surface through plasma treatment is only a temporary effect. In other words, plasma-treated surfaces are known to be prone to ageing effects. A surface has the tendency to go to the lowest possible energy state and this is the main driving force regarding surface adaptation. In air, this results in reorientation of polar groups towards the bulk, minimizing the interfacial free energy. In a solvent, these polar groups are still present on the surface but the interfacial energy is minimized by expanding the polar groups towards the polar solvent [56]. When rinsing the treated surface with water or other polar solvents, partial recovery of the original wettability occurs. According to Kostov et al. this behaviour is caused by dissolution of lower molecular weight oxidized material (LMWOM), which consists of short, highly oxidized polymer fragments, loosely bounded to the surface and produced during plasma exposure. The loss of these functional groups due to dissolution in polar solvents or evaporation results in recovery of surface wettability [66]. Also temperature is an important factor with respect to hydrophobicity. An increased temperature results in a decreased wettability, it is insinuated that this is caused by polymer chain motion, as there is a reorientation of the polar group into the bulk. After activation post-plasma reactions occur, as radicals react with atmospheric O_2. The post-plasma reactions

are very likely caused by stable radical sites (long-lived radical sites in the substrate surface) formed by UV- radiation from the plasma or by excited molecules [71]. Because of this ageing effect, wettability again decreases, but remain higher in respect to its initial condition. It is important to characterize the surface chemistry at the time biological tests are conducted in order to correlate surface chemistry and physics to biological findings. Plasma treatment thus results in a combination of different functionalities, often with a low long-term stability [64].

2.2.2   Plasma polymerisation

Plasma polymerisation is an easy technique to introduce polymer nano-films onto a substrate. Here, an organic monomer is converted into reactive fragments, which are polymerised and deposited onto the surface [56]. This transition into reactive fragments happens when the monomer gas interacts with the plasma and the energy of the gas particles is transmitted to the monomer causing fragmentation, visualized in Figure 2.6. The monomer can react in different ways when it comes in contact with plasma. For example, a dissociation-ionization reaction will lead to different reactive fragments than a protonation reaction, which is followed by a dehydrogenation reaction. Different conditions such as power, pressure, *etc.* will favour one of these chemical pathways. Depending on the chemical nature of the monomer, the coating possesses different chemical and physical properties. Also monomer flow, power, treatment time and plasma gas flow influence the characteristics of the coating. A DBD plasma polymerisation set-up is presented in Figure 2.7. Plasma-polymerised coatings have different physical and chemical characteristic compared to polymers that are formed through traditional polymerisation. These plasma-polymerised films are pinhole-free, completely amorphous, insolvable in most solvents and highly cross-linked leading to good thermal, chemical and mechanical stability [50].
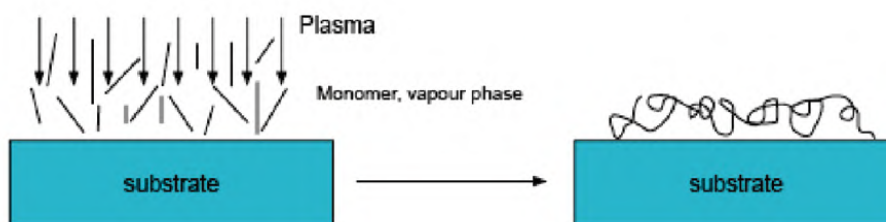

Figure 2.6: Plasma polymerisation [56].

De Geyter et al. investigated the deposition of PMMA on polypropylene substrates using an atmospheric pressure DBD. They state that when the monomer concentration becomes too low, the amount of ester-function groups decreases and the amount of ether and alcohol

groups increases [65]. The fragmentation also depends upon the amount of discharge power supplied to maintain the plasma. At high discharge powers and low monomer concentrations, molecules are subjected to heavy fragmentation, which leads to a large loss of monomer functional groups and oxygen. Methyl methacrylate is then highly fragmented causing a low amount of ester groups and a higher amount of ether and alcohol groups [65]. Research done by Cools et al. and Van Vrekhem et al. also states that low monomer concentration leads to a high energy/monomer ratio and so results in high fragmentation [50, 72]. This then again leads to a more profound loss of functionalities and a modified surface [50]. Resistance towards hydrolysis and the stability of coatings over time was observed to be higher for increased plasma power. This can be explained by high cross-linking at high powers and so resulting in a better stability. In comparison to plasma activated surfaces, plasma-polymerised coatings are not so prone to ageing [56]. This characteristic makes plasma polymerisation more applicable than plasma activation industry-wise, as often components are stored for a relatively long time. Research by Van Vrekhem et al. shows that after 48 hours of plasma polymerisation, the pull-out stress of plasma polymerised UHMWPE cemented into PMMA did not change, indicating a stable coating. It was found that a short treatment time gives rise to thinner films, which are more stable over time than thicker ones [56].
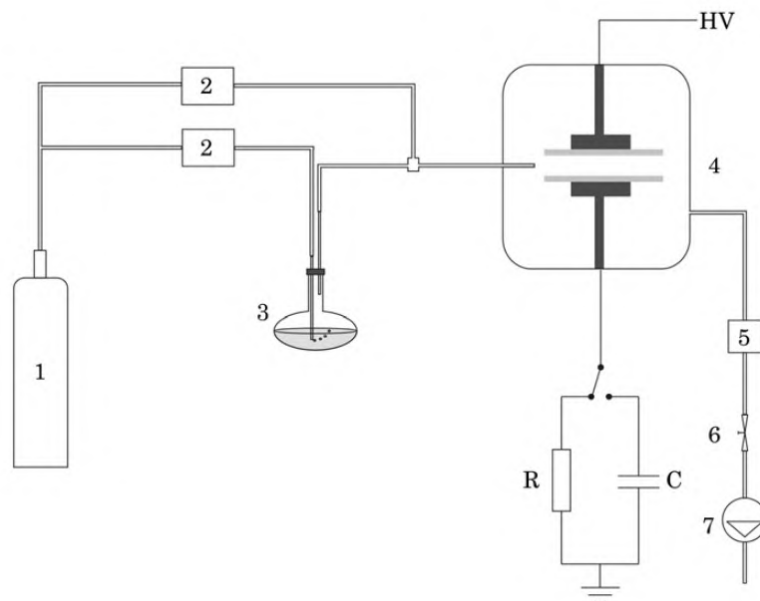

Figure 2.7: DBD plasma polymerisation reactor [50].

2.3 Plasma activation regarding surface adhesion

Cools et al. indicate that plasma activation is an excellent tool to modify and enhance wettability of hydrophobic UHMWPE by incorporation of polar groups like alcohols, ketones and ethers. They claim that the integrity of the substrate is conserved, which allows treatment of delicate components like biomedical implants [50]. A follow-up paper by Van Vrekhem et al. states that this plasma activation significantly improves the adhesion to bone cement (PMMA), as the pull-out stress of untreated UHMWPE was 0.47 MPa in comparison to an Ar plasma activated sample with a mean pull-out stress of 1.43 MPa, leading to almost a three fold increase [72]. Lommatzsch et al. suggest similar results when working with a plasma jet using dry air and N_2. They report that plasma treatment improves the adhesive bond strength of PE from 0.5 MPa to approximately 2 MPa [71]. This improvement is the result of an increased surface tension and the incorporation of functional groups containing O_2 and N_2 on the PE surface. It are dipole attractions and the formation of chemical bonds between substrate and the adhesive that are mainly responsible for the bond strength [71]. Van Deynse et al. used an atmospheric pressure plasma jet to modify the surface of low-density PE. Her research involved characterisation of the plasma operation conditions. She showed that an increase in discharge power leads to an increased incorporation of oxygen containing groups. Gas flow has to be high enough to provide a sufficient amount of particles, but turbulent flow, starting from 1.5 standard liters per minute (slm), should be avoided as these flows are less efficient in transporting plasma particles [69]. Just like Chen et al., Kostov et al. indicate that the atmospheric pressure plasma jet exhibits higher oxygen content and better hydrophilicity than substrates treated with a DBD. They state that this finding is the result of two effects. First, the interaction of Ar metastables with air molecules results in the production of a large amount of reactive species. Secondly, the gas stream of the plasma jet carries active oxygen species to the surface, resulting in higher oxygen levels [66, 67]. Research by Van Deynse et al. indicates that for low-density PE treated with Ar using an atmospheric pressure plasma jet at treatment distances from 5 to 15 mm, the water contact angle reduces with more than 70 %. This can be explained by the increased incorporation of oxygen containing groups, especially the increased implementation of O-C=O has a big influence. Starting from 15 mm, the plasma effect starts to decrease. Van Deynse et al. also reported that ageing after 14 days is restricted to only a 25 % loss of treatment efficiency [70].

2.4 Plasma activation regarding cell adhesion and proliferation

Biocompatibility of biomaterials relates, amongst others, to the absence of adverse cellular reactions and depending on the application results in cell interaction (e.g. bone implant) or

inert cell conditions (e.g. heart valves). Research shows that multiple factors influence the proliferation of cells on a substrate, like surface chemistry, topography and wettability. By surface modification or surface coating, it is possible to change cell interactions of materials which in their natural state are not able to support cell adhesion, spreading and proliferation [73].

Adhesion and spreading of cells are morphologic phenomena resulting from a series of molecular events, occurring in and around the cell. Generally, cells bind to the extra cellular matrix through cell membrane receptors. There are several classes of receptors. These receptors sense the environment of the cell and when the receptor finds a suitable binding site, also called a receptor binding side, it binds and a feedback-signalling pathway within the cell allows more receptors to be localized in that cell region. One class of receptors are integrins. Integrins, also known as receptor proteins, not only allow binding to matrix proteins, like vitronectin, laminin and fibronectin, but are also thought to be involved in signalling events towards gene transcription and cell proliferation. Focal adhesion kinase (FAK) and Ras homolog gene family, member A (RhoA) are proteins typically involved in intracellular signalling with respect to adhesion [73]. Within focal adhesion, integrins are highly enriched relative to their average membrane distribution. Hydrophobic substrates generally do not sustain cell adhesion. This is probably due to inaccessibility of adhesion sites on fibronectin and vitronectin absorbed to the surfaces, resulting in a lack of organisation of integrins. Not only chemical but also physical properties like surface roughness influence cell adhesion and morphology. This is usually reflected in a difference in cell morphology. The interaction between a polymer implant and the surrounding tissue can be divided into 4 stages. Within a few nano-seconds, a water shell is formed around the material during implantation. Secondly, a layer of plasma proteins consisting out of albumin, fibrinogen, immunoglobin type-G and fibronectin is adsorbed. During the third stage, a few minutes to days after implantation, cells reach the surface and interact with the implant through protein coating. This complex process depends on surface properties. The final stage includes further development of the early implant stages. The adsorption of proteins to biomaterials has a strong influence on inflammatory responses [56, 73].

Many polymeric surfaces are not optimal with regard to cell adhesion, compared to their mechanical bulk characteristics, which are most often very well suited for the purpose of the device. If cell adhesion must be enhanced, plasma activation represents a good fit. Plasma treatment is highly versatile due to its many parameters. Functional groups responsible for enhanced cell adhesion are amino-, hydroxyl- and carboxyl-entities making the material more polar. This by itself can enhance cell attachment and growth. It is also possible to add spacer coupling, which means that amine or carboxylic segments are added and used to bind proteins. By adding proteins like albumin, cells will not perceive the surface to be foreign. It

is also possible to add growth factors like cytokines. These can be fixed onto the surface in order to accelerate cell growth. The pictures in Figure 2.8 represent all these features. Possible applications are the production of artificial skin and artificial cornea cells. It is indicated that several protein components of the extracellular matrix, such as gelatin, collagen, laminin and fibronectin can be immobilized by plasma activation of the polymer surface and thereby effectively improve the cell adhesion force and its proliferation rate [60, 73, 74].
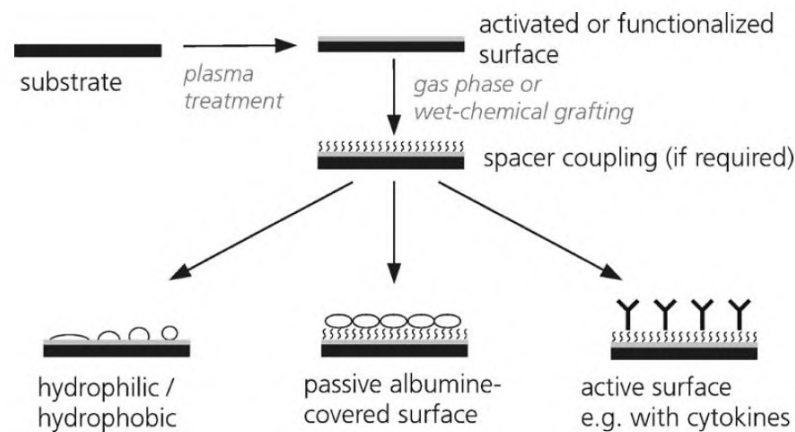

Figure 2.8: Aspects of plasma surface modifications regarding enhancement of cell growth on surfaces [74].

Van Kooten et al. used plasma activation on polystyrene material to create series with increasing oxygen surface incorporation and as a result decreasing water contact angles. Cell populations demonstrated a decreased growth rate on surfaces with low wettability. They reported that the individual morphology of cells was not influenced by surface treatment, but cell proliferation on surfaces increased with rising oxygen incorporation, ending at a maximum of 21 % O_2. The expression of adhesion-related proteins, like cadherin-h, FAK and RhoA was increased on surfaces with higher wettability [73]. Tutak et al. investigated the impact of the physical and chemical properties of a surface on osteoblasts. They found that the two fundamental steps regarding cell growth, the initial attachment to the substrate surface and proliferation, were strongly depended on the energy and the roughness of the surface. Best growing conditions were provided by a medium roughness (mean square roughness (Rq) around 100 nm) [60]. Tamada et al. modified different polymer surfaces using a glow discharge. Substrates included PE, polytetrafluorethylene, poly(ethylene terephthalate), polystyrene and polypropylene. The surface wettability of all materials decreased as treatment time increased and for each polymer a different dependence of cell adhesion with regard to the length of the treatment was observed. Overall, all samples appointed an optimal water contact angle for cell adhesion of approximately 70° [75]. Van Vrekhem et al. showed in a recent study that adhesion and proliferation of osteoblast cells on the surface of UHMWPE

is increased after plasma activation. Adhesion enhancement was observed through cell morphology, as literature states that when cells have a round shape, they are not sufficiently attached to the surface [72].

2.5   Goal of research

Glenoid loosening is indicated to be the number one problem regarding anatomic TSA [13]. As metal-backed glenoid models are not the answer to this major problem, optimization of glenoid cementation fixation is a must [46]. In TSA, the glenoid component is mostly made out of UHMWPE and the main cause of failure regarding this procedure is partly due to the chemical surface properties of UHMWPE. As mentioned before, UHMWPE is a linear homo-polymer, making it non-polar. PMMA cement, which is used in regard to prosthesis fixation, is a more polar molecule and contains ester-functionalities. The region of failure is most frequently the interface between the UHMWPE glenoid prosthesis and the PMMA used to fixate it. Increasing adhesion between the UHMWPE surface and PMMA, can lead to superior component fixation. Many polymers, like UHMWPE could benefit from modification of their surface properties in order to improve the adhesion strength, biocompatibility and lifespan of the implant. This can also result in improved cell interactions, migration and might eventually be an answer to the high prevalence of glenoid component loosening. For an optimal result, process parameters of the treatment (plasma activation) have to be determined for each set-up/application and material individually, as plasma surface interactions depend strongly on the substrate and operation properties [71]. The purpose of this master thesis is to improve the adhesion properties a UHMWPE glenoid component towards bone cement (PMMA) and bone by looking at the influence of different plasma activation conditions like treatment time, jet velocity, gas flow and power on surface characteristics of UHMWPE, ageing, adhesion and proliferation with regard to cells and adhesion towards bone cement by using an atmospheric pressure Ar plasma jet [50, 72].

Chapter 3

Plasma activation of UHMWPE using a plasma jet

3.1 Introduction

As described in Chapter 1, glenoid component loosening is the number one problem regarding anatomic total shoulder arthroplasty and can be the result of incorrect positioning or insufficient component fixation. Chapter 2 introduced plasma technology and elucidated that plasma activation can modify surfaces like UHMWPE, by implementing functional groups, which can lead to an increased adhesion towards bone cement and enhanced cell interactions.

Plasma activation is an excellent method to modify the surface chemistry of polymers without affecting bulk properties. There are several applications that can benefit from this method and therefore plasma is a very popular research topic. However as it might work well in theory, it is not guaranteed that these methods will be successful in practice. Different set-ups, gasses and parameters lead to different types of surface modification regarding plasma activation. This chapter will examine the influence of the treatment time, jet velocity, gas flow and power of an atmospheric pressure plasma jet on surface chemistry of UHMWPE using Ar gas. First surface characterisation tests are conducted, through which the chemical and physical properties of the modified surface are examined, using contact angle goniometry, atomic force microscopy (AFM) and X-ray photoelectron spectroscopy (XPS). In total five different activation conditions are selected and further tested. After analysing the modified surface chemistry, a large scale ageing test is conducted to examine how plasma surface modification changes as a function of time. In order to see if plasma activation of UHMWPE leads to better cell interaction and increases adhesion towards bone cement, cell and pull-out tests are conducted for the five different plasma activation conditions.

3.2   Experimental set-up

The experimental set-up with regard to plasma activation, using an atmospheric pressure plasma jet is displayed in Figure 3.1. Plasma is generated within a quartz capillary, which has an inside and outside diameter of 1.3 and 3.0 mm and serves as a dielectric barrier. The needle (tungsten wire) within the quartz capillary is connected to a high voltage source and represents the high voltage electrode (electrode 1). It has a diameter of 0.5 mm and a half-sphere-shaped tip. The ring electrode surrounding the quartz capillary is grounded and has a height of 10 mm (electrode 2). It is placed at a distance of 35 mm from the high voltage electrode and 20 mm from the lower edge of the capillary. During activation pure Ar gas flows through the capillary. When a high voltage is applied to the tungsten wire, plasma is generated in the inter-electrode gap and propagates into the surrounding air as a result of the gas flow through the quartz capillary. This set-up leads to a plasma afterglow effect, as only the afterglow of the plasma comes in contact with the sample. Plasma is generated by applying an AC high voltage, with a fixed frequency of 27 KHz to the high voltage electrode 1. UHMWPE samples are modified by scanning the surface with a constant velocity for a number of times using a CNC portal milling machine PF 600 P from BZT (Germany). The UHMWPE samples are placed 20 mm from the lower end of the capillary. Experimental parameters and detailed instrument information are summarized below in Table 3.1, 3.2 and 3.3.
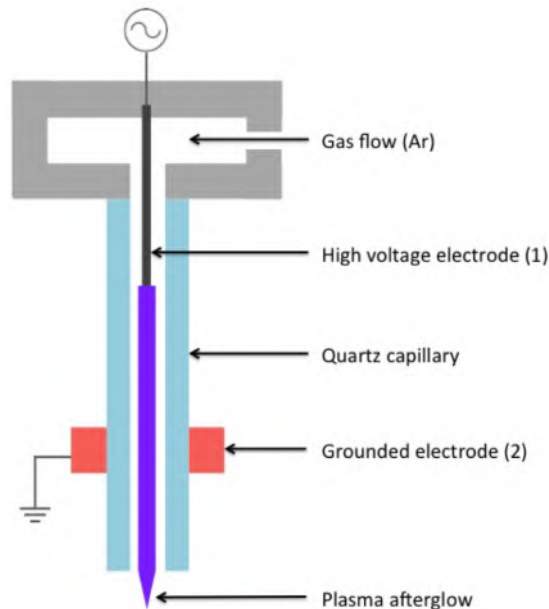

Figure 3.1: The atmospheric pressure plasma jet configuration used during experiments.

Instruments

Quartz capillary diameter: inside 1.3 mm, outside 3.0 mm
Quartz capillary as dielectric barrier
Tungsten wire (electrode 1) diameter: 0.5 mm
Copper ring electrode (electrode 2) diameter: inner 3.0 mm, outer 4.0 mm
Copper ring electrode (electrode 2) height: 10 mm
Inter-electrode distance: 35 mm
Distance copper ring electrode (electrode 2) and edge capillary: 20 mm
High voltage source: 27 KHz
Bronckhorst EL-flow gas flow controllers: max. of 10 l/min gas feed
CNC portal milling machine PF 600 P from BZT

Table 3.1: Instruments used in the plasma jet set-up.

Fixed parameters

Plasma jet distance from sample: 20 mm
Plasma glow diameter: 1 mm
Pressure: atmospheric
Gas: Ar

Table 3.2: Parameters kept fixed during plasma treatment.

Variable parameters

Treatment time: [0.13, 6 s]
Repetition: [1, 45]
Plasma jet velocity: 50, 150 or 450 mm/min
Gas feed during activation: 0.75 or 2 l/min
Voltage: 4 or 5 kV

Table 3.3: Variable parameters.

Each time, UHMWPE-films purchased from GoodFellow (England), with a thickness of 0.50 mm, are cut 20 mm (x-direction) by 10 mm (y-direction). The plasma jet is programmed to scan the whole sample area using WINPC-NC software. As the plasma afterglow has a diameter of 1 mm, the sample is scanned in 15 steps in the y-direction and passes a length of 22 mm in x-direction, in order to make sure the whole area is treated. An example of the UHMWPE-film and the jet pathway is provided in Figure 3.2 and 3.3.
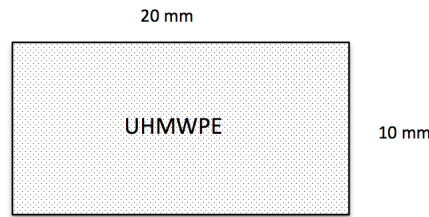
Figure 3.2: UHMWPE-film size and shape used during plasma activation in regard to surface characterisation.
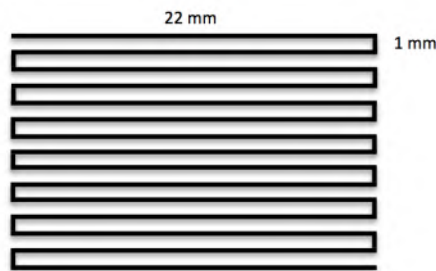

Figure 3.3: The plasma jet pathway, which is used to scan (activate) the whole area of the sample.

For cell tests round circles, with a diameter of 12 or 15 mm are punched out of the UHMWPE-film, so they fit a in a 24-well plate. With regard to the pull-out tests, medical grade UHMWPE blocks are used, which are 30 mm in length (x-axis), 9 mm wide (y-axis) and 4 mm high (z-axis). Plasma jet movements are adjusted so the whole surface of the circles and blocks are scanned.

3.3   Electrical characterization of the discharge

The atmospheric pressure plasma jet is electrically characterized by measuring the applied high voltage and the resulting discharge current. The voltage that is applied to the high voltage electrode (electrode 1) is measured by a 1000:1 high voltage probe (Tektronic P6015A). For the discharge current the voltage is measured by a 60 MHz oscilloscope probe (Picotech MI007) across a 47 Ω resistance. This resistance is placed in-between the ring electrode and grounding. Because there are two different applied voltages, characterization is done twice, one time for an applied voltage of 4 kV and a flow of 2 l/min and one time for an applied voltage of 5 kV and a flow of 0.75 l/min. By using a digital oscilloscope (Picoscope 3204A) the measured voltage and current are plotted as a function of time and the following wave forms are obtained (Figure 3.4 and 3.5).
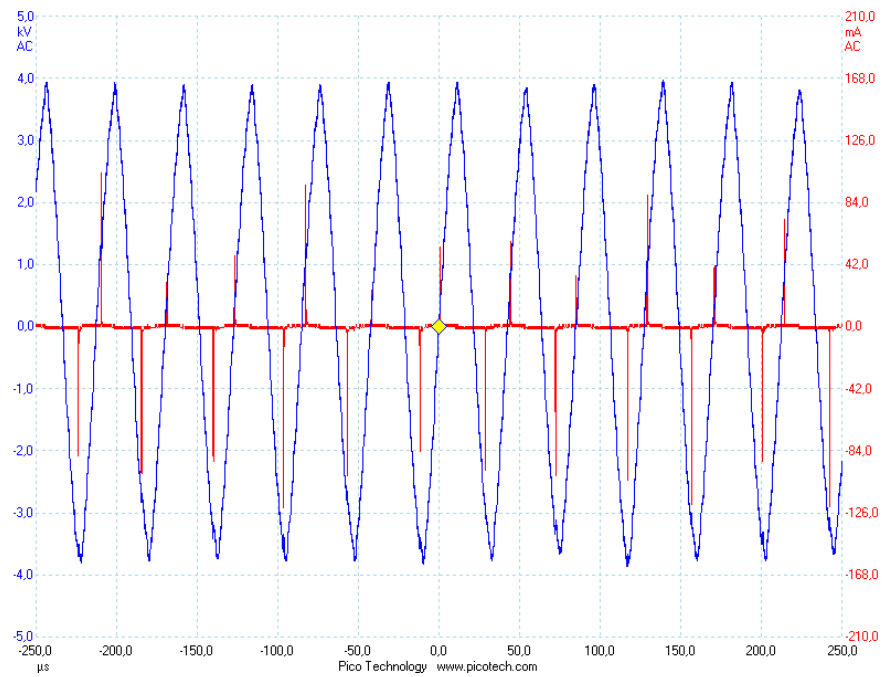
Figure 3.4: Electrical characterization of the discharge after applying a high voltage of 4 kV and a flow of 2 l/min: voltage (blue) and current (red) as a function of time.
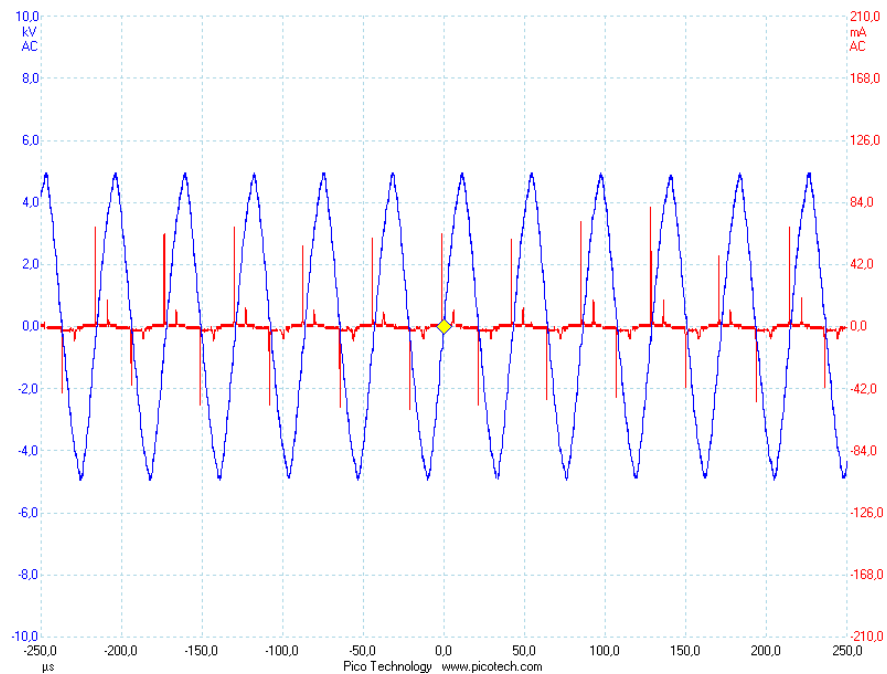

Figure 3.5: Electrical characterization of the discharge after applying a high voltage of 5 kV and a flow of 0.75 l/min: voltage (blue) and current (red) as a function of time.

One can see that the applied voltage is sinusoidal ranging from -4 kV to 4 kV (Figure 3.4) or -5 kV to 5 kV (Figure 3.5). The current on the other hand contains peaks which are a result of filamentary discharges. The wave form for an applied voltage with an amplitude of 4 kV and a gas flow of 2 l/min, indicates one current discharge spike every half voltage cycle, either negative or positive, depending on the voltage sign. The wave form for an applied voltage with an amplitude of 5 kV and a gas flow of 0.75 l/min, shows every half cycle of the applied voltage one large current spike and one smaller current spike. The current pulses indicate microdischarge activity and represent the plasma mode, which gives more information on ionizing efficiency. Literature states that a homogeneous mode, also refered to as a glow mode, is characterized by a single current pulse per half cycle. A multi-glow mode contains several wide current pulses per half cycle, while a filamentary mode is represented by a large number of spike current pulses every half cycle. Research reveals that filamentary mode leads to diminished ionizing efficiency compared to homogeneous mode. In this set-up the plasma mode is equal to a homogeneous mode [76, 77].

Based on these measurements (voltage and current as a function of time), the discharge power of the atmospheric pressure plasma jet can be calculated using the following equation, where P represents power (W), I stands for current (A), U indicates voltage (V), T is equal to the total time interval (s) and t represents the time interval (s) at which the measurements are conducted:

$$P = \frac{1}{T} \int_0^t U.I dt$$

By taking the measurements of 15 different time intervals of 500 μs and calculating the discharge power over each time interval, the average discharge power is obtained for the two different electrical conditions and are summarized in Table 3.4.

Flow (l/min)	Voltage (kV)	Power (W)
2	4	1.60 $\pm$0.02
0.75	5	2.62 $\pm$0.08

Table 3.4: Discharge power for the two different electrical plasma conditions.

3.4   Surface characterisation

Surface characterization examines the effect of plasma activation with regard to surface alterations. In order to see chemical changes, three tests are performed to study this surface

modification: water contact angle (WCA) measurements, AFM and XPS. Measuring the WCA of a droplet on a surface gives a fast and basic idea on surface hydrophilicity. Several sets of parameters such as treatment time, jet velocity, gas flow and power are tested and five conditions are selected through measurement of the WCA. Next, AFM is conducted, which gives more information on how plasma activation changes the surface roughness. In a last step the chemical surface composition is examined using XPS, which accurately determines the chemical composition in terms of carbon and oxygen concentrations and functional groups.

3.4.1 Contact angle measurement

The contact angle is the angle at which the droplet meets the solid surface and is the result of interactions across liquid, vapour and solid interfaces. WCA measurements give an indication on the wettability of a surface. For a hydrophilic surface the WCA is low as the droplet (deionized water) spreads out over the surface, starting at 0° for strong hydrophilic surfaces, up to 90° for weak hydrophilic surfaces. For a hydrophobic surface the WCA is higher than 90°, as it tries to minimize contact with the surface and becomes more convex. This method is used to evaluate the effect of plasma activation based on hydrophilicity and also gives more information about possible interactions with other materials. Surfaces that have a high contact angle are more hydrophobic and will have low affinity with polar, hydrophilic materials. More information regarding this measurement technique is provided in Appendix B.1.

The liquid used to deposit the water droplet is deionized water, 1 μl drops are produced at a speed of 150 μl/min. The instruments and software used to measure the WCA are called Easydropp and Drop Shape Analysis (DSA) and are both acquired from the company Krüss (Germany). Each measurement is performed in duplicate.

Parameter selection

In order to examine the effect of treatment time on the WCA, Ar flow and power are kept fixed (summarized in Table 3.5), while treatment time is increased by increasing the repeats of the travelled pathway. The treatment time T (s) is calculated by dividing the plasma diameter D (mm) by the plasma jet velocity v (mm/min) and multiplying this with the amount of repetitions R and 60 to transform the time from minutes to seconds:

$$T = \frac{D}{v}.R.60$$

Three different jet velocities (50 mm/min, 150 mm/min and 450 mm/min) are tested. The WCA as a function of treatment time is plotted in Figure 3.6. As the treatment time increases, the WCA decreases exponentially for each of the three plasma jet velocities, until a plateau

is reached and the WCA is no longer influenced by further treatment. The point at which this saturation starts to take place is defined as the saturation point. For this configuration (fixed flow and power) the saturation point is reached after approximately 3.6 s for all three jet velocities and for longer treatment times the jet velocities do not influence the measured WCA, all angles lie on the same trend-line. This considerable decrease in WCA, going from untreated UHMWPE at 87° towards approximately 47° gives a first indication that plasma activation can strongly increase surface wettability.

Fixed parameters	
Gas flow (l/min)	2
Power (W)	1.60

Table 3.5: Fixed parameters, which are used to find the saturation point for plasma activation of the UHMWPE-film.
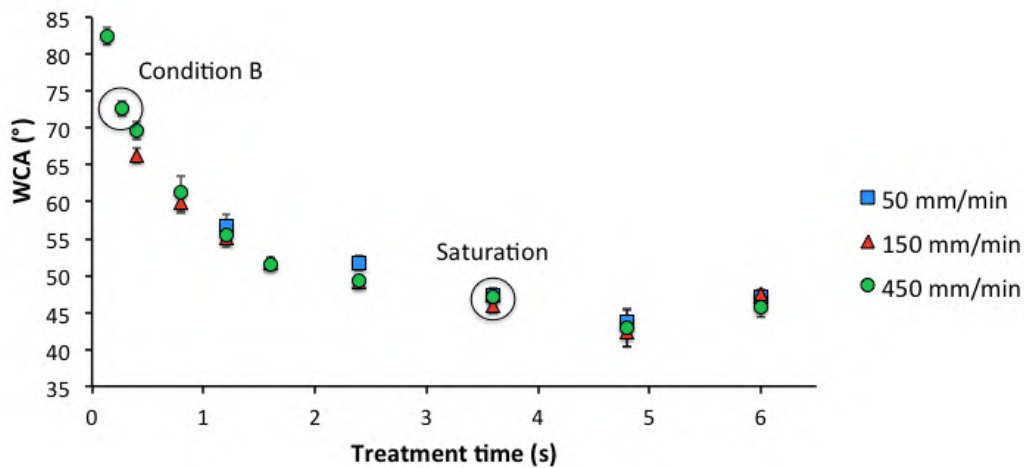

Figure 3.6: WCA measurements during different treatment times for three types of jet velocities, using a gas flow of 2 l/min and a power of 1.6 W.

Based on this graph, three saturation points, each reached at the same treatment time (3.6 s) but at different velocities and repetition times, are selected. Their parameters are summarized in Table 3.6 and they are labelled Saturation 1 (450 mm/min), Saturation 2 (150 mm/min) and Saturation 3 (50 mm/min). The measured WCA of these saturation points are given in Table 3.7.

Label	Treatment time (s)	Repetition	Jet velocity (mm/min)
Saturation 1	3.6	27	450
Saturation 2	3.6	9	150
Saturation 3	3.6	3	50

Table 3.6: The parameters of the saturation points for the three different jet velocities, at a gas flow of 2 l/min and a power of 1.60 W.

Label	WCA (°)
Saturation 1	47.1 ±0.7
Saturation 2	46.0 ±1.1
Saturation 3	47.3 ±1.0

Table 3.7: WCA of the Saturation conditions.

As discussed in section 2.4, Tamada et al. suggest that cell adhesion is best on plasma modified PE surfaces with a measured contact angle of 70° [75]. In order to obtain a surface modification that corresponds more to these findings, the same configuration is taken (same flow and power, Table 3.5) but the treatment time is set much shorter. This condition is referred to as Condition B. Its WCA as a function of treatment time is marked in Figure 3.6. After a treatment time of 0.27 s, at a speed of 450 mm/min, an Ar flow of 2 l/min and an applied power of 1.60 W, the original WCA of UHMWPE drops from 87° to 72.3°. The parameters and obtained WCA of Condition B are summarized in Table 3.8 and 3.9.

Label	Treatment time (s)	Repetition	Jet velocity (mm/min)
Condition B	0.27	2	450

Table 3.8: The parameters of Condition B, at a gas flow of 2 l/min and a power of 1.60 W.

Label	WCA (°)
Condition B	72.6 ±1.0

Table 3.9: WCA of Condition B.

Literature also suggests that too much oxygen can lead to the production of free radicals, which are highly reactive towards vital molecules like DNA and proteins, leading to cell lysis [78]. In an attempt to find a contact angle even lower than the Saturation point, the fixed configuration is adjusted (gas flow and power). Literature states that the gas flow during

plasma activation co-determines the amount of gas ionisation, high flows lead to high gas volumes that have to be ionized by a fixed power. When lowering the flow, the amount of ionisation and radical formation will increase as the energy per gas volume increases. Van Deynse et al. indicate that this mainly leads to an increase in hydrophilic oxygen groups on the surface and thereby increases polarity [69]. Figure 3.7 confirms this theory, by decreasing the gas flow, the WCA simultaneously decreases and hydrophilicity increases. When the flow becomes lower than 0.75 l/min, the WCA again increases as the amount of particles becomes to low in regard to optimal ionisation. This experiment is conducted at a treatment time of 3.6 s, a jet velocity of 50 mm/min and a power of 1.60 W.
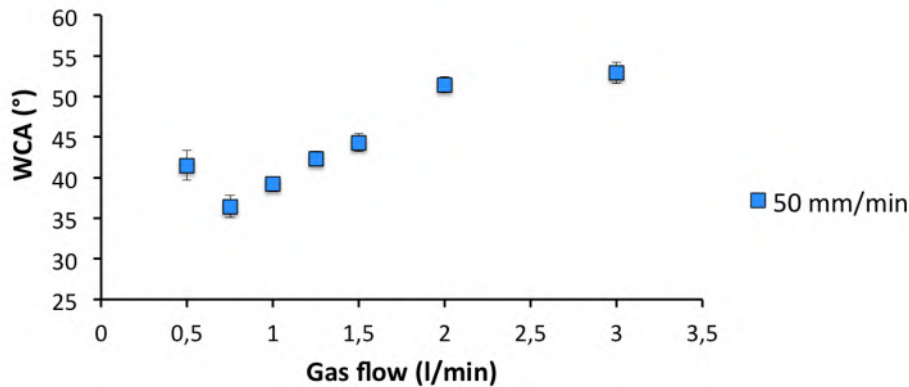

Figure 3.7: WCA as a function of different gas flows, using a treatment time of 3.6 s, a jet velocity of 50 mm/min and a power of 1.6 W.

Van Deynse et al. also state that a higher power leads to a higher concentration of reactive plasma species, resulting in a more profound surface activation and increased hydrophilicity [69]. By applying 2.62 W instead of 1.60 W and by using a gas flow of 0.75 l/min instead of 2 l/min (Table 3.10), the WCA decreases from 87° to 25.5°. The treatment time and jet velocity is taken at 50 mm/min and 3.6 s. This condition is labelled Condition F and its parameters are summarized in Table 3.11, the corresponding WCA can be found in Table 3.12.

Fixed parameters	
Gas flow (l/min)	0.75
Power (W)	2.62

Table 3.10: For Condition F the gas flow and power parameters are changed in order to reach a less hydrophobic surface in respect to the Saturation conditions.

Label	Treatment time (s)	Repetition (x)	Jet velocity (mm/min)
Condition F	3.6	3	50

Table 3.11: The parameters of Condition F, at a gas flow of 0.75 l/min and a power of 2.62 W.

Label	WCA(°)
Condition F	25.5 ±2.2

Table 3.12: WCA of Condition F.

So by variating several parameters like treatment time, jet velocity, gas flow and power and by measuring the resulting WCA on the modified surface, five different plasma activation conditions are selected. Each of these five conditions are labelled and from now on referred to similar. Table 3.13 gives a final overview of the selected conditions. Through these five different treatment conditions, it is possible to examine the influence of treatment time (compare Saturation 1 with Condition B), jet velocity (compare Saturation 1, 2 and 3) and gas flow, power (compare Saturation 3 with Condition F) on surface modification of UHMWPE after plasma activation.

Label	Treatment time (s)	Jet velocity (mm/min)	Flow (l/min)	Power (W)	WCA(°)
Saturation 1	3.6	450	2	1.60	47.1 ±0.7
Saturation 2	3.6	150	2	1.60	46.0 ±1.1
Saturation 3	3.6	50	2	1.60	47.3 ±1.0
Condition B	0.27	450	2	1.60	72.6 ±1.0
Condition F	3.6	50	0.75	2.62	25.5 ±2.2

Table 3.13: The different parameters of the five selected plasma activation treatments.

3.4.2 Atomic force microscopy

It is known that plasma activation can lead to surface etching which might smoothen or roughen the surface [50]. In the case of an atmospheric pressure plasma jet, the exited and ionized Ar atoms from the discharge can create reactive species, like atomic oxygen, ozone and OH-radicals by their reaction with ambient air. These reactive particles can subsquently etch and roughen the samples surface [66]. This change in surface roughness has an influence on the measured WCA as a higher surface roughness enhances the WCA compared to its smoother equal. In order to see how plasma activation of UHMWPE influences the surface roughness in this set-up, AFM is performed on untreated and treated samples using the five different activation settings. AFM creates an image of the material surface by scanning it with a probe, thereby the surface morphology can be examined before and after surface modification. Based on these images the root-mean-squared surface roughness (Rq) of the whole surface is determined. A more detailed explanation regarding AFM is provided in Appendix B.2.

During this experiment a cantilever (PPP-NCHR) XE-70 set-up from Park systems (Korea) is used in non-contact mode. The image quality is set on 256x256 with a scan size of 30 μm and a scan rate of 0.3 to 1.0 Hz. The operating software (XEP) and data processing software (XEI) both come from Park systems. The Park Systems XEI data processing software allows to determine several roughness measures for each sample. For each sample, the Rq value of the surface roughness is determined in triplicate.

The acquired roughness values are given in Table 3.14. For this set-up plasma activation using an atmospheric pressure plasma jet does not significantly influence surface roughness. Overall, UHMWPE is a material with a relative high surface roughness, as untreated UHWMPE has an Rq value of 139 nm with a standard deviation of 8 nm. For treated samples this leads to an average in the same order but with an even higher deviation, which makes it difficult to compare different types of plasma activation. It is clear that for this set-up, plasma activation has only a small influence on surface roughness and etching effects that might appear when using plasma activation can be neglected regarding this experiment. This corresponds to literature as Wang et al. already reported that the hydrophilic effect of remote Ar plasma enhances radical reactions and restrain electron and ion etching effects, see section 2.2 [67].

3.4.3 X-ray photoelectron spectroscopy

XPS can determine the chemical composition of a surface. Through a survey scan the atomic composition is defined as a relative percentage and through detailed recordings of C1s peaks

Label	Rq (nm)
Untreated UHMWPE	139 ±8
Saturation 1	145 ±22
Saturation 2	142 ±34
Saturation 3	140 ±27
Condition B	124 ±19
Condition F	133 ±27

Table 3.14: Root-mean-squared (Rq) surfaces roughness before (Untreated UHMWPE) and after plasma activation.

the type of chemical bonds between e.g. carbon and oxygen can be determined, as every chemical bond has its own specific binding energy. By deconvolving the recorded C1s peaks, a spectrum of individual peaks is obtained. If the binding energy of a specific carbon bond is known, it is possible to determine its relative intensity from the spectrum. The peak intensity indicates a quantity and the peak position declares the element and the type of chemical bond. Literature proposes the following energy values: 285.0 eV for the C-C/C-H bond, 286.7 eV for the C-O bond, 287.7 eV for the C=O bond and 288.9 eV for the O-C=O bond [65]. An example of a curve fitting that is applied for the deconvolution of the C1s peak for plasma activated UHMWPE is given in Figure 3.8. A technical description on XPS is provided in Appendix B.3.

The XPS measurements are performed on a Physical Electronics PHI (United States), 5000 VersaProbe II spectrometer employing a monochromatic Al K_α X-ray source (hν = 1486.6 eV). Experimental parameters include a pressure lower than 5.10^{-6} Pa, a point measurement of 200 μm, an area measurement of 600 μm x 100 μm and an applied power of 50 W. For the spectrum recordings a survey scan region of 0 to 1100 eV is taken, with a survey pass energy of 187.75 eV. This was dome for three points per sample. The detail scan region is set on 20 eV with a detail pass energy of 23.5 eV. The survey scans are processed using PHI MultiPak software (Physical Electronics PHI, United States) and from the peak area ratios, the elemental composition can be determined. PHI MultiPak is used to curve-fit the high resolution C1s peaks, the calibration point is taken at 285 eV for C-C bond. For each sample, three different points on the surface are measured.
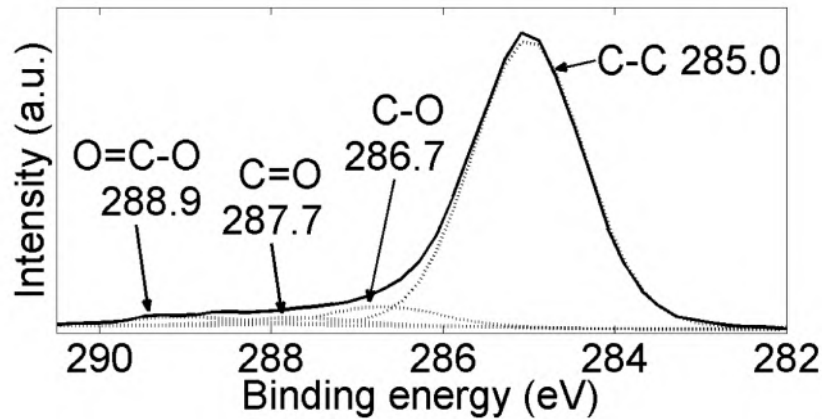
Figure 3.8: Curve fitting that is applied for the deconvolution of the C1s peak regarding plasma activated UHMWPE [50].

Percentage composition

In order to see how different plasma activation conditions influence surface chemistry, treated samples are analysed using XPS. Table 3.15 gives the atomic concentration regarding carbon and oxygen, expressed in relative percentage. Also the oxygen/carbon ratio is present in this graph.

Label	C %	O %	O/C
Saturation 1	70.0 ±1.2	30.0 ±1.2	0.43 ±0.03
Saturation 2	71.1 ±1.6	29.0 ±1.6	0.41 ±0.03
Saturation 3	71.6 ±0.9	28.4 ±0.9	0.40 ±0.02
Condition B	79.3 ±1.8	20.7 ±1.8	0.26 ±0.03
Condition F	70.5 ±1.2	29.5 ±1.2	0.42 ±0.02

Table 3.15: Relative percentage of carbon and oxygen present on the surface and their ratio for each plasma activation condition.

As expected Condition B has an oxygen concentration that is much smaller compared to Saturation 1 (20.7 and 30.0 %), as the treatment time is 14 times shorter than the Saturation conditions. Lower treatment times thus result in a lower oxygen concentration. XPS measurements indicate that there is a strong statistical difference (p <0.01) in oxygen concentration between Saturation 1 and Condition B and this corresponds with the WCA measurements. The oxygen concentration of all three Saturation points is approximately 30 %, this corresponds and explains the results from the WCA measurements which decrease after plasma treatment and for all three Saturation conditions reach the same plateau value of approximately 47°. Based on XPS results, a higher power and lower flow, used during Condition F

compared to Saturation 3 does not affect the amount of oxygen incorporation (no statistical difference between Saturation 3 and Condition F) but WCA measurements state otherwise, as the measured contact angle does further decrease compared to the Saturation conditions, with a WCA of approximatly 47° for the Saturation conditions and 25.5° for Condition F. This conflicting outcome can be due to the fact that when the WCA is measured only the top surface, with a depth of approximately 1 nm is analysed, while XPS measurements have an analysing depth of approximately 10 nm [79].

Functional groups

By deconvolving the C1s peaks the relative percentage of functional groups present on the surface is determined. Table 3.16 represents the relative percentage of functional groups like C-C, C-O, C=O and O-C=O for each plasma activation condition.

Label	C-C %	C-O %	C=O %	O-C=O %
Saturation 1	63.2 ±2.4	14.2 ±3.7	10.0 ±2.1	12.6 ±1.2
Saturation 2	62.3 ±4.9	17.2 ±5.8	8.0 ±1.5	12.5 ±1.0
Saturation 3	65.9 ±6.4	18.5 ±7.8	6.4 ±1.6	9.1 ±1.2
Condition B	72.6 ±3.1	14.0 ±3.5	8.4 ±0.9	5.0 ±0.6
Condition F	62.0 ±3.7	20.5 ±5.4	8.0 ±2.2	9.5 ±0.8

Table 3.16: Relative percentage of functional groups present on the surface for each plasma activation condition.

It is seen that longer treatment times (Saturation 1 compared to Condition B), lead to equal concentrations of C-O and a statistical increase ($p < 0.01$) in O=C-O functionalities. This phenomenon is graphically represented in Figure 3.9, where the relative percentage of functional groups is expressed as a function of treatment time for a jet velocity of 450 mm/min, a gas flow of 2 l/min and a power of 1.60 W. Overall standard deviations are high so no finite conclusion can be made.

The use of different jet velocities leads to a similar hydrophilicity (similar amounts of oxygen), but different functional group incorporation. Higher jet velocities like Saturation 1 (450 mm/min) compared to Saturation 3 (50 mm/min) lead to a higher amount of C=O and O-C=O functionalities, with a statistical difference ($p < 0.01$) between Saturation 1 and Saturation 3 regarding the relative percentage of O-C=O functionalities, a statistical difference ($p < 0.05$) for O=C functionalities and no statistical significance regarding relative oxygen percentage. Also between Saturation 2 and Saturation 3 there is a strong statistical difference ($p < 0.01$) in relative percentage of O-C=O functionalities. When comparing the
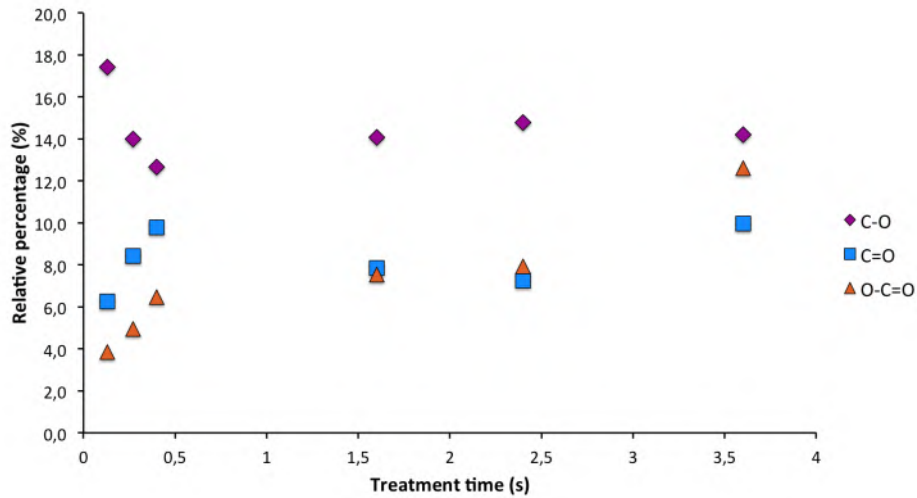
Figure 3.9: Relative percentage of functional groups as a function of treatment time for a jet velocity of 450 mm/min, a power of 1.60 W and a gas flow of 2 l/min.

pronounced plasma activation condition, Condition F, with Saturation 3 (same jet velocities, same treatment time, lower gas flow and higher power), it is seen that the overall relative percentage of functionalities remain in the same range.

3.4.4 Conclusion

Plasma activation of UHMWPE using an atmospheric pressure Ar plasma jet leads to increased surface hydrophilicity of UHMWPE, as the initial WCA decreases and the amount of oxygen containing functionalities increases. According to Van Deynse et al. an atmospheric pressure plasma jet causes dissociation and ionization of the atmosphere, which contains N_2, O_2 and H_2O resulting in O-atoms and OH-radicals. When these radicals reach the surface of UHMWPE, they will interact with C-C, C-H and other bonds. Only if the energy of these radicals is higher than the bond energy, they will be able to break these bonds. The energy required to break a C-H or a C-C bond is approximately 4.4 eV and 3.6 eV and this results in an unpaired electron configuration, which is highly reactive. These created polymer radicals will react with atomic O, molecular O_2, OH-radicals from Ar plasma or with atmospheric oxygen, leading to implementation of oxygen containing groups [69].

As treatment time increases, the contact angle continues to decrease until a saturation plateau is reached. Further plasma treatment will no longer influence the WCA as the surface is saturated with oxygen. An increase in treatment time, from 0.27 s to 3.6 s, lead to a statistical increase in O=C-O functionalities. Different jet velocities and equal treatment time result in an equal saturation plateau regarding WCA measurements and an equal oxygen concentra-

tion but different types of functional groups are incorporated. Faster jet movements induce a statistically higher amount of C=O and O-C=O functionalities and slow movements seem to have higher C-O functionalities. A decrease in flow and an increase in power result in a further decrease of the WCA but the overall amount of oxygen is not further influenced. This is probability due to the different analysing depths of WCA measurements and XPS analysis.

3.5 Ageing tests

Ageing of plasma-treated polymers has been investigated by several researchers and chemical changes induced by plasma activation are often found to be either partially or totally reversible as time increases. Williams et al. indicate two main events that take place, (i) post-treatment chemical reactions and (ii) surface relaxation [79]. With respect to an industrial product, ageing should be avoided or controlled as much as possible. In order to assess how plasma activated UHMWPE is influenced by time and the enviroment an ageing experiment is conducted. Three interesting environments are evaluated. A first test environment includes ageing in vacuum in order to see if long-term storage at vacuum conditions preserves this alternated surface chemistry in regard to this plasma set-up. A second environment comprises ageing in ambient air, it is said that plasma activation has only a transient effect and fades when exposed to ambient air. However, research done by Van Deynse et al. indicates that ageing in a controlled ambient air environment after plasma activation using an atmospheric pressure plasma jet, results in a loss of treatment efficiency restricted to only 25% after 14 days of ageing, which is overall much better than for a DBD reactor set-up [70]. In a last experiment the implant environment is simulated, as treated samples are incubated in a phosphate-buffered saline solution (PBS) resembling physiological implant conditions. Different time intervals are selected to see how this fading effect evolves as a function of time for each of these three different environments. The five selected time slots include 4 h, 8 h, 24 h, 7 days and 14 days. After incubation the WCA is measured. Each measurement is conducted in duplicates in order to confirm the observed ageing effects. All five different plasma activation conditions are tested this way.

Ageing of plasma-treated surfaces strongly depends on the environment, time, temperature, humidity etc., so in order to control this process, specific ageing conditions are defined [79, 80]. During vacuum incubation the activated sample is placed in a closed Petri dish and the temperature of the vacuum oven is programmed at approximately 20 °C. For the ageing tests in ambient air treated samples are incubated at 20 °C and a humidity of 50 %, resembling controlled open air conditions. In order to mimic physiological conditions a 1 liter PBS solution is made using 8.0 g sodium chloride (NaCl), 0.2 g potassium chloride (KCl), 1.42 g di-sodium phosphate (Na_2HPO_4), 0.24 g mono-potassium phosphate (KH_2PO_4), solved in

800 ml of deionized water, supplemented with hydrogen chloride (HCl) to reach a pH of 7.4. In a last step the solution is further diluted using deionized water in order to reach a total volume of 1 l. Samples are incubated for a specific amount of time in this PBS solution at 37 °C and after incubation they are washed with deionized water and dried using dry air or N_2.

3.5.1   WCA measurements after ageing

After plasma treatment, samples are stored for a selected time slot of 4 h, 8 h, 24 h, 7 days and 14 days, subsequently the WCA is measured. The graphs below show the evolution of the WCA as a function of storage time, for vacuum, ambient air and PBS. Each plasma activation condition has its own graph and for each graph a relaxation plateau value is reached after approximately 24 h, this relaxation phenomena is also described in literature regarding ageing in ambient air [70, 80].

The loss in treatment efficiency L (%) during storage up to 7 days is calculated using the following equation [70]:

$$L = 100.\frac{\theta_{s1} - \theta_{s2}}{\theta_{s1} - \theta_{untreated}}$$

Where θ_{s1} is the saturation value of the WCA after plasma treatment, θ_{s2} is the plateau value of the WCA after 14 days of storage and $\theta_{untreated}$ is the WCA value of the untreated material, which is equal to 87° for UHMWPE.

For each plasma activation condition an ageing graph is shown, where the dotted lines represent the plateau value reached after approximately 24 h for vacuum (purple) and for air (blue). Figure 3.10 shows ageing as a function of time for Saturation 1. After 24 h in vacuum an ageing plateau is reached as the WCA increases from 47.5° towards approximately 52.9° and remain relatively constant from then on. For air this plateau value is equal to 54.2°. Ageing in PBS results in an initial increase in WCA and after 24 h the WCA starts to decrease. The loss in treatment efficiency for vacuum is equal to 14 %, for air this is 17 %.
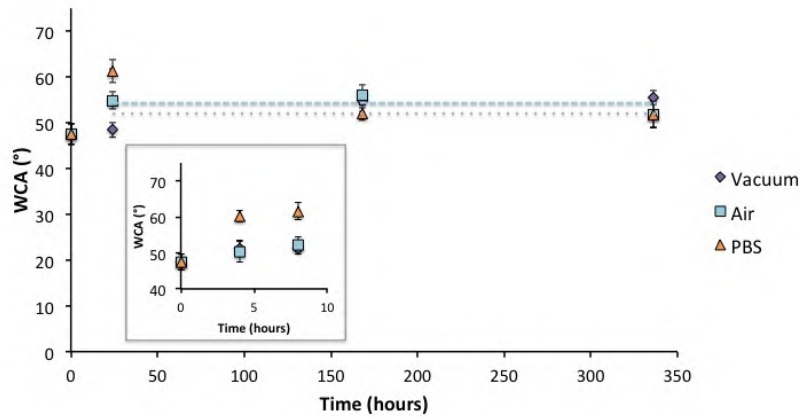
Figure 3.10: Ageing of plasma activated samples using Saturation 1 plasma activation. The WCA
angle is expressed as a function of storage time for vacuum, ambient air and PBS. The
dotted lines represent the plateau value reached after approximately 24 h for vacuum
(purple) and for air (blue).

As visualized in Figure 3.11 the WCA for vacuum increases from 46.5° towards a plateau
values of approximately 51.9° for ageing of Saturation 2. For air this plateau value is equal
to 55.2°. Also here ageing in PBS results in an initial increase in WCA and after 24 h the
WCA starts to decrease. For vacuum this leads to a loss in treatment efficiency of 13 %, for
air this is equal to 21 %.

The vacuum ageing graph for Saturation 3 visualizes an increase in WCA angle going from
45.0° towards 52.5°, ageing in air leads to a plateau value of 57.4° (Figure 3.12). The WCA for
ageing in PBS increases until 24 h of storage and afterwards it decreases again. This results
in a loss in treatment efficiency of 18 % for vacuum and 30 % for air.

Plasma activation Condition B is a very short treatment, leading to a non-pronounced surface
modification. After plasma treatment the WCA drops from the initial 87.0° towards 68.6°
and storage in vacuum or air leads towards plateau values of respectively 69.8° or 69.6°, seen
in Figure 3.13. Almost no hydrophic recovery is seen for this mild surface modification and
this results in a very small loss in treatment efficiency of approximately 7 % for vacuum and
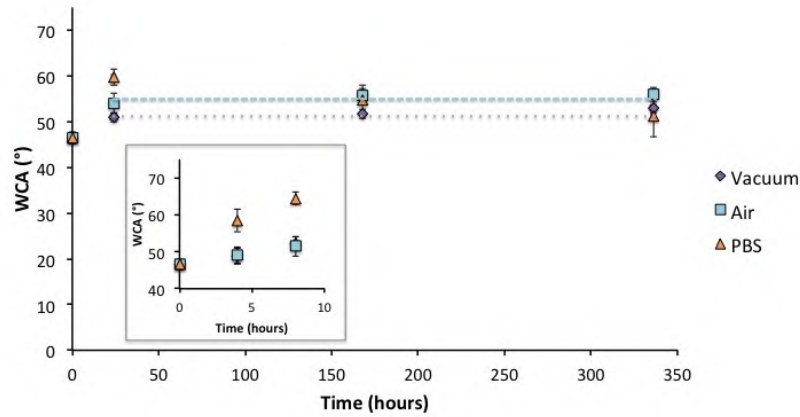6 % for air. The values for PBS remain stable here.

Figure 3.11: Ageing of plasma activated samples using Saturation 2 plasma activation. The WCA angle is expressed as a function of storage time for vacuum, ambient air and PBS. The dotted lines represent the plateau value reached after approximately 24 h for vacuum (purple) and for air (blue).
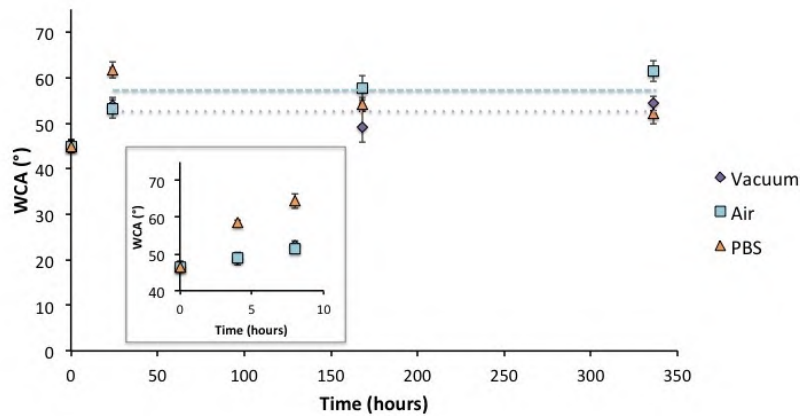

Figure 3.12: Ageing of plasma activated samples using Saturation 3 plasma activation. The WCA angle is expressed as a function of storage time for vacuum, ambient air and PBS. The dotted lines represent the plateau value reached after approximately 24 h for vacuum (purple) and for air (blue).

In contrast to Condition B, the more hydrophilic plasma treatment, Condition F, leads to a very pronounced surface modification. Plasma treatment causes a decrease in WCA from 87° towards 25.5°. Ageing in vacuum results in a plateau value of 33.3° and ageing in air leads to a plateau of 37.8°. The loss in treatment efficiency is therefore equal to 13 % and 20 %, which lies in the same range as the loss in treatment efficiencies of the Saturation conditions

1 and 2. Here ageing in PBS leads to a sharp increase in WCA until 24 h of storage, followed by a fast decrease. These findings are shown in Figure 3.14.
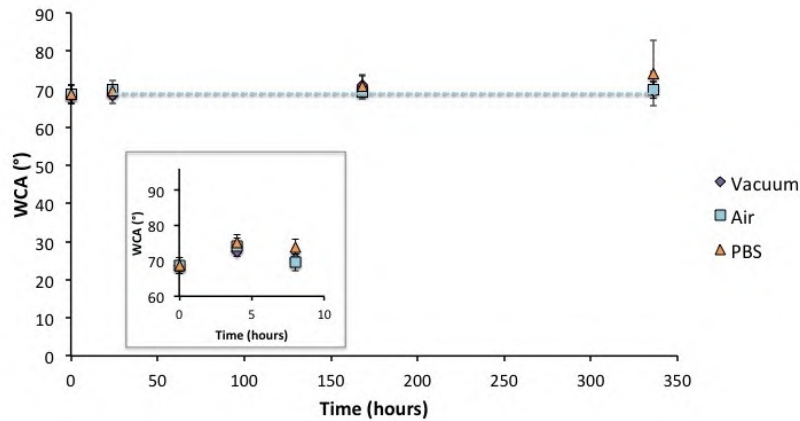

Figure 3.13: Ageing of plasma activated samples using Condition B plasma activation. The WCA angle is expressed as a function of storage time for vacuum, ambient air and PBS. The dotted lines represent the plateau value reached after approximately 24 h for vacuum (purple) and for air (blue).

Ageing as a function of time shows that after plasma treatment the WCA quickly increases during the first hours of storage, except for Condition B, here the increase is minimal. Hydrophobic recovery of treated UHMWPE is most pronounced for Saturation 3 and less apparent for the Condition B for both vacuum and air. Condition F has a loss that is in the same range as Saturation 1 and 2. After approximately 24 h of ageing, all five conditions reach a WCA plateau value. For each condition the percentage of remaining surface modification regarding 14 days of ageing in vacuum and air is calculated. This parameter is just like the loss in treatment efficiency very sensitive to small deviations. By using the plateau WCA value for ageing in vacuum and air the percentage of remaining surface modification (R) is determined and summarized in Table 3.17. This is equal to 100 % - L (loss in treatment efficiency). Except for Saturation 3 and Condition B, all types of plasma activation lead to the same percentage of conservation of approximately 86 % for vacuum and around 80 % for air. It seems like shorter treatment times (Condition B) or higher jet velocities (Saturation 1) lead to better plasma preservation. Overall these values of preservation are much higher than those reported in literature regarding ageing in a DBD-reactor, here plasma activation is known for its transient effect [80]. This high maintenance of surface modifications as a function of time makes atmospheric pressure plasma jets very promising in regards to plasma activation.
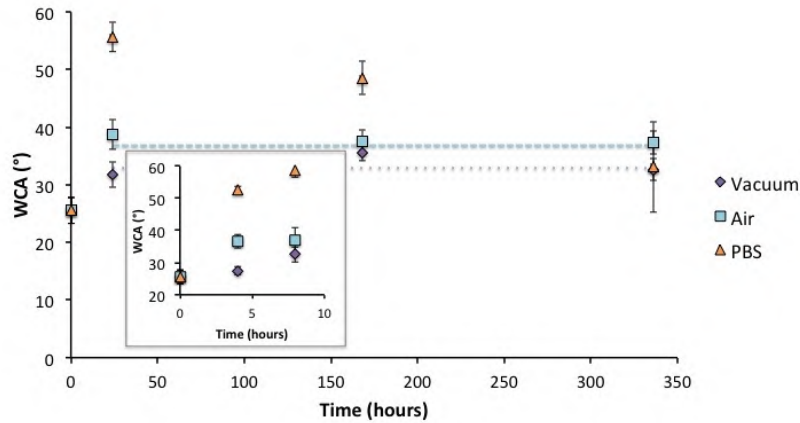
Figure 3.14: Ageing of plasma activated samples using Condition F plasma activation. The WCA angle is expressed as a function of storage time for vacuum, ambient air and PBS. The dotted lines represent the plateau value reached after approximately 24 h for vacuum (purple) and for air (blue).

Label	R_{vacuum} (%)	R_{air} (%)
Saturation 1	86 ±10	83 ±6
Saturation 2	87 ±2	79 ±3
Saturation 3	82 ±7	70 ±10
Condition B	93 ±7	94 ±2
Condition F	87 ±3	80 ±1

Table 3.17: R represents the percentage of remaining surface modification after 14 days ageing in vacuum or air.

3.5.2 XPS measurements after ageing

Percentage composition

In order to see how ageing influences the chemical composition of an activated UHMWPE surface XPS measurements are performed after 7 days of storage in vacuum, air and PBS. The relative percentage of oxygen and carbon and their ratio are summarized in Table 3.18.

Label	Environment	C %	O %	O/C
Saturation 1	Vacuum	77.0 ±0.8	23.0 ±0.8	0.30 ±0.01
Saturation 2		76.9 ±1.9	23.1 ±1.9	0.30 ±0.03
Saturation 3		79.3 ±1.7	20.7 ±1.7	0.26 ±0.03
Condition B		81.9 ±2.1	18.1 ±2.1	0.22 ±0.03
Condition F		75.3 ±2.8	24.7 ±2.8	0.33 ±0.05
Saturation 1	Air	78.5 ±0.6	21.5 ±0.6	0.27 ±0.01
Saturation 2		81.6 ±1.7	18.4 ±1.7	0.23 ±0.03
Saturation 3		81.5 ±1.3	18.5 ±1.3	0.23 ±0.02
Condition B		89.0 ±1.2	11.0 ±1.2	0.12 ±0.02
Condition F		81.1 ±2.5	18.9 ±2.5	0.23 ±0.04
Saturation 1	PBS	92.2 ±3.0	7.8 ±3.0	0.09 ±0.04
Saturation 2		85.5 ±0.4	14.6 ±0.4	0.17 ±0.01
Saturation 3		89.4 ±1.5	10.6 ±1.5	0.12 ±0.02
Condition B		92.6 ±2.2	7.4 ±2.2	0.08 ±0.03
Condition F		92.4 ±0.6	7.6 ±0.6	0.08 ±0.01

Table 3.18: Relative percentage of carbon and oxygen present on the surface and their ratio for each plasma activation condition after 7 days of ageing in vacuum, air or PBS.

By comparing the relative percentage of oxygen concentrations after 7 days of ageing with XPS data directly after treatment (Table 3.15) it is seen that ageing results in a decrease in oxygen concentration. This outcome is explained by the fact that during ageing post-treatment chemical reactions and surface relaxation takes place. Functional groups react with the environment and reorganise in order to lower their surface energy, leading to hydrophobic recovery [79]. The Saturation conditions seem to have an overall equal response to ageing in vacuum and air. The fact that Saturation 3 has a higher hydrophobic recovery based on WCA measurements is observed in a lesser extent during relative oxygen concentration measurements. However, even after 7 days of ageing in air Saturation 1 has a statistical higher amount of oxygen compared to Saturation 3 ($p < 0.05$). Condition B shows a decrease in oxygen concentration starting from 20.7 % at day zero, towards 18.1 % after 7 days of storage in vacuum and 11.0 % after 7 days of storage in air. This does not correspond to WCA measurements as the percentage of remaining surface modification are for both vacuum and air approximately 94 %. A similar effect is observed for Condition F, here ageing in vacuum results in an oxygen concentration of 24.7 % while ageing in air leads to an oxygen concentration of 18.9 % and WCA measurement lead to a hydrophobic recovery of which both plateau values lie very close to each other, 33.3° and 37.8°. WCA measurements indicate that ageing in air does not lead to a significant hydrophobic recovery (similar to that of vacuum), while XPS results contradict these findings. XPS data indicate that ageing in air does cause

hydrophobic relaxation with a significant difference regarding ageing in vacuum for all activation conditions (p <0.05). For ageing in vacuum, results regarding the WCA and XPS do match. As explained before, WCA measurements have a penetration depth of approximately 1 nm into the surface while XPS goes up to 10 nm and based on these results it might be that ageing in air leads to deeper lying post-treatment chemical reactions compared to ageing in vacuum. During ageing in vacuum, chemical reaction will not fully take place as there is no reagent present, but due to this big experimental set-up, vacuum conditions are often interrupted, which might lead to hydrophobic recovery after all. PBS is just like the human body a reactive environment, much more reactive than air and vacuum. During 7 days of ageing, PBS might interact with the surface of UHMWPE which might explain these random results regarding carbon and oxygen concentrations. Overall, these interactions are not fully understood which makes it hard to interpret what is happening.

Functional groups

By looking deeper into detail and analysing the relative percentage of functional groups present on the surface after 7 days of ageing, it is possible to see what type of changes occur at the surface during ageing. The relative percentage of functional groups after 7 days of ageing in vacuum, air or PBS is given in Table 3.19.

It is seen that 7 days of ageing in various environments, leads towards hydrophobic recovery as the amount of oxygen starts to decrease. This recovery is caused by a change in functional group configuration, which at first sight seems to lead to values that lie closer to each other (for different plasma activation conditions) compared to XPS data measured at day zero, see Table 3.16. Overall vacuum has the highest amount of oxygen containing functional groups, confirming that this environment preserves plasma modification best. Ageing, even in air leads to a small decrease in functionalities. This decline is most profound for O-C groups and goes for all ageing environments towards a plateau value of approximately 12 %, also for Condition B. The decline in C=O and O-C=O functionalities is not so profound for ageing in vacuum or air but decreases for the PBS environment. Ageing in PBS leads to a loss of oxygen containing functional groups as the relative percentage of C-C bonds increases to approximately 81 % for all conditions, compared to vacuum and air. The decrease in O-C=O-groups is the most profound for PBS, as vacuum and air values lie approximately 5 and 4 times higher. Overall, 7 days of ageing in PBS leads to levelling of the different plasma activation conditions, all the different conditions have approximately equal amounts of functional groups and the more pronounced the surface modification, the intenser the interaction with PBS. This is also seen during WCA measurements as ageing in PBS for Condition F resulted in a pronounced wave (see Figure 3.14) and for Condition B the measured contact angles are more on one line (see Figure 3.13). Longer treatment times (Saturation 1 compared to Condition

B) lead to a significant higher amount of O=C and O-C=O functionalities even after 7 days of storage in vacuum or air (p <0.05). Higher jet velocities (Saturation 1) result in a higher relative percentage of carboxyl-groups, even after 7 days of ageing in vacuum or air. Also noticeable is the fact that Condition B has relative low C=O and O-C=O concentrations, but a C-O concentration that is equally high as all the other activation conditions regarding ageing in vacuum, air and PBS, a phenomena that was already seen during direct XPS measurements.

Label	Environment	C-C %	C-O %	C=O %	O-C=O %
Saturation 1	Vacuum	70.4 ±1.5	11.7 ±0.6	9.4 ±0.1	8.5 ±1.0
Saturation 2		68.2 ±1.5	12.5 ±0.8	9.6 ±0.3	9.6 ±0.9
Saturation 3		72.7 ±1.0	11.6 ±1.0	8.0 ±0.4	7.6 ±0.4
Condition B		75.6 ±1.3	12.1 ±0.4	7.9 ±0.4	4.4 ±0.6
Condition F		68.0 ±0.8	13.9 ±0.7	7.3 ±0.4	10.7 ±0.8
Saturation 1	Air	73.1 ±0.2	11.9 ±0.2	8.2 ±0.3	6.9 ±0.4
Saturation 2		72.6 ±0.5	12.7 ±0.1	8.1 ±0.1	6.7 ±0.5
Saturation 3		74.1 ±0.8	12.0 ±0.5	7.5±0.4	6.4 ±0.5
Condition B		79.4 ±0.8	12.4 ±0.4	5.9 ±0.5	2.3 ±0.1
Condition F		73.3 ±0.4	11.7 ±0.1	7.6 ±0.4	7.5 ±0.3
Saturation 1	PBS	81.4 ±2.6	11.4 ±1.2	5.8 ±1.2	1.3 ±0.5
Saturation 2		79.9 ±2.2	13.0 ±3.0	5.7 ±1.1	1.4 ±0.2
Saturation 3		79.9 ±0.7	11.5 ±0.5	6.6 ±0.1	2.0 ±0.1
Condition B		83.4 ±1.7	11.0 ±0.5	4.7 ±1.5	1.0 ±0.5
Condition F		83.0 ±1.1	9.7 ±0.9	5.4 ±0.3	1.9 ±0.1

Table 3.19: Relative percentage of functional groups present on the surface for each plasma activation condition after 7 days of ageing in vacuum, air or PBS.

Based on these findings it is possible to say that double bonds like in C=O and O-C=O functionalities are more stable regarding ageing in vacuum and air than single bond C-O, as functional reorganisation is much more pronounced for the latter. From XPS data measured at day zero it is concluded that higher jet velocities like Saturation 1 contains more of these double bonds, compared to Saturation 3, what might explain the fact that hydrophobic recovery is more pronounced for Saturation 3.

3.5.3 Conclusion

Storage of plasma-treated UHMWPE in vacuum, air or PBS modifies the surface chemistry and wettability, this is due to the fact that during ageing chemical interactions and surface relaxation takes place. Functional groups react with the environment and reorganise in order

to lower their surface energy, leading to hydrophobic recovery [79]. Storage in vacuum preserves surface modification best, but the difference with air (based on WCA measurements) is smaller than initially thought. Ageing in air, which is a reactive environment, causes hydrophobic relaxation that takes place deeper in the bulk surface compared to ageing in vacuum. This explains why hydrophobic recovery in air was not pronounced during WCA measurements but indicates a significant difference regarding ageing in vacuum based on XPS measurements. This apparent contradiction is explained by the analysing depth of the two techniques [79]. For XPS elemental information is obtained from a depth of about 10 nm. However WCA measurements have an analising depth of only 1 nm. Ageing in PBS for a period up to 14 days suggests chemical interactions and reorganisation leading to results that are difficult to interpret. Literature indicates that storage in PBS enhances wetttability by chemical reactions with the storage medium, leading to an increase in polar content of the surface [81]. The more pronounced the plasma activation, the higher the interactions with PBS. According to WCA measurements ageing reaches a stable configuration after approximately 24 h. Hydrophobic recovery was low compared to DBD data found in literature as the percentage of remaining surface modification after 14 days of ageing in vacuum was 82 to 93 % and in air the range is equal to 70 to 94 %. Overall, the different Saturation conditions had a similar ageing pathway but the condition with the slowest jet velocity, Saturation 3 (50 mm/min) shows a higher hydrophobic recovery compared to Saturation 1 (450 mm/min) and 2 (150 mm/min) based on WCA measurements and XPS data. This is due to the fact that higher jet velocities result in a higher amount of double bond functionalities C=O and O-C=O, which are more stable than C-O functionalities, leading to less hydrophobic recovery.

3.6   Cell tests

When a UHMWPE glenoid component is placed *in vivo* during anatomical TSA it will immediately start to interact with its surrounding environment. In order to maintain sufficient component fixation over time anatomical integration is essential, so cell (osteoblast) adhesion and proliferation towards UHMWPE is of great importance. Therefore cell tests are conducted on untreated and surface-activated UHWMPE samples and the effect of plasma activation regarding cell adhesion and proliferation is investigated. For the five conditions, plasma activated UHMWPE samples are prepared and kept in vacuum. Meanwhile mouse calvaria 3T3 (MC3T3) cells are cultured *in vitro*. MC3T3 is a subclone osteoblast precursor cell line, driven from the skull of a mouse embryo and preserved in liquid nitrogen. This cell line is chosen based on research by Van Vrekhem et al. that stated that it gives sufficient cell adhesion results with a relative percentage of viable attached cells ranging from 68 to 78 %, using plasma activated UHMWPE [72]. In a next step MC3T3 are expanded in Modified Eagle's Medium (MEM) (Gibco, Thermofisher, United States), a standard culture media

to which 10 % fetal bovine serum (FBS) (Gibco), 1 % sodium pyruvate (Gibco) and 0.5 % penicillin streptomycin (PS) (Gibco) is added and is referred to as complete (c)MEM. After expansion, cells are rinsed twice with phosphate buffer saline (PBS) (VWR, Belgium) and enzymatically released from its surface using Tryple Express (Gibco). Next the cell suspension is spon down, re-suspended in cMEM and cultured onto untreated and plasma activated samples. Cell counting is performed with a hemocytometer (Burker, Marienfield) using trypan blue (Sigma Aldrich, Belgium) under a bright-field microscope. The cell experiments consist of two parts: cell adhesion and cell proliferation. In order to see how plasma activation affects cell adhesion and proliferation, morphologic and quantitative cell tests are conducted. The adhesion test compares the different treated samples and the untreated UHMWPE sample, 24 h after seeding. The proliferation experiment compares 24 h with 7 days after seeding to see how cell configuration and amount changes over time.

In a first step round samples are pushed out of a UHMWPE-film. Each plasma condition is tested and also untreated UHMWPE samples are tested. The samples are placed in a 24-well suspension plate (Greiner CELLSTAR, Sigma Aldrich) so cells can not attach to the bottom surface. As a positive control, cells are seeded in a regular 24-well plate (Corning Costar, Sigma Aldrich), which does not contain UHMWPE. As a negative control, treated samples are covered with medium that does not contain any cells and are used to measure the background signal during quantitative measurements. Before cell seeding, all UHMWPE samples are placed under a UV-light for at least 30 min to prevent contamination. In house research by R. Ghobeira indicates that this type of sterilisation does not effect the applied surface modification. For the adhesion test a cell suspension of 1 ml containing 100 000 cells is added to each well and for the proliferation test a cell suspension of 1 ml containing 40 000 cells is added to each well. For both adhesion and proliferation tests cell morphology, viability and density are assessed by a LIVE/DEAD cell viability assay (duplicates). Each sample is washed two times with 0.5 ml of PBS and incubated in a solution containing 0.5 ml PBS, 2.5 μl calcein AM (Anaspec, United States) and 2.5 μl propidium iodide (PI) (Sigma Aldrich). Calcein AM is used to indicate intracellular esterase activity and thereby gives living cell a green fluorescent color, while PI indicates the loss of the cell plasma membrane integrity and leads to a red fluorescent color, indicating dead cells. Quantitative cell viability tests include a CellTiter 96 Aqueous Non-Radioactive Cell Proliferation, MTS (3-(4,5-dimethylthiazol-2-yl)-5-(3-carboxymethoxyphenyl)-2-(4-sulfophenyl)-2H-tetrazolium) assay, which is a calorimetrical method and a PrestoBlue assay, which is a fluometrical method. Here each sample is tested in triplicates. MTS (Promega, United States) produces in the presence of phenazine methosulfate (PMS) and cells, a formazan product that has an absorbance maximum at 490-500 nm in PBS. This MTS assay measures the cellular conversion of MTS into soluble formazan by mitochondrial NADH/NADPH-dependent dehydrogenase. Each sample (well) is washed with PBS and a solution containing 0.5 ml of colorless media and 100 μl PMS/MTS mixture

(1 μl PMS per 20 μl MTS) is added. After 4 h of incubation at a temperature of 37 °C, 400 μl of the colored compound is taken out and the absorbance of the formazan dye in the solution is measured with a 490 nm Universal Microplate Reader EL 800 (BioTek Instruments, USA). PrestoBlue (Invitrogen, United States) is a resazurin-based compound, which is converted to its reduced form by mitochondrial enzymes of viable cells. As a consequence of the reduction, the reagent exhibits a change in color, as well as a shift in its fluorescence and this can be quantified by using either a fluorometric or a spectrophotometric approach. To each well 450 μl normal culture media is added together with 50 μl PrestoBlue compound. After 1 h incubation at 37 °C, 400 μl of the colored PrestoBlue solution is taken out and its fluorescence is measured at 535-605 nm.

3.6.1 Cell adhesion

During a first cell adhesion set-up, treated and untreated UHMWPE samples with a diameter of 12 mm are used regarding LIVE/DEAD imaging, MTS and PrestoBlue measurements. On day zero a cell amount of 100 000 cells/well is seeded and after 24 h visual inspection and quantitative measurements are conducted. Directly after placing the UHMWPE samples in cell suspension, the samples started to float on top of the medium. As a result there are almost no cells present on the surface of the UHMWPE samples, only a small amount of cells adhered on the outer edges. This can be seen in the following LIVE/DEAD images (Figure 3.15), which represent samples: Saturation 1 (A), Saturation 2 (B), Saturation 3 (C), Condition B (D), Condition F (E) Untreated sample (F) and the Positive control (G). The positive control, where cells are seeded on a regular cell adhering surface, shows good cell viability and density. MTS measurements confirmed this low amount of cell adhesion as the signal of the samples on which cells are seeded is approximately equal to the negative control, which does not contain any cells and is used to measure the signal background during quantitative measurements. Because of these two negative outcomes the PrestoBlue test was not performed.
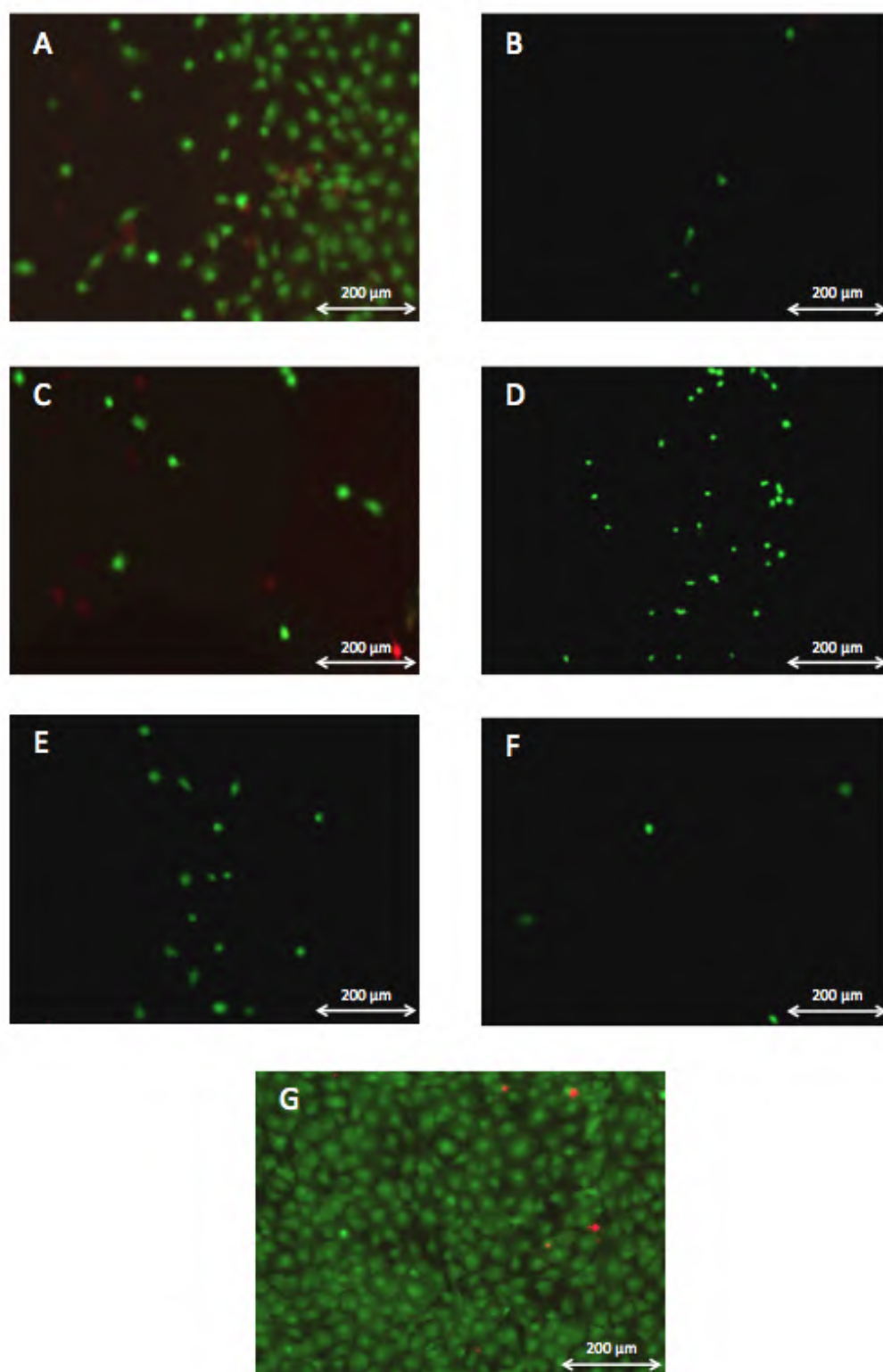
Figure 3.15: Fluorescence images of MC3T3 cells after 24 h in culture regarding cell adhesion set-up one. Green indicates living cells, red indicates dead cells. Images presented are Saturation 1 (A), Saturation 2 (B), Saturation 3 (C), Condition B (D), Condition F (E), Untreated sample (F) and the Positive control (G).

In a second set-up, the diameter of the UHMWPE samples is increased from 12 mm to 15 mm and metal rings made out of stainless steel are placed on top of the samples to avoid floating. In order to assess if cells are truly attached to the surface cell morphology is observed through fluorecent images. When cells are attached to a surface they have an elongated or triangular shape and when they are not firmly bound to the surface their morphology is much more round. When looking at LIVE/DEAD data, it is seen that the untreated sample has a very low cell density, containing clusters of cells that seem barely attached to the surface (Figure 3.16: F). The treated samples display a much better, elongated morphology (Figure 3.16: A, B, C, D, E). Also the positive control shows good cell density. Unfortunately all samples contained a lot of death cells on the outer diameter. This is seen in Figure 3.16: G, which represents the positive control. Especially for this image magnification is decreased to 4 instead of 10. This outer border of death cells corresponds to the metal ring diameter, which probably interacts with its fluid environment and releases toxic metal impurities. MTS data shows that the amount of cells present on the untreated UHMWPE samples is lower than those present on the plasma-treated samples. The relative percentage of viable cell attachment ranges from 37 % for the untreated sample to 70 % for Saturation 3 relative to the positive control (100 %). This visual inspection and quantitative MTS test does not correspond well with PrestoBlue measurement as here all UHMWPE samples have approximately the same relative percentage of cell attachment, indicating that plasma activation does not influence cell adhesion. The fact that the cell amount present on the untreated sample does not correspond well to LIVE/DEAD images can be due to the fact that cells, which did not adhere well are still present during quantitative measurements and give an incorrect impression regarding adhesion. The difference in quantitative measurements might be caused by a too high plating density regarding the PrestoBlue assays. According to Invitrogen there is not one ideal plating density regarding the PrestoBlue reagent, the linear range depends on the cell type. Highly active cells have a linear correlation range that is much smaller than less active cells. For example Jurkat cells show a linear correlation within a range of 100 to 1000 000 cells/well, whereas U-2SO cells have a linear range of 100 to 20 000 cells/well. When the cell amount is not in this linear range it is not possible to correlate different fluorescent values. This is a result of the fact that resazurin within the solution is being reduced to resorufin, which makes a secondary reduction to hydro-resorfin and results in a colorless, non-fluorescent compound [82]. During this set-up the seeding density is equal to 100 000 cell/well which probability does not lie in the linear range of PrestoBlue. For this, it can be concluded that for quantitative measurement regarding high cell amounts, it is better to use the MTS assay.
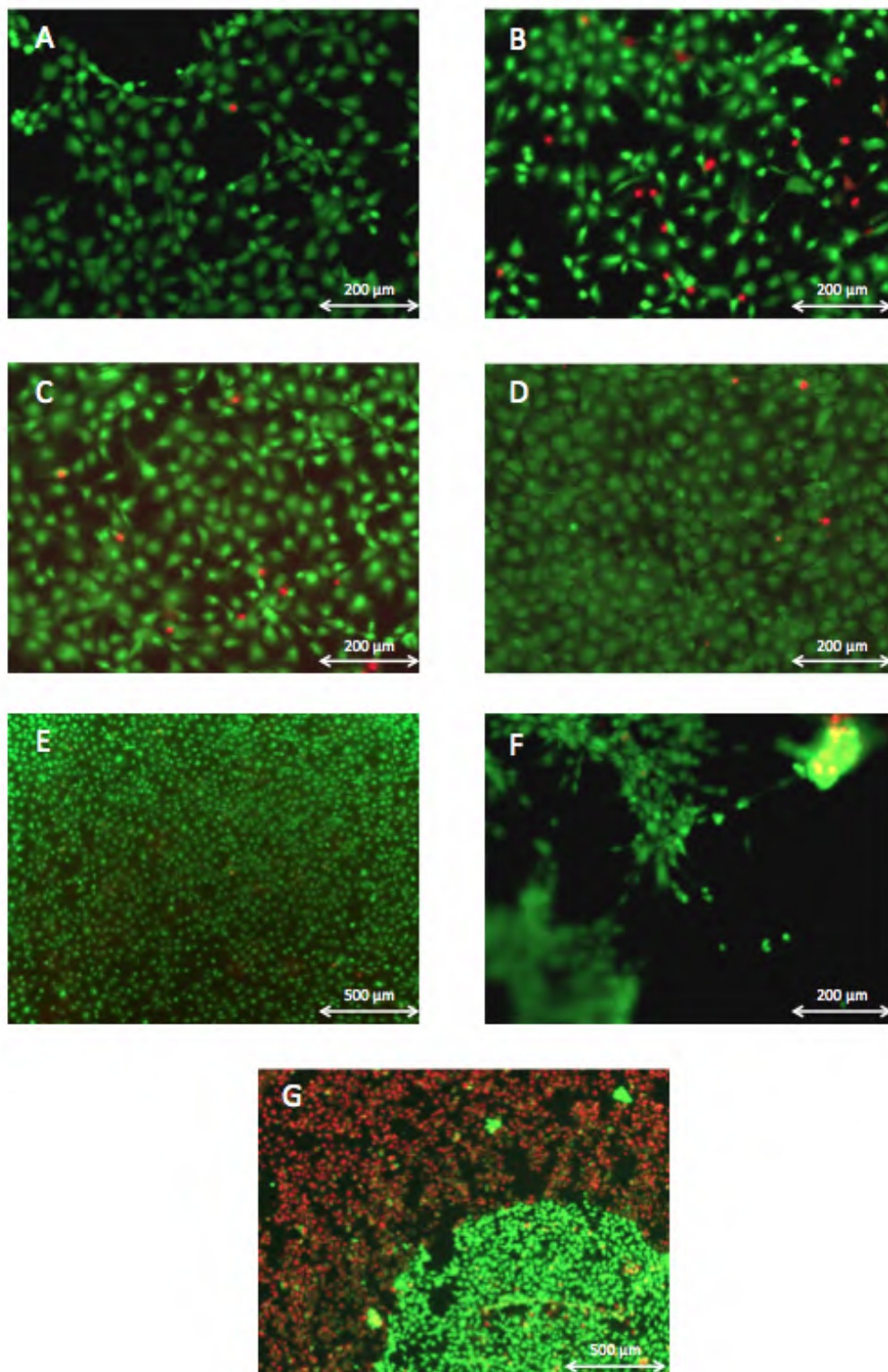
Figure 3.16: Fluorescence images of MC3T3 cells after 24 h in culture regarding cell adhesion set-up two. Green indicates living cells, red indicates dead cells. Images presented are Saturation 1 (A), Saturation 2 (B), Saturation 3 (C), Condition B (D), Condition F (E), Untreated sample (F) and the Positive control (G).
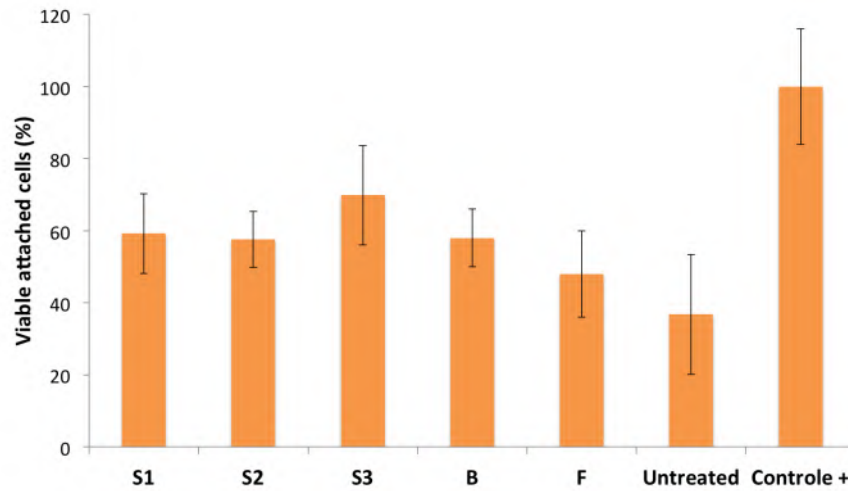
Figure 3.17: Results of a MTS assay adhesion test of MC3T3 cells after 24 h in culture for treated and untreated UHMWPE samples.
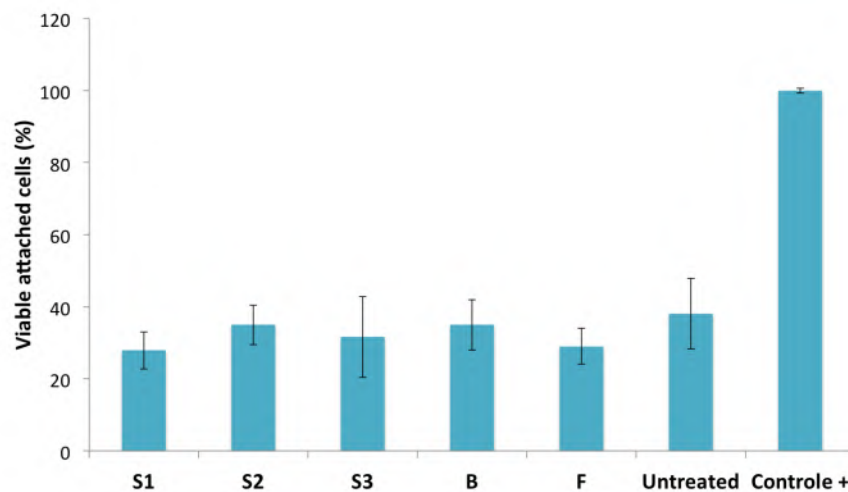

Figure 3.18: Results of a PrestoBlue assay adhesion test of MC3T3 cells after 24 h in culture for treated and untreated UHMWPE samples.

3.6.2 Cell proliferation

For the proliferation set-up, tests are conducted after 24 h and 7 days of seeding. Instead of metal rings, inert glass rings are used on a sample diameter of 15 mm for both MTS and PrestoBlue experiments. For the LIVE/DEAD images, no rings are used as there were only a limited amount available but due to the increase in sample diameter the floating effect is less pronounced.

After 24 h of incubation treated samples show an elongated cell configuration (Figure 3.19:

A, B, C, D, E) and also the positive control contains a proper amount of viable cells (Figure 3.19: G). After 24 h in culture, LIVE/DEAD images regarding untreated samples show a variable outcome. One sample of the untreated condition contains a sufficient amount of cells with elongated cell morphology and the other sample contains almost no cells (Figure 3.19: F). MTS data regarding this set-up is not usable because this assay is not a sensitive measuring agent and cell density after 24 h of seeding is still very low, with a high background signal, leading to standard deviations that are higher than the remaining signal (the average measured signal subtracted by the measured background). PrestoBlue indicates a relative percentage of viable attached cells ranging from 45 % for the untreated sample to 63 % for Saturation 3 relative to the positive control (100 %). This corresponds well with the MTS measurements during the second adhesion set-up. This PrestoBlue assay is much more sensitive in regard to cell detection. Invitrogen indicates a cell sensitivity of 12 cell/well compared to MTS with a sensitivity of 1000 cells/well [82]. This is also seen during these experiments as the fluorescence PrestoBlue signal measured has much higher values compared to MTS, where variations in cell signal directly result in very high standard deviations. Also the background signal coming from PrestoBlue is much lower. In regard to a low cell amount, it is better to use PrestoBlue as a quantitative assay.

After 7 days in culture, samples for the LIVE/DEAD staining are floating as they did not contain glass rings. Overall cell amount increased and cells on the treated samples indicate an elongated morphology (Figure 3.21: A, B, C, D, E). Also the positive control displays a high cell density and elongated morphology (Figure 3.21: G). Again one sample of the untreated condition indicates good cell adhesion and one sample has almost no cells present (Figure 3.21: F). An error occurred during culture or MTS measurements as MTS quantification indicates a signal that lies lower than that measured at 24 h. Therefore this data is not taking into account. As PrestoBlue does not cause cell lysis, the same cells are used to measure the fluorescent signal at 24 h and day 7. This makes comparison in regard to proliferation more valuable. Figure 3.22 indicates the multiplication in cell signal from 24 h to day 7. From this it is possible to see that cell proliferation is more pronounced for Saturation 3, Condition B and Condition F compared to the other UHMWPE samples but no statistical differences are observed. This is somewhat contradictory to what is seen on the fluorescent images and published in literature as plasma activation of UHMWPE is known to increase proliferation of MC3T3 cells after a culture time of 7 days [72].
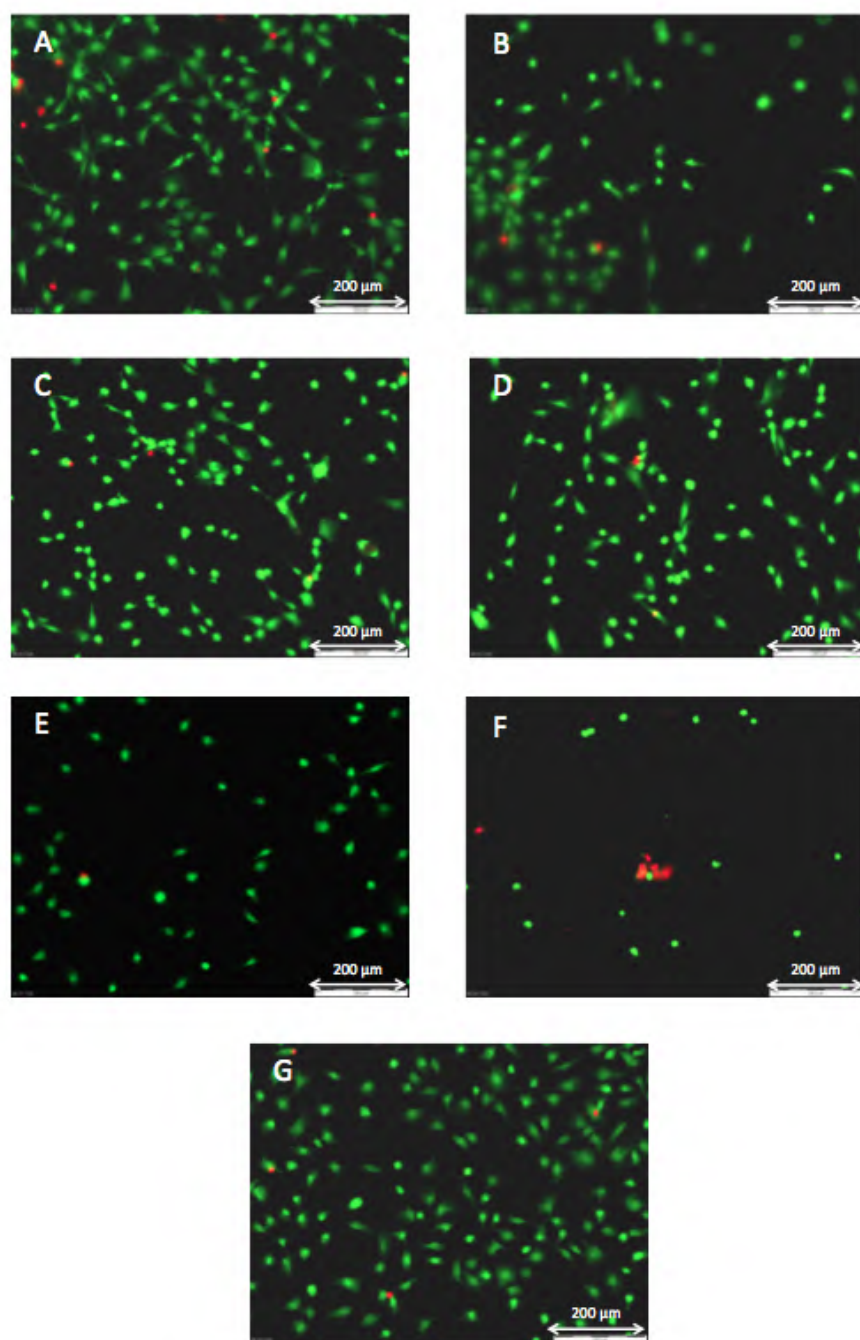
Figure 3.19: Fluorescence images of MC3T3 cells after 24 h in culture regarding a cell proliferation test. Green indicates living cells, red indicates dead cells. Images presented are Saturation 1 (A), Saturation 2 (B), Saturation 3 (C), Condition B (D), Condition F (E), Untreated sample (F) and the Positive control (G).
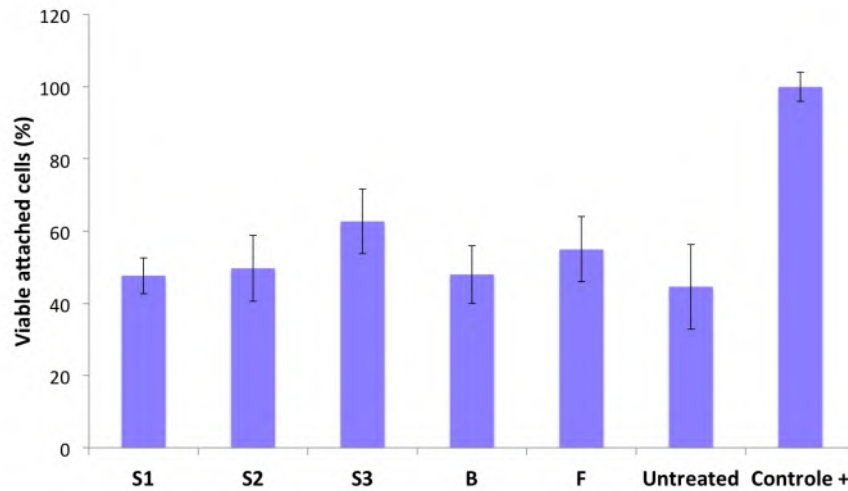
Figure 3.20: Results of a PrestoBlue assay proliferation test of MC3T3 cells after 24 h in culture for treated and untreated UHMWPE samples.

3.6.3 Conclusion

Based on fluorescent images, cell adhesion regarding plasma activated UHMWPE shows better cell morphology, viability and density compared to untreated UHMWPE. For this set-up (cell amount >100 000 cells/well) the MTS assay gives a more reliable outcome compared to PrestoBlue measurements. MTS quantification suggests that plasma activation leads to a an increase in cell adhesion. Overall plasma activation seems to improve initial biocompatibility of UHMWPE as cell configuration on treated samples indicate sufficient surface adhesion, elongated cell morphology and higher quantitative amounts based on MTS results. When quantifying small cell amounts, like during the proliferation test after 24 h of seeding (cell amount >40 000 cells/well), it is better to use PrestoBlue, as it is much more sensitive towards smaller cell amounts compared to MTS. Visual inspection through fluorescent imaging suggests a good cell morphology, density and viability, similar to the positive control, at day 7 of the proliferation test. Quantitative measurements (PrestoBlue) regarding cell proliferation does not show a significant improvement by plasma activation of UHMWPE and also no statistical difference regarding different plasma treatment methods is observed. Further optimization of these cell test set-ups is needed to draw a clearer conclusion regarding visual inspection and quantitative measurements.
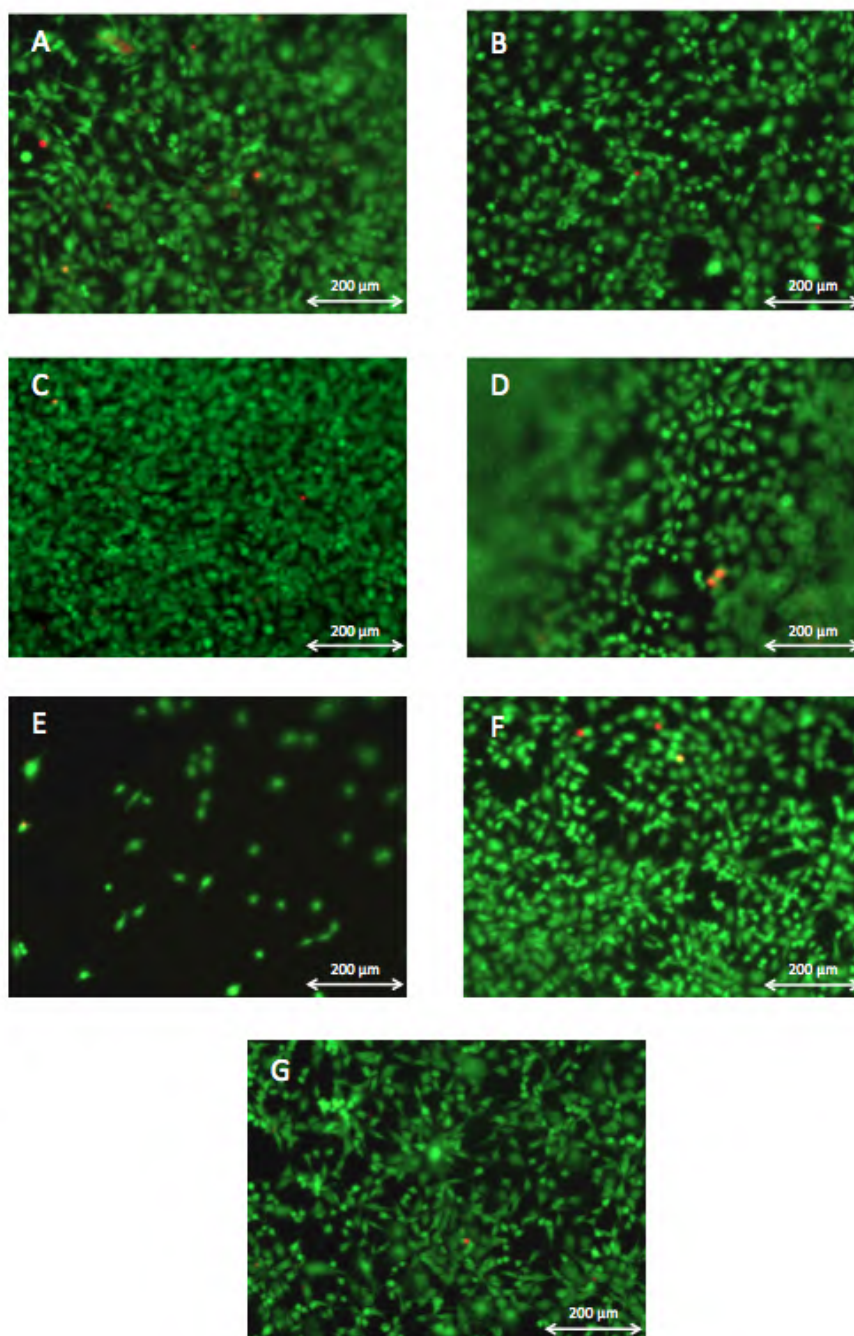
Figure 3.21: Fluorescence images of MC3T3 cells after 7 days in culture regarding a cell proliferation test. Green indicates living cells, red indicates dead cells. Images presented are Saturation 1 (A), Saturation 2 (B), Saturation 3 (C), Condition B (D), Condition F (E), Untreated sample (F) and the Positive control (G).
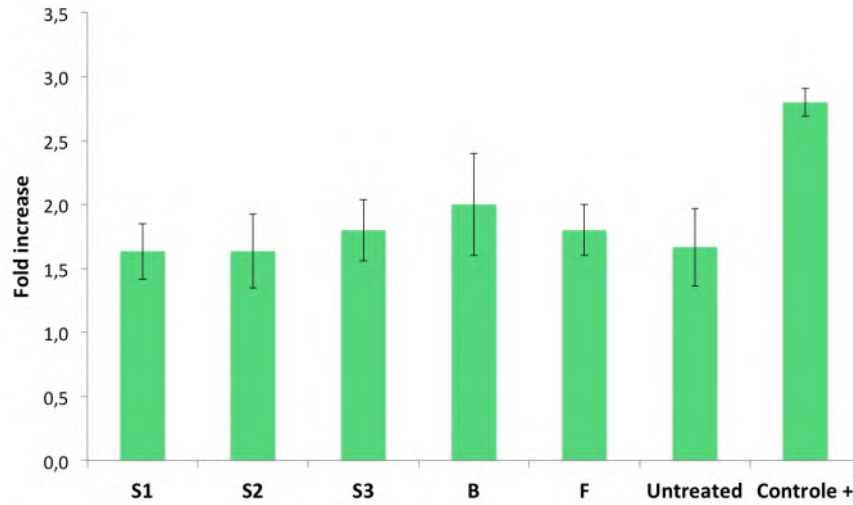
Figure 3.22: The multiplication in cell signal from 24 h to day 7 regarding a PrestoBlue assay proliferation test using MC3T3 cells for treated and untreated UHMWPE samples.

3.7 Pull-out tests

A glenoid prosthesis is made out of medical grade UHMWPE, which is a linear homo-polymer, making it non-polar. Bone cement (PMMA), which is used in regard to prosthesis fixation, is more polar and contains ester-functionalities. By increasing adhesion between the UHMWPE surface and PMMA, component fixation can be improved. Through surface characterization it is seen that plasma activation using an atmospheric pressure Ar plasma jet increases hydrophilicity by implementing oxygen containing functional groups on the surface. In order to assess the effect of plasma treatment regarding adhesion of UHMWPE and bone cement (PMMA), pull-out tests are performed. For each of the five activation conditions, 10 samples are prepared and fixed in bone cement right after plasma treatment. Also 10 untreated samples are cemented.

3.7.1 Surface characterization of medical grade UHMWPE

During hardening of PMMA a lot of heat is produced, namely 82–86 °C, which lies above the working temperature of the UHMWPE-film, that is according to the supplying company GoodFellow 55-95 °C [30]. Therefore medical grade UHMWPE (Chirulen 1020, Quadrant, Belgium) is used. Because the composition of this material might deflect from the UHMWPE-film that was used during previous experiments, surface characterization is performed to assess the effect of plasma surface modification regarding this medical grade UHMWPE. All five plasma activation methods are tested. Directly after treatment the WCA is measured. First the Saturation conditions are tested, for Saturation 1, 2 and 3 this results in a contact

angle of 45.5°, 45.9° and 45.1°, which is similar to the WCA measurements of the UHMWPE-film, see section 3.4.1. Increasing treatment time from 3.6 s to 4.8 s, results in a WCA of 44.0°, from which can be concluded that increasing treatment time does not longer affects hydrophilicity and surface saturation is reached. Plasma activation using Condition B or F gives a WCA of 69.8° or 27.7°, which also matches the values from the UHMWPE-film. Based on these results, no modifications regarding the five plasma treatment conditions are made. In regard to plasma activation, the top and bottom (x= 30 mm and y= 9 mm) of the medical grade UHMWPE samples are treated. In order to see if this also covers treatment of the samples sides, which has a thickness of 4 mm (z), WCA of these sides is measured after top and bottom treatment. For Saturation type-3 activation, the sides have a WCA of 55.3°, due to a limited amount of time, this decrease in WCA is considered to be adequate. Based on these findings only the top and bottom of medical grade UHMWPE is treated during sample preparation.

3.7.2 Sample preparation

During cementation the UHMWPE samples are placed into a teflon mold, which fixes the dimensions of the obtained bone cement cylinder and positions the UHMWPE sample correctly in bone cement. Figure 3.23 shows one half of this cementation mold. The bone cement is made by mixing 24 g of radiopaque polymer powder (Denture base polymers from Huge Dent, China) and 11 ml of MMA monomer liquid (Huge Dent). This results in a bone cement paste that hardens after 20 to 30 minutes. Within 30 s of adding the two components together and mixing them, the paste is poured into the mold that contains the sample. The dimensions of the used UHMWPE samples are visualized in Figure 3.24. The obtained bone cement cylinder containing the UHMWPE sample has a diameter of 20 mm and a height of 40 mm. The activated part of the sample is cemented in the mold for a length of about 4 mm, Figure 3.25 represents a sample after cementation.

3.7.3 Pull-out tests

After all samples are fixed into PMMA bone cement, a universal testing machine LRX plus (Lloyd Instruments, Bognor Regis, UK) is used to perform a uni-axial pull-out test on each sample, with a fixed moving speed of 2 mm/min. Figure 3.26 gives an example of the change in load as a function of time during one of these pull-out tests.

During pull-out tests the maximal force needed to pull the UHMWPE samples out of bone cement is measured. By normalizing this value over the measured contact area, the pull-out stress is determined. The mean stress needed to pull the sample out of the bone cement is

about 0.11 MPa for an untreated sample and in between 0.31 and 0.97 MPa for the plasma activated samples. The mean pull-out stress thus clearly increases after plasma treatment. Figure 3.27 displays these values and indicates a statistical significant difference (p $<$0.05) regarding (all) treated and untreated samples. In order to give a good overview only Condition B and Untreated is marked as significantly different in this figure.
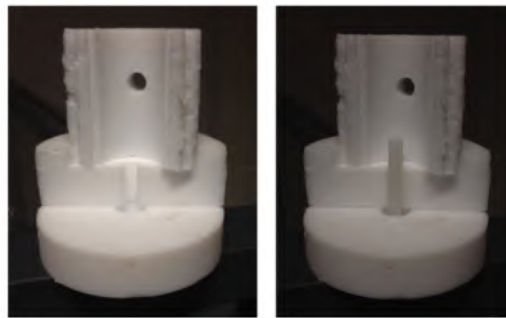

Figure 3.23: The cementation mold; **Left**: Mold without sample. **Right**: Mold with sample.
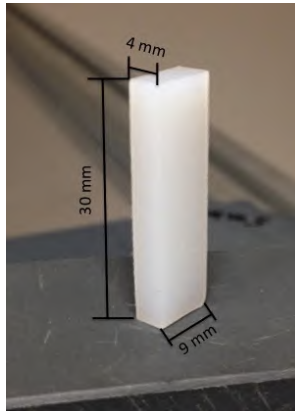

Figure 3.24: Dimension of the medical grade UHMWPE sample used for cementation.

Figure 3.25: Sample after cementation.

Together with WCA measurements and XPS-results this shows that incorporating oxygen containing functional groups on the polymer surface enhances adhesion between UHMWPE and PMMA. The greater the difference in electronegativity between atoms in a bond, the more polar the bond. Oxygen has an electronegative value of 3.44 and carbon 2.5. High oxygen concentrations increase polarity of the surface and thereby the amount of intermolecular forces regarding other materials. When looking at C-C, C-O, C=O and O-C=O bonds,

carboxyl-functionalities have the highest polarity as both oxygen atoms pull the electrons away from carbon, through which carbon gets a partially positive load and the oxygen atoms get a partially negative load. When this oxygen-rich surface comes in contact with PMMA which also contains oxygen (ester) functionalities, an increase in intermolecular forces (mainly Van der Waals forces) can improve surface adhesion, leading to better component fixation.

Even for a plasma treatment time of only 0.27 s (Condition B), a significant increase in pull-out stress is obtained. Increasing treatment time (Condition B versus Saturation 1), leads to a significant increase in pull-out stress (p <0.01). This correlates to the significant increase in oxygen concentrations between both conditions (p <0.01). There is also a significant difference between the pull-out stress of Saturation 1 and Saturation 3, which have no statistical difference in oxygen concentration. However the amount of carboxyl-groups on the Saturation 1 surfaces is higher than the amount present on Saturation 3 surfaces. As said before, higher carboxyl-functionalities lead to greater Van der Waals interaction and thus better surface adhesion towards PMMA. Higher jet velocities (450 mm/min compared to 50 mm/min) during plasma activation thus result in an equal amount of oxygen concentrations but a statistical higher amount of carboxyl-functionalities and therefore significantly increase adhesion towards PMMA. There seems to be no significant difference in decreasing gas flow and increasing power, as the mean pull-out stress needed to pull-out Saturation 3 and Condition F is almost equal. This corresponds with XPS measurements as there was also no real difference in oxygen concentration and functionalities.
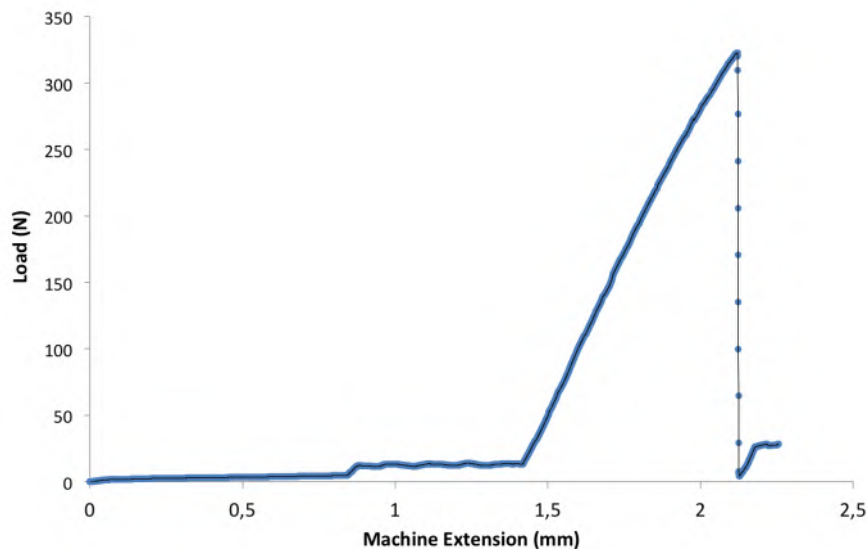

Figure 3.26: Example of the load as a function of strain during a uniaxial pull-out test for an UHMWPE sample treated using Saturation 1.
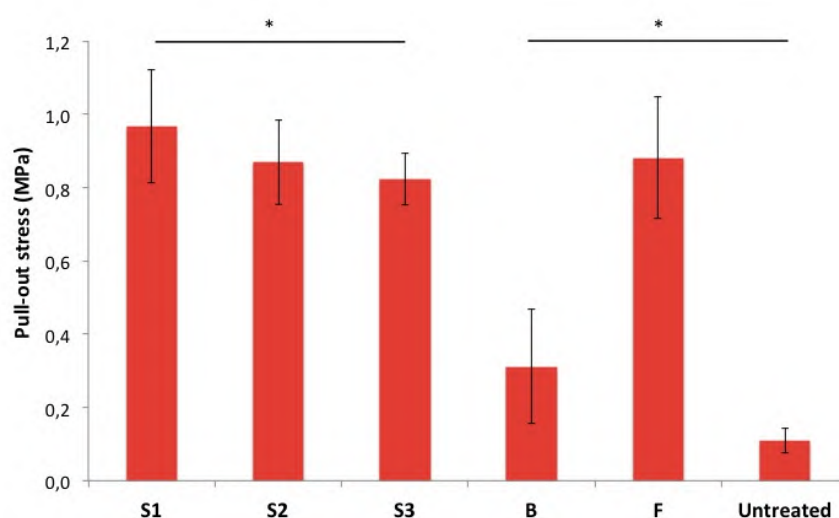
Figure 3.27: Pull-out stress for the plasma activated and untreated UHMWPE samples, with a statistical difference between Saturation 1 and 3. All treated samples have a pull-out stress that is significant higher than the pull-out stress of the untreated sample. This figure only displays the statistical difference regarding Untreated and Condition B.

3.7.4 Conclusion

Plasma activation significantly increases the adhesion of UHMWPE towards bone cement, due to an increase in surface polarity. Even a short treatment time of 0.27 s leads to a significant increases in pull-out stress and raising treatment time towards 3.6 s leads to even higher pull-out stresses as a result of enhanced oxygen concentrations. Increased jet velocities (from 50 mm/min to 450 mm/min) results in a significant raise in pull-out stress because of the increase in carboxyl-functionalities (O-C=O). Lowering the gas flow and amplifying the power, does not affect the acquired pull-out stress, which relates to XPS results as also the relative percentage of oxygen remain unchanged.

3.8 Conclusion

The aim of this master thesis was to improve adhesion properties a UHMWPE glenoid component towards bone cement (PMMA) and bone by looking at the influence of different plasma activation conditions like treatment time, jet velocity, gas flow and power. This chapter proved that plasma activation of UHMWPE samples results in a modification of the surface. By using an atmospheric pressure plasma jet, selected regions can be modified under normal ambient pressure. Plasma activation using Ar gas results in an increase in surface hydrophilicity by incorporation of oxygen containing functional groups and does not significantly affect surface roughness.

Longer treatment times lead to more incorporation of C=O and O-C=O and has an overall higher relative amount of oxygen present on the surface. Even for a short treatment time, the pull-out stress is significantly increased compared to untreated UHMWPE. Different jet velocities at equal treatment time lead to the same oxygen concentration but different types of functional groups are incorporated. Faster jet movements have a statistical higher amount of C=O and O-C=O functionalities, slower movements seem to have more C-O functionalities. This is reflected in the pull-out tests as faster jet velocities have a higher mean pull-out stress, due to increased adhesion towards PMMA which also contains carboxyl-functionalities. A smaller flow and higher power result in a further decrease of the WCA but the overall amount of oxygen based on XPS results is not further influenced, also no difference in pull-out stress is observed. Based on cell morphology plasma activation seems to have a positive effect on cell adhesion and proliferation, which should benefit anatomical integration of the glenoid component. However, plasma activation is a transient type of surface modification as hydrophobic recovery will take place. Storage of plasma-treated UHMWPE in vacuum, air or PBS modifies the surface chemistry and wettability. During WCA measurements it was seen that the measured contact angle initially increased until 24 h and maintained stable from then on. Storage in vacuum preserves surface modification best. XPS data indicated that ageing in air does cause hydrophobic relaxation with a significant difference regarding ageing in vacuum for all activation conditions, in contrast to WCA measurements. Ageing in PBS simulates physiological conditions, which is a very reactive environment, leading to surface interactions. Faster jet movements lead to a statistical higher amount of C=O and O-C=O functionalities, slower movements seem to have higher C-O functionalities. In respect to ageing faster jet movements lead to a more stable configuration and therefore hydrophobic recovery was less profound here.

It is obvious that TSA glenoid fixation using bone cement can benefit from plasma activation and this surface modification technique might tackle current complications regarding component loosening, leading to improved glenoid performance.

Appendix A

Plasma polymerisation of MMA on UHMWPE using a plasma jet

A.1 Introduction

Plasma polymerisation is an interesting technique to deposit polymer nano-films on a substrate without affecting the mechanical bulk properties of the material. Plasma polymerized films are pine-hole free and highly cross-linked and therefore insoluble, thermally stable, chemically inert and mechanically tough [83]. In this set-up, plasma polymersation of MMA will deposit a plasma-PMMA layer on the pre-activated UHMWPE surface using an atmospheric pressure plasma jet. This jet has the main advantage of selective polymerisation; selective areas can be treated for a specific amount of times, which results in different polymer film thicknesses and composition. As the PMMA polymer film on UHMWPE consists of the same material as the bone cement that is used in TSA, fixation should be improved [50].

A.2 Experimental set-up

Plasma polymerisation is performed by the identical instruments used during plasma activation, only the head of the jet is changed. The design of this polymerisation head is visualized in Figure A.1. A second gas flow controller regulates the amount of Ar gas that flows through the liquid MMA solution and thereby controls the quantity of MMA.
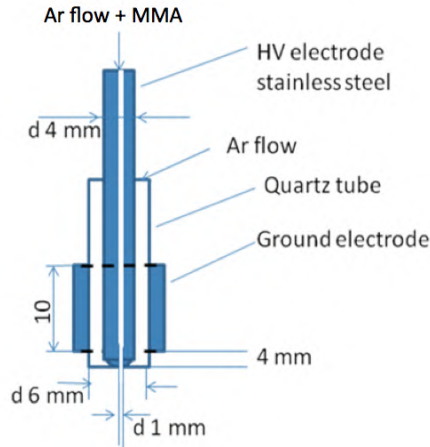
Figure A.1: The atmospheric pressure plasma jet configuration used during polymerisation.

A.3 Conclusion

One of the initial purposes of this master thesis was to investigate plasma polymerisation of methyl methacrylate (MMA) on UHMWPE using a plasma jet. A similar trail was already conducted by Van Vrekhem et al. using a DBD instead of a plasma jet [50, 72]. Nevertheless early in the process it was seen that polymerisation took place inside the tubing of the plasma jet and so a coating was formed within. This would lead to various plasma environment conditions and therefore it was suggested to use N_2 instead of Ar as a carrier gas for the monomer flow. The afterglow of N_2 contains metastables that have a longer lifespan than those of Ar, they keep their energy longer to themself before transferring it to the monomer [84]. It was assumed that polymerisation now would take place further down the tube and this would prevent deposition inside the plasma jet. Even though there was not a direct visible sign of polymerisation inside the tube, results regarding the WCA were inconclusive, the plasma glow was non-consistent and sometimes even unstable. After demounting the plasma jet, a gold colour coating was found within the tube. It became clear more extensive and long-term research is necessary regarding this set-up.

Even so plasma polymerisation of MMA on UHMWPE using a atmospheric pressure plasma jet has the potential to lead to promising results regarding the application of increased shoulder prosthesis fixation, as selective areas can be treated and because plasma polymerisation is not as prone to ageing as plasma activation. Further research is needed until working conditions are optimized.

Appendix B

Surface characterisation

B.1   Contact angle measurement

Static water contact angle goniometry is a simple and widely used test to evaluate the wettability of a surface, like for example polymer films. By putting a small droplet of deionized water or other liquid on the material surface it is possible to measure the contact angle of this droplet with the surface. The contact angle is defined as the angle between the solid surface and the tangential line drawn through the three phase boundary, where the liquid, gas and solid interact. An example is given in Figure B.1. The contact angle will depend on the hydrophilicity of both the liquid and the surface. When a droplet of distilled water is used, a hydrophobic surface will result in a relative high contact angle as opposed to a hydrophilic surface. The contact angle is a measure of the relative amount of adhesion (liquid to solid) and cohesive (liquid-liquid) forces counteracting each other and varies over the range of 0 to 180°[85].
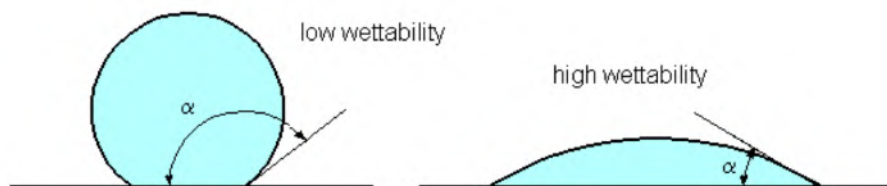

Figure B.1: Principle of contact angle measurment; **Left**: Surface with low wettability, leading to a high water contact angle. **Right**: Surface with high wettability, leading to a low water contact angle [85].

B.2   Atomic force microscopy

Atomic force microscopy (AFM) was invented in 1986 by Gerd Binning, Calvin Quate and Christoph Gerber. It combines the mechanical profilometer, using the mechanical tip to sense forces and scanning tunnel microscopy, using piezoelectric transducers for scanning. The probing tip is attached to a cantilever-type spring. Images are taken by scanning the sample and digitizing the deflection arm in the z-direction or by analysing a change in tapping frequency according to the xy-plane. Typical forces between the probing tip and the sample range from 10^{-11} to 10^{-6} N and the smallest measurable distance goes to 10^{-14} m. Two operation types are possible, contact and non-contact mode. During non-contact mode, also known as dynamic mode or tapping mode, there is a constant tip-sample separation of 10 to 100 nm. Here the cantilever taps at or close to its resonance frequency. Forces present on the surface deform this frequency and data is driven from this change. The tip senses attractive forces such as Van der Waals, electrostatic, magnetic and capillary forces, giving information about surface topography, distribution of charges, wall structures and liquid film distribution. When the tip of the cantilever is in contact with the sample, ionic repulsion forces allow the surface topography to be traced with high resolution. Also frictional forces and elastic or plastic deformations can be detected, given that conditions are optimal. This mode is called contact mode, or static mode. In this case the force is kept constant leading to a change in cantilever height. Because of the interaction between the tip and the surface, the cantilever is deflected. A laser is reflected on the cantilever and detected by photodiodes. The position of the reflected laser beam on the surface of the photodiode determines the z-position of the cantilever, this principle is visualised in Figure B.2. AFM contains a feedback system that reads data and prevents the tip from breaking [86, 87, 88].
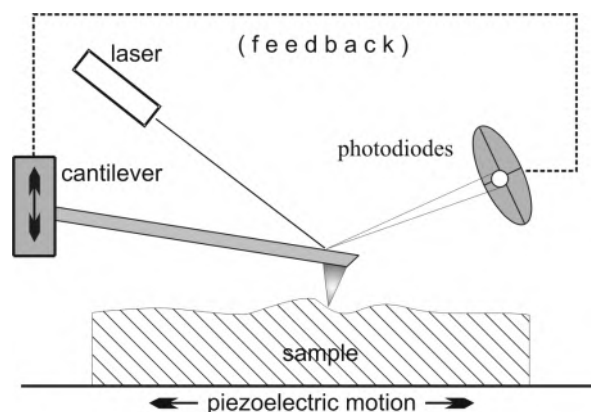

Figure B.2: Basic principle of AFM as the tip of the cantilever moves over the surface in static mode, its position is determined by reflection of the laser beam [89].

B.3 X-ray photoelectron spectroscopy

X-ray photoelectron spectrometers exists for quite some time now and during the intervening years this technique has been optimized into a routine, surface analysis method in which the chemical stage of near surfaces regions is determined. This technique provides a semi-quantitative analysis of the atomic surface composition and can resolve different types of chemical bonds at the surface. The basic principles of XPS includes the interaction of an X-ray photon with a sample, leading to the ejection of an electron from either the valence electron shell or an inner core electron shell, these electrons are called photoelectrons. These ejected photoelectrons are focussed onto the entrance slit of an electrostatic analyser by an electromagnetic lens system. The electrons then pass through a hemispherical electron analyser, which can disperse the emitted electrons according to their kinetic energy. Thereby the flux of emitted electrons of a particular energy is measured. These electrons are detected using an electron multiplier. The kinetic energy E_{kin} of the emitted electron is given by the following formula [90]:

$$E_{kin} = h\nu - E_b - \phi$$

where hν is the energy of the incident monochromatic X-ray photon, E_b the binding energy of the electron towards the atom and ϕ the work function of the specimen. The work function is the minimum energy that is needed to liberate an electron from the surface, this formula is graphically shown in Figure B.3. Looking at the photoelectric effect, a photon with an energy bigger than the working function is needed in order for photoeletric emission to occur. Any excess energy is given to the electron as kinetic energy. By measuring the energy of the photoelectron and knowing the energy of the incident photons, the electron binding energy can be determined. It is this binding energy that permits identification of the atom under investigation and that provides information concerning its chemical state. For each atomic element, there is a characteristic binding energy associated with each core atomic orbital, i.e. each element will give rise to a characteristic set of peaks determined by the photon energy and the respective binding energies. The presence of peaks at specific energies therefore indicates a specific element in the sample. The exact binding energy of an electron depends not only on the electron shell from which photo emission occurs, but also on the local chemical and physical environment. A major strength of XPS is the ability to identify chemical state changes that occur at a surface when two or more atoms combine. When two atoms combine to from a bond, electron transfer occurs between the atoms, one becomes more positive and the other more negative. This results in a shift in electron binding energies of the electrons by a small amount, usually a fraction between 1 to a few eV. These small shifts in the peak position are responsible for peak broadening. Through this way, XPS can also provide infor-

mation on the type of bonds formed at the surface. The intensity of the peaks is expressed by the peak area and is proportional to the relative abundance of the element within the analysed region of the sample surface. A quantitative analysis of atomic surface composition is determined through a so-called survey scan, i.e. an XPS spectrum with a wide energy frame and a relatively low resolution. When doing XPS experiments this is the first spectrum recorded. For an accurate determination of the binding energy of a specific electron level, a narrow energy frame is place around a specific XPS peak (like carbon), here the spectrum is recorded with a high resolution and a small energy step. In this high resolution spectrum, deconvolution of overlapping peaks is performed to resolve the different types of chemical bonds. The intensity of the XPS peak is only determined by the photoelectrons that reach the detector without loss of energy. The photoelectrons that loose energy deviate from the detection line. Consequently an XPS spectrum only provides information on the top atomic layers (up to 5-10 nm, or roughly 20-40 atomic layers). The spectra can be strongly influenced by the relative orientation of the source, sample and detector.

XPS requires an ultra-high vacuum environment, lower than 5.10^{-6} Pa to prevent contamination of the specimen surface and interaction of the background gas. Therefore the instrument normally consist out of a preparation chamber to carry out initial manipulations and remove any gaseous contaminants left in the sample. The preparation chamber is followed by an analytical chamber at ultra-high vacuum, with a photon source, an electron analyser and a detector, here the monochromatic source of radiation is focused on the specimen. Figure B.4 visualizes the XPS set-up.
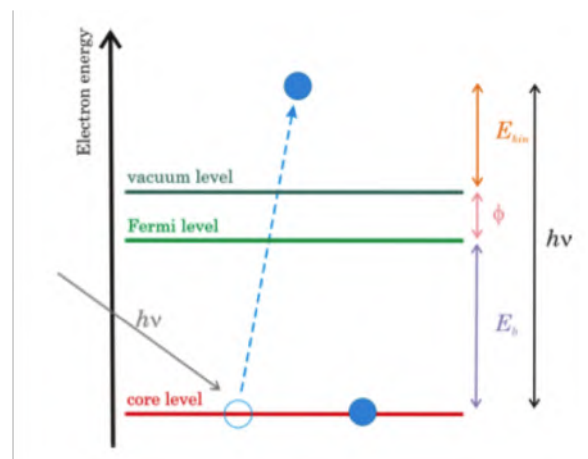

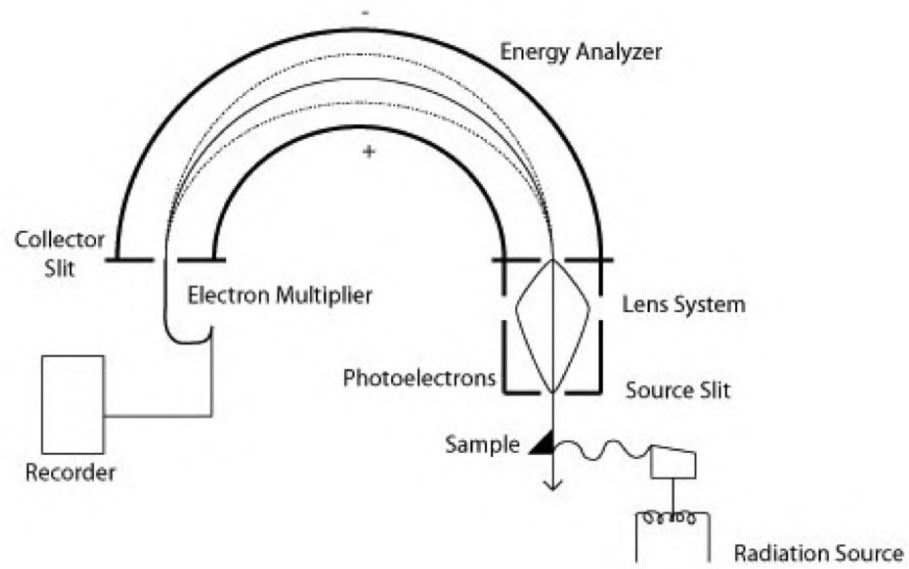**Figure B.3:** Energy diagram of the photo-ionisation process [90].

Figure B.4: Schematic representation of an XPS set-up [91].

Bibliography

[1] L. Kaback, A. Green, and T. Blaine, "Glenohumeral arthritis and total shoulder replacement," *Medicine and Health*, vol. 95, no. 4, pp. 120–4, 2012.

[2] L. De Wilde, "Shoulderprosthesis: A biomechanical perspective," *Course: Biomechanics UGent*, 2015.

[3] Sports-Injury-Clinic, "Rotator cuff tear."

[4] S. M. Kurtz, *Ultra-high molecular weight polyethylene in total joint replacement and medical devices*. UHMWPE Biomaterials Handbook, United States: Matthew Deans, 2015.

[5] R. A. Brand, M. A. Mont, and M. M. Manring, "Biographical sketch: Themistocles gluck (1853-1942)," *Clin Orthop Relat Res*, vol. 469, no. 6, pp. 1525–7, 2011.

[6] E. L. Flatow and A. K. Harrison, "A history of reverse total shoulder arthroplasty," *Clin Orthop Relat Res*, vol. 469, no. 9, pp. 2432–9, 2011.

[7] C. S. Neer, "Articular replacement for the humeral head," *J Bone Joint Surg Am*, vol. 37, pp. 215–28, 1955.

[8] J. Sanchez-Sotelo, "Total shoulder arthroplasty," *The Open Orthopaedics Journal*, vol. 5, pp. 106–14, 2011.

[9] C. S. Neer, K. C. Watson, and F. J. Stanton, "Recent experience in total shoulder replacement," *The journal of bone and joint surgery*, vol. 64, no. 3, p. 319, 1982.

[10] R. H. Cofield, "Status of total shoulder arthroplasty," *Arch Surg*, vol. 112, pp. 1088–91, 1977.

[11] C. S. Neer, "Replacement arthroplasty for glenohumeral osteoarthrisis," *J Bone Joint Surg Am*, vol. 56, pp. 1–13, 1974.

[12] P. Walch, G.; Boileau, "Prosthetic adaptability: a new concept for shoulder arthroplasty," *J Shoulder Elbow Surg*, vol. 8, pp. 443–51, 1999.

[13] K. I. Bohsali, M. A. Wirth, and J. Rockwood, C. A., "Complications of total shoulder arthroplasty," *J Bone Joint Surg Am*, vol. 88, no. 10, pp. 2279–92, 2006.

[14] J. S. Day, E. Lau, K. L. Ong, G. R. Williams, M. L. Ramsey, and S. M. Kurtz, "Prevalence and projections of total shoulder and elbow arthroplasty in the united states to 2015," *J Shoulder Elbow Surg*, vol. 19, no. 8, pp. 1115–20, 2010.

[15] C. Chillemi and V. Franceschini, "Shoulder osteoarthritis," *Arthritis*, vol. 2013, pp. 1–7, 2013.

[16] T. Norris and J. Iannotti, "Functional outcome after shoulder arthroplasty for primary osteoarthritis: A multicenter study," *Journal of Shoulder and Elbow Surgery*, vol. 11, no. 2, pp. 130–135, 2002.

[17] A. Papadonikolakis, M. B. Neradilek, and F. A. Matsen, "Failure of the glenoid component in anatomic total shoulder arthroplasty," *J Bone Joint Surg Am*, vol. 95, no. 24, pp. 2205–12, 2013.

[18] E. Ricchetti and G. R. Williams, "Total shoulder arthroplasty—indications, technique, and results," *Operative Techniques in Orthopaedics*, vol. 21, no. 1, pp. 28–38, 2011.

[19] S. D. Martin, D. Zurakowski, and T. S. Thornhill, "Uncemented glenoid component in total shoulder arthroplasty," *The journal of bone and joint surgery*, vol. 87-A, no. 6, pp. 1284–92, 2005.

[20] E. Ibrahim and M. Thomas, "Hemiarthroplasty of the glenohumeral joint," *Orthopaedics and Trauma*, vol. 29, no. 5, pp. 287–296, 2015.

[21] Cedars-Sinai, "Arhtroplasty fixation."

[22] S. Churchill, B. Kopjar, and E. Fehringer, "Humeral component modularity may not be an important factor in the outcome of shoulder arthroplasty for glenohumeral osteoarthritis," *Medical journal of orthopedics*, 2015.

[23] B. Schoch, J. D. Werthel, C. Schleck, J. W. Sperling, and R. H. Cofield, "Does an increase in modularity improve the outcomes of total shoulder replacement? comparison across design generations," *Int Orthop*, vol. 39, no. 10, pp. 2053–60, 2015.

[24] M. Rocha, A. Mansur, and H. Mansur, "Characterization and accelerated ageing of uhmwpe used in orthopedic prosthesis by peroxide," *Materials*, vol. 2, no. 2, pp. 562–576, 2009.

[25] A. A. Young and G. Walch, "Fixation of the glenoid component in total shoulder arthroplasty: what is modern cementing technique?," *J Shoulder Elbow Surg*, vol. 19, no. 8, pp. 1129–36, 2010.

[26] M. Schrumpf, T. Maak, S. Hammoud, and E. V. Craig, "The glenoid in total shoulder arthroplasty," *Curr Rev Musculoskelet Med*, vol. 4, no. 4, pp. 191–9, 2011.

[27] H. D. Clitherow, C. M. Frampton, and T. M. Astley, "Effect of glenoid cementation on total shoulder arthroplasty for degenerative arthritis of the shoulder: a review of the new zealand national joint registry," *J Shoulder Elbow Surg*, vol. 23, no. 6, pp. 775–81, 2014.

[28] L. V. Gulotta, K. L. Chambers, R. F. Warren, D. M. Dines, and E. V. Craig, "No differences in early results of a hybrid glenoid compared with a pegged implant," *Clin Orthop Relat Res*, vol. 473, no. 12, pp. 3918–24, 2015.

[29] E. J. Strauss, C. Roche, P. H. Flurin, T. Wright, and J. D. Zuckerman, "The glenoid in shoulder arthroplasty," *J Shoulder Elbow Surg*, vol. 18, no. 5, pp. 819–33, 2009.

[30] R. Vaishya, M. Chauhan, and A. Vaish, "Bone cement," *J Clin Orthop Trauma*, vol. 4, no. 4, pp. 157–63, 2013.

[31] T. Choi, M. Horodyski, A. M. Struk, D. T. Sahajpal, and T. W. Wright, "Incidence of early radiolucent lines after glenoid component insertion for total shoulder arthroplasty: a radiographic study comparing pressurized and unpressurized cementing techniques," *J Shoulder Elbow Surg*, vol. 22, no. 3, pp. 403–8, 2013.

[32] D. R. Respoli, J. W. Sperling, G. S. Athwal, and C. D. Schleck, "Humeral head replacement for the treatment of osteoarthritis," *Journal of bone and joint surgery*, vol. 88-A, no. 12, pp. 2637–44, 2006.

[33] G. M. Gartsman, H. A. Elkousy, K. M. Warnock, T. B. Edwards, and D. P. O'Connor, "Radiographic comparison of pegged and keeled glenoid components," *J Shoulder Elbow Surg*, vol. 14, no. 3, pp. 252–7, 2005.

[34] C. P. Roche, N. J. Stroud, P. H. Flurin, T. W. Wright, J. D. Zuckerman, and M. J. DiPaola, "Reverse shoulder glenoid baseplate fixation: a comparison of flat-back versus curved-back designs and oval versus circular designs with 2 different offset glenospheres," *J Shoulder Elbow Surg*, vol. 23, no. 9, pp. 1388–94, 2014.

[35] T. W. Throckmorton, P. C. Zarkadas, J. W. Sperling, and R. H. Cofield, "Pegged versus keeled glenoid components in total shoulder arthroplasty," *Journal of Shoulder and Elbow Surgery*, vol. 19, no. 5, pp. 726–733, 2010.

[36] T. Mamatha, R. P. Shakuntala, B. V. Marlimanju, G. K. Sneha, M. P. Mangala, and K. Brijesh, "Morphology of glenoid cavity," *Journal of health and allied science*, vol. 10, no. 3, 2011.

[37] D. Raj, "Shoulder resurfacing (arthrosurface) with a beverly hills orthopedic surgeon."

[38] S. Hsu, R. Greiwe, C. Saifi, and C. Ahmad, "Reverse total shoulder arthroplasty, biomechanics and rationale," *Operative Techniques in Orthopaedics*, vol. 21, no. 1, pp. 52–59, 2011.

[39] T. K. Kiet, B. T. Feeley, M. Naimark, T. Gajiu, S. L. Hall, T. T. Chung, and C. B. Ma, "Outcomes after shoulder replacement: comparison between reverse and anatomic total shoulder arthroplasty," *J Shoulder Elbow Surg*, vol. 24, no. 2, pp. 179–85, 2015.

[40] N. Purohit and I. Katsimilis, "The "whys and wheres" of metal work around the shoulder," 2015.

[41] I. Shoulder Options, "Luna™ stemless humeral prosthesis."

[42] M. E. Torchia, R. H. Cofield, and C. R. Settergren, "Total shoulder arthroplasty with the neer prosthesis: long-term results," *Journal of Shoulder and Elbow Surgery*, vol. 6, pp. 495–550, 1997.

[43] P. H. Flurin, M. Janout, C. Roche, T. Wright, and J. D. Zuckerman, "Revision of the loose glenoid component in anatomic total shoulder arthroplasty," *Bulletin of the hospital for joint diseases*, vol. 71, pp. 68–76, 2013.

[44] H. Iwaki, G. Scott, and M. Freeman, "The natural history and significance of radiolucent lines at cemented femoral interface," *The journal of bone and joint surgery*, vol. 84, no. B, pp. 550–5, 2002.

[45] L. M. Kwong, M. Jasty, R. D. Mulroy, W. J. Maloney, C. Bragdon, and W. H. Harris, "The history of the radiolucent line," *Journal of bone and joint surgery*, vol. 74, no. B, pp. 67–73, 1992.

[46] P. Boileau, C. Avidor, S. G. Krishnan, G. Walch, J. F. Kempf, and D. Mole, "Cemented polyethylene versus uncemented metal-backed glenoid components in total shoulder arthroplasty: a prospective, double-blind, randomized study," *J Shoulder Elbow Surg*, vol. 11, no. 4, pp. 351–9, 2002.

[47] T. M. Provencher and A. A. Romeo, *Shoulder instability: A comprehansive approach.* 2012.

[48] J. F. Mano, R. A. Sousa, L. F. Boesel, N. M. Neves, and R. L. Reis, "Bioinert, biodegradable and injectable polymeric matrix composites for hard tissue replacement: state of the art and recent developments," *Composites Science and Technology*, vol. 64, no. 6, pp. 789–817, 2004.

[49] E. Brach del Prever, A. Bistolfi, P. Bracco, and L. Costa, "Uhmwpe for arthroplasty: past or future?," *Journal of Orthopaedics and Traumatology*, vol. 10, no. 1, pp. 1–8, 2008.

[50] P. Cools, S. Van Vrekhem, N. De Geyter, and R. Morent, "The use of dbd plasma treatment and polymerization for the enhancement of biomedical uhmwpe," *Thin Solid Films*, vol. 572, pp. 251–259, 2014.

[51] S. L. Brown and A. T. Holme, *Chemistry for Engineering Students*. 2011.

[52] S. M. Kurtz, *The Clinical performance of historical and conventional UHMWPE in hip replacements*. 2015.

[53] A. Firas, G. Michael, K. Georgina, F. Bronwyn, and P. Paul, "Adhesion of polymers," *Progress in Polymer Science*, vol. 34, no. 9, pp. 948–68, 2009.

[54] J. A. Stone, *The theory of intermolecular forces*. 2013.

[55] W. Taylor and B. Welt, *Synopsos of plasma surface treatments*. 2009.

[56] T. Desmet, R. Morent, N. De Geyter, C. Leys, E. Schacht, and P. Dubruel, "Nonthermal plasma technology as a versatile strategy for polymeric biomaterials surface modification: A review," *Bio-macromolecules*, vol. 10, no. 9, pp. 2351–69, 2009.

[57] M. Strobel, C. S. Lyons, and K. L. Mittal, *Plasma surface modification of polymers: relevance to adhesion*. 1994.

[58] M. Strobel, M. J. Walzakn, J. M. Hill, A. Lin, E. Karbashewski, and C. S. Lyons, "A comparison of gas-phase methods of modifying polymer surfaces," *Journal of adhesion science technology*, vol. 9, no. 3, pp. 365–83, 1995.

[59] P. K. Chu, J. Y. Chen, L. P. Wang, and N. Huang, "Plasma-surface modification of biomaterials," *Materials science and engineering*, vol. 36, pp. 143–206, 2002.

[60] S. Yoshida, K. Hagiwara, T. Hasebe, and A. Hotta, "Surface modification of polymers by plasma treatments for the enhancement of biocompatibility and controlled drug release," *Surface and Coatings Technology*, vol. 233, pp. 99–107, 2013.

[61] I. Langmuir and L. Tonks, "A general theory of the plasma of an arc," *APS journals*, vol. 34, no. 6, p. 876, 1929.

[62] E. Gomez, D. A. Rani, C. R. Cheeseman, D. Deegan, M. Wise, and A. R. Boccaccini, "Thermal plasma technology for the treatment of wastes: a critical review," *J Hazard Mater*, vol. 161, no. 2-3, pp. 614–26, 2009.

[63] V. Scholtz, J. Pazlarova, H. Souskova, J. Khun, and J. Julak, "Nonthermal plasma, a tool for decontamination and disinfection," *Biotechnol Adv*, vol. 33, no. 6 Pt 2, pp. 1108–19, 2015.

[64] T. Von Woedtke, S. Reuter, K. Masur, and K. D. Weltmann, "Plasmas for medicine," *Physics Reports*, vol. 530, no. 4, pp. 291–320, 2013.

[65] N. De Geyter, R. Morent, C. Leys, L. Gengembre, and E. Payen, "Treatment of polymer films with a dielectric barrier discharge in air, helium and argon at medium pressure," *Surface and Coatings Technology*, vol. 201, no. 16-17, pp. 7066–7075, 2007.

[66] K. G. Kostov, T. M. C. Nishime, A. H. R. Castro, A. Toth, and L. R. O. Hein, "Surface modification of polymeric materials by cold atmospheric plasma jet," *Applied Surface Science*, vol. 314, pp. 367–75, 2014.

[67] W. Chen, C. Jie-rong, and L. Ru, "Studies on surface modification of poly(tetrafluoroethylene) film by remote and direct ar plasma," *Applied Surface Science*, vol. 254, no. 9, pp. 2882–88, 2008.

[68] S. Bornholdt, M. Wolter, and H. Kersten, "Characterization of an atmospheric pressure plasma jet for surface modification and thin film deposition," *The European Physical Journal D*, vol. 60, no. 3, pp. 653–60, 2010.

[69] A. Van Deynse, P. Cools, C. Leys, N. De Geyter, and R. Morent, "Surface activation of polyethylene with an argon atmospheric pressure plasma jet: Influence of applied power and flow rate," *Applied Surface Science*, vol. 328, pp. 269–78, 2014.

[70] A. Van Deynse, P. Cools, C. Leys, R. Morent, and N. De Geyter, "Surface modification of polyethylene in an argon atmospheric pressure plasma jet," *Surface and Coatings Technology*, vol. 276, pp. 384–90, 2015.

[71] U. Lommatzsch, D. Pasedag, A. Baalmann, G. Ellinghorst, and H. Wagner, "Atmospheric pressure plasma jet treatment of polyethylene surfaces for adhesion improvement," *Plasma Processes and Polymers*, vol. 4, no. 1, pp. 1041–45, 2007.

[72] S. Van Vrekhem, P. Cools, H. Declercq, A. Van Tongel, C. Vercruysse, M. Cornelissen, N. De Geyter, and R. Morent, "Application of atmospheric pressure plasma on polyethylene for increased prosthesis adhesion," *Thin Solid Films*, 2015.

[73] T. G. van Kooten, H. T. Spijker, and H. J. Busscher, "Plasma-treated polystyrene surfaces: model surfaces for studying cell–biomaterial interactions," *Biomaterials*, vol. 25, no. 10, pp. 1735–47, 2004.

[74] C. Oehr, "Plasma surface modification of polymers for biomedical use," *Nuclear Instruments and Methods in Physics Research Section B: Beam Interactions with Materials and Atoms*, vol. 208, pp. 40–7, 2003.

[75] Y. Tamada and Y. Ikada, "Cell adhesion to plasma-treated polymer surfaces," *Polymer*, vol. 34, no. 10, pp. 2208–12, 1992.

[76] A. Sublet, C. Ding, J. L. Dorier, C. Hollenstein, P. Fayet, and F. Coursimault, "Atmospheric and sub-atmospheric dielectric barrier discharges in helium and nitrogen," *Plasma Sources Science and Technology*, vol. 15, no. 4, pp. 627–34, 2006.

[77] C. Meyer, S. Muller, B. Gilbert-Lopez, and J. Franzke, "Impact of homogeneous and filamentary discharge modes on the efficiency of dielectric barrier discharge ionization mass spectrometry," *Anal Bioanal Chem*, vol. 405, no. 14, pp. 4729–35, 2013.

[78] V. Stern, "The oxygen dilemma: Can to much o2 kill?."

[79] R. L. Williams, D. J. Wilson, and N. P. Rhodes, "Stability of plasma-treated silicone rubber and its influence on the interfacial aspects of blood compatibility," *Biomaterials*, vol. 25, no. 19, pp. 4659–73, 2004.

[80] A. Van Deynse, P. Cools, C. Leys, R. Morent, and N. De Geyter, "Influence of ambient conditions on the aging behavior of plasma-treated polyethylene surfaces," *Surface and Coatings Technology*, vol. 258, pp. 359–67, 2014.

[81] D. J. Wilson, R. L. Williams, and R. C. Pond, "Plasma-treated surfaces following storage in air or pbs," *Surface and interface analysis*, vol. 31, pp. 397–408, 2001.

[82] Invitrogen, "Prestoblue cell viability reagent," report, 2012.

[83] N. De Geyter, R. Morent, S. Van Vlierberghe, P. Dubruel, C. Leys, L. Gengembre, E. Schacht, and E. Payen, "Deposition of polymethyl methacrylate on polypropylene substrates using an atmospheric pressure dielectric barrier discharge," *Progress in Organic Coatings*, vol. 64, no. 2-3, pp. 230–37, 2009.

[84] V. Guerra, P. Sa, and J. Loureiro, "Electron and metastable kinetics in the nitrogen afterglow," *Plasma sources science and technology*, vol. 12, pp. 8–15, 2003.

[85] R. Averyard and D. A. Haidon, *An introduction to the principles of surface chemistry.* 1973.

[86] G. Binnig, C. F. Quate, and C. Gerber, "Atomic force microscope," *Phys Rev Lett*, vol. 56, no. 9, pp. 930–3, 1986.

[87] E. Meyer, "Atomic force microscopy," *Surface Science*, vol. 41, pp. 3–49, 1992.

[88] ArtificialOxideNanostructures, "Afm and imaging of the surface."

[89] S. Montanari, *Atomic Force Microscope.* Thesis, 2005.

[90] N. De Geyter, *Plasma modification of polymer surfaces in the subatmospheric pressure range.* Thesis, 2008.

[91] L. Sabbatini, "Photoelectron spectroscopy: Application," 2014.